The contribution of cortical feedback projections to sensory representations in the mouse primary visual cortex

Gabriela Tondolo Fioreze

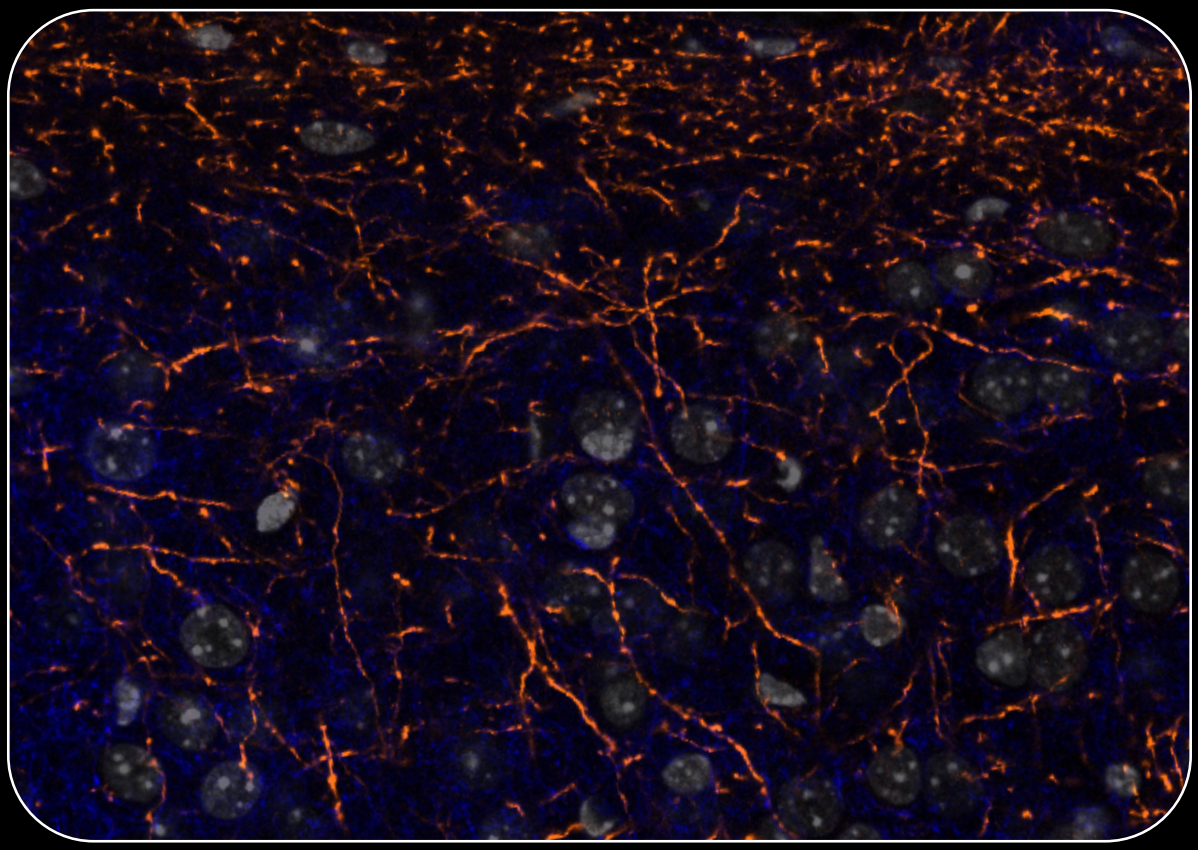

Dissertation presented to obtain the Ph.D degree in Neuroscience

Instituto de Tecnologia Química e Biológica António Xavier | Universidade Nova de Lisboa

Oeiras,
July, 2022

The contribution of cortical feedback projections to sensory representations in the mouse primary visual cortex

Gabriela Tondolo Fioreze

Dissertation presented to obtain the Ph.D degree in Neuroscience

Instituto de Tecnologia Química e Biológica António Xavier | Universidade Nova de Lisboa

Research work coordinated by: Fundação Champalimaud

Oeiras, July, 2022

The contribution of cortical feedback projections to sensory representations in the mouse primary visual cortex

Gabriela Tondolo Fioreze

A Dissertation
Presented to the Faculty
of Universidade Nova de Lisboa
in Candidacy for the Degree
of Doctor of Philosophy

Supervised by: Leopoldo Petreanu
International Neuroscience Doctoral Programme
Champalimaud Research
Lisbon, Portugal

2022

To my family

Acknowledgments

I want to take this opportunity to say some *obrigadas* to everyone who was fundamental to this thesis. The work presented here was only possible because of an extensive number of people. Some contributed to the scientific work presented in this document, and others, as importantly, with motivation and support.

Muito obrigada to:

Leopoldo Petreanu, my supervisor, for welcoming me into his lab. Thank you for sharing your knowledge, love for science and being present in every moment of the way.

All members of the Cortical Circuits Laboratory, for being great lab mates. Thank you: Nico M. (for the vauquitas and good advice), Tiago (for the collaborations and for the extensive time debugging missing triggers), Rodrigo (for the yummy cakes), Bass (for making me think higher and deeper), Julia (for the company during late nights of work), Hedi (for the great sense of humor), Radhika (for making the 2-photon room a nice place to be at nights and weekends and for the encouraging words), Oihane (for exploring unknown dimensions at my dataset and friendship), Margarida (for the most beautiful craniotomies and all the much-needed breaks), Beatriz B. (for her initial implementation of Bpod), Beatriz M. (for the patched cells presented in this thesis), Camille (for valuable comments at the project), Flora and Gonçalo (both new to the lab, but already doing new and exciting experiments). I would like to especially thank Marina Fridman, who contributed immensely to the research presented in this thesis, and, most importantly, for the constant support to cheer and ground me when needed.

My thesis committee, Megan Carey and Zach Mainen, for watching over my progress and for the constant encouraging words.

The graduate office, in particular Tânia, Simone, and Teresa, for their kindness and infinite patience towards bureaucracy.

The CCU community, for making the CCU a fun place to do science. In particular, thank you: Ricardo Gonçalves, Patrícia Francisco, Samantha Herbert, João Marques, Dennis Herrmann, Veronica Corrales, Simone Lackner, Eric DeWitt, Raphael Steinfeld, Lorenza Calcaterra, Jovin Jacobs, Michael Pereira, Matheus Farias and Susana

Lima.

All CCU platforms, for the scientific support and making the experimental work exponentially more enjoyable. The Hardware Platform (for the debugging and explanations), Rodent Platform (for keeping a careful watch over all mice), Histology Platform (for all beautifully processed brains), Molecular Biology Platform (for the viruses and genotyping), and the Glass Wash and Media Preparation (for every last minute PFA).

My Portuguese family, for making Lisbon a home. Thank you for the pure love and the most enjoyable gatherings: Marina Fridman, Marco Demma, Michael Pereira, Thiago Paiva, and Gábor Halmai. Thank you for the best moves on the dance floor and the beautiful friendship: Cristina Ferreira and Ricardo Neto. Thank you for the siblinghood and for making the quarantine fun: to all my flatlings at Rua Maria.

My friends back in Brazil, for making those few days a year special. Thank you Sophia Scomazzon, Thayne Kowalski, Ana Paula Canabarro, Gustavo Stumpf, Lenise Kim, Alan Fleck, Darlan Misussi, Grasiele Sausen and Patrícia Bock.

A minha família, muito obrigada pelo amor incondicional e apoio. Esta tese é uma conquista que dividimos. Obrigada por investirem e acreditarem em mim, por sempre instigarem minha curiosidade e promoverem um ambiente em que questionar é bem-vindo e formar opiniões é algo contínuo. Também que, às vezes, rir é a única solução! Obrigada mãe, pai, vó, mano, Dani, Maria, Isa, tia, tio e Pedro.

Título

A contribuição das projeções de feedback corticais para representações sensoriais no córtex visual primário do ratinho

Resumo

À medida que a informação visual viaja ao longo da hierarquia cortical, nosso cérebro constrói representações do mundo exterior, que por fim guiam comportamento. Áreas da hierarquia cortical comunicam-se por meio de conexões corticais recíprocas. Enquanto o papel de conexões *feedforward* no processamento visual é razoavelmente compreendido, contribuições de conexões de *feedback* são menos claras. A principal fonte de conexões de *feedback* para o córtex visual primário do ratinho (V1) é um conjunto de áreas visuais de ordem superior (HVAs). As HVAs modulam a atividade de V1 e têm sido implicadas na percepção visual e modulações contextuais. No entanto, o impacto das HVAs em V1 tem sido tradicionalmente estudados inibindo sua atividade, tornando esses estudos incapazes de distinguir as contribuições das conexões de *feedback* diretas e das vias indiretas. Este estudo teve como objetivo investigar as contribuições das conexões de *feedback* diretas HVA→V1 nas representações visuais e não visuais de neurônios em V1. Nós simultaneamente inibimos a atividade de conexões de *feedback* diretas oriundas de várias HVAs enquanto registramos a atividade de neurônios em V1 evocada por *drifting gratings*, imagens naturais, filmes naturais e durante escuridão no ratinho acordado e sem comportamento. Descobrimos que a preferência de *tuning* dos neurônios em V1 - por exemplo, preferência em orientação - não depende de conexões de *feedback* diretas HVA→V1. No entanto, o *feedback* córtico-cortical direto inibe seletivamente as respostas para a orientação e direção de movimento preferidas. Além disso, o *tuning* à filmes naturais, mas não à imagens naturais estáticas, era dependente de conexões de *feedback* diretas HVA→V1, sugerindo que as correlações espaço-temporais do estímulo recrutam *feedback* córtico-cortical. Em particular, enquanto no nível de um único neurônio, as curvas de *tuning* para filmes naturais alteram-se ao silenciarmos as conexões de *feedback* diretas HVA→V1, respostas de diferentes neurônios em V1 tornaram-se mais semelhantes através da população. Além disso, nós descobrimos que as conexões de *feedback* diretas HVA→V1 inibem a facilitação induzida pela locomoção de respostas visualmente evocadas. Assim, o *feedback* córtico-cortical direto é um participante crucial no processamento da informação visual em V1 e constitui a base de mecanismos de supressão pelo *surround*, diversificação de representações em V1 e modulações de estado em processamento sensorial.

Abstract

As visual information travels along the cortical hierarchy, our brain builds representations of the outside world, which ultimately guide behavior. Areas in the cortical hierarchy communicate through reciprocal cortical connections. While the role of feedforward connections in visual processing is reasonably understood, the contributions of feedback connections are less clear. The main source of feedback inputs to the mouse's primary visual cortex (V1) is a set of higher-order visual areas (HVAs). HVAs modulate the activity of V1 and have been implicated in visual perception and contextual modulations. Nevertheless, the impact of HVAs in V1 has been traditionally studied by inhibiting their activity, rendering these studies unable to distinguish the contributions of direct cortico-cortical feedback and indirect pathways. This study aimed to investigate the contributions of direct HVA→V1 feedback in shaping visual and non-visual representations of V1 neurons. We simultaneously inhibited the activity of direct feedback inputs from multiple HVAs while recording the activity of V1 neurons elicited by drifting gratings, natural images, natural movies, and during darkness in the awake non-behaving mouse. We found that the tuning preference of V1 neurons - e.g., preferred orientation - is not dependent on direct HVA→V1 feedback inputs. However, direct cortico-cortical feedback selectively inhibits responses to the preferred orientation and direction of motion. Moreover, the tuning of natural movies, but not of static natural images, was dependent on direct HVA→V1 feedback inputs, suggesting the stimulus' spatial-temporal correlations recruit direct cortico-cortical feedback. In particular, whereas at the single neuron level, tuning curves to natural movies changed upon silencing direct HVA→V1 feedback, responses of different V1 neurons became more similar across the population. Furthermore, we found that direct HVA→V1 feedback inhibits the locomotion-induced facilitation of visually-evoked responses. Thus direct cortico-cortical feedback is a crucial player in the processing of visual information in V1 and underlies mechanisms of surround suppression, diversification of V1 representations, and state modulations of sensory processing.

Author Contributions

Author contributions are listed at the beginning of every chapter. Overall, Gabriela Tondolo Fioreze (GF) and Leopoldo Petreanu designed all experiments and analyses described here. GF wrote the thesis.

Financial Support

This research was funded by the Champalimaud Foundation. GF was supported by the Fundação para a Ciência e Tecnologia grant number PD/BD/52449/2013.

Contents

Chapter 1

General introduction

.

Published results

Marques, T., Nguyen, J., **Fioreze, G.**, and Petreanu, L. (2018a). The functional organization of cortical feedback inputs to primary visual cortex. Nature Neuroscience, 21(5):757–764.

Author contributions: Fioreze, G. processed histological tissues, acquired and quantified images, and prepared a figure for the manuscript.

Marques, T., Summers, M. T., **Fioreze, G.**, Fridman, M., Dias, R. F., Feller, M. B., and Petreanu, L. (2018b). A Role for Mouse Primary Visual Cortex in Motion Perception. Current Biology, 28(11):1703–1713.

Author contributions: Fioreze, G. collected all data and assisted in the analysis of the 2-photon imaging experiments in anaesthetised naive mice.

The work presented in this thesis aims to investigate the role of direct cortico-cortical feedback connections in shaping cortical representations. The following sections aim to provide a general understanding of how the brain represents the world through vision and, what are the current theories and evidence pointing to the functional role of cortical feedback on visual processing.

1.1 Vision: forward model vs. inference

The survival of an organism is dependent on its ability to interact with the world. Thus building a representation of the external world is fundamental to one's success. From a simple flash of light to complex representations such as a painting, our brain transforms photons into meaningful visual representations of the external world that ultimately instruct behavior. Mechanisms involving a variety of molecules, cell types, brain areas, time scales, and computations have been at the center of vision research. How does the brain build visual representations?

Visual information travels from the retina to the cortex and is transformed into meaningful visual representations. As the visual information ascends into the cortex, neurons extract relevant features from the visual scene. In the retina, photoreceptors transform photons into electrical signals. Then, visual information travels to the lateral geniculate nucleus of the thalamus (LGN) whose projections direct information to the primary visual cortex (V1) - the first stage of visual processing in the cortex. Alternatively, visual information can also be rooted from the retina to the superior colliculus. The cortex is a hierarchically organized brain structure, and V1 is at the bottom of the cortical visual hierarchy. After V1, the genicular information proceeds to two main routes: the higher-order visual cortical areas (HVA) and the lateral posterior nucleus of the thalamus (LP). In turn, LP sends its inputs to the HVA. Finally, from the HVA, visual information is distributed to other cortical and subcortical areas (Fig.1.1A) (for review, see (Busse, 2018)).

In each processing step, neurons represent more extensive portions of the visual field (Siegle et al., 2021). The region in space where a sensory stimuli can elicit action potentials in sensory neurons is defined as the receptive field (RF) (Sherrington, 1904). The RF structure is composed of ON and OFF subfields. Subfields are classified according to their response to light in the visual system. For instance, positioning a light source over ON subfields results in the neuron spiking. On the other hand, neurons also spike when a light source placed over OFF subfields is turned off (Hubel and Wiesel, 1959, 1962). RFs in the early processing stages are small, representing narrow regions of space. In later processing stages, such as HVA, RFs are larger and

neurons encode more complex features (Siegle et al., 2021). Thus, representations become more complex at each processing stage, rendering a more complete picture of the world.

The RF structure, and the observation that neurons in the cat V1 selectively respond to edges of light (Hubel and Wiesel, 1962), inspired the forward model for vision. In this model, a V1 neuron acquires orientation-selective responses from the proper alignment of the RF's subfields of LGN inputs. For instance, moving a bar of light iso-oriented to the arrangement of ON subfields will simultaneously activate most ON-center LGN cells. Activation of a large number of LGN neurons results in strong excitation of LGN →V1 inputs, generating action potentials. In contrast, a cross-oriented bar would only activate a subset of ON subfields at one time, resulting in weak depolarization and no spikes. Interestingly, the forward model exemplifies how neurons in an area can extract features of the visual scene that are not captured by any individual neurons from which they receive input (for review, see Niell and Scanziani 2021).

A pure forward model of vision can explain visual processing by looking into the visual stimuli exciting the RF. However, information beyond the RF, or a context, can influence the perception of a visual stimulus (for review, see Gilbert and Li 2013). In this case, context can be defined as an animal's behavioral state (e.g., foraging vs. resting), the visual scene surrounding a visual stimulus (e.g., a candle placed in a cake or at a tomb), or information from other sensory modalities (e.g., the crisp sound of a potato chip), among others. Contextual modulations can affect the activity of neurons in all stages of processing. Given their significance, modern theories of vision include contextual modulations in their models, e.g., predictive coding theories (Friston, 2005; Rao and Ballard, 1999). These theories propose that the brain's main function is to build hypotheses, or inferences, about the world. By constantly trying to predict the upcoming sensory stimulus and updating the internal model of the world, the brain reduces the sensory uncertainty, increasing the likelihood of desired outcomes.

How does information not captured by the RF arrive at each processing stage? It is thought that contextual information arrives at the early processing stages from the neurons that project back to the early processing stages from later processing stages. These projections are called feedback projections. Hence, visual processing comprises two streams of information: (1) feedforward stream or bottom-up, which carry sensory input, and (2) feedback stream or top-down, which provide contextual signals (for review, see Gilbert and Li 2013). Thus, animals utilize a range of information beyond the photon's exciting RFs to build visual percepts successfully.

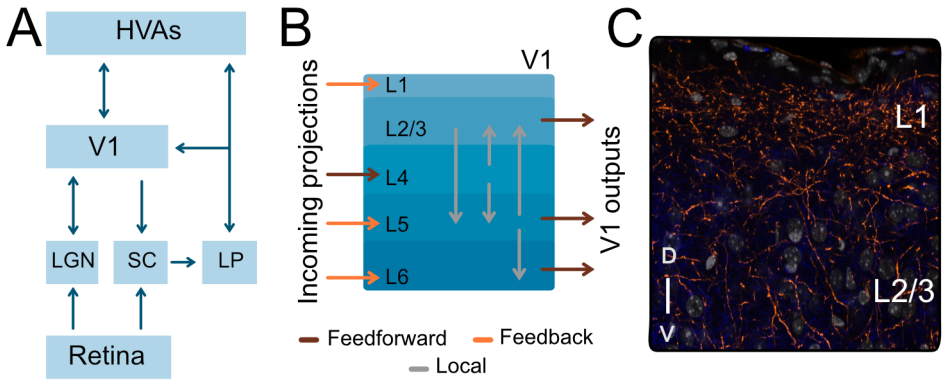

Figure 1.1: Anatomy of the visual system
(A) Diagram of the visual system. Light enters the retina and its transformed by each stage of processing in the visual system. Visual information reach the primary visual cortex (V1) from the lateral geniculate nucleous of the thalamus (LGN) via feedforward connections. From V1, genicular information is sent to the HVA and from there to other cortical and subcortical areas. The HVA also receives inputs from the lateral posterior nucleus of the thalamus (LP), which roots information from the superior colliculus. In turn, HVA and LP send feedback projections to V1. Adapted from (Glickfeld and Olsen, 2017) (B) Schematic of V1 canonical connectivity. Incoming feedforward connections (brown arrow) preferentially target layer 4 (L4) whereas feedback connections (brown orange) innervate layer 1 (L1), 5 (L5) and 6 (L6). Cortical layers also send stereotypical local connections (gray arrows) to each other. The outputs of V1 originate from layers 2/3 (L2/3), L5 and L6. Adapted from (Niell and Scanziani, 2021). (C) HVA →V1 feedback inputs in V1. Example confocal image of V1 top layers showing feedback projections (GCaMP6s, orange) from LM, AL, RL, AM and PM. Cell nuclei are labelled with DAPI (white).

1.2 The neocortex

The neocortex makes up 82% of the average 1.5 kg human brain. In the mouse, the neocortex represents a smaller portion of the brain mass, only 42%. The cortical mass corresponds to about 13 to 28% of all brain neurons in a wide range of species (Herculano-Houzel, 2009). Its late development in evolution suggests the neocortex might be the site for the human's unique cognitive abilities and rich behavior repertoire (Preuss, 2007). A rudimentary neocortex first appeared in reptiles during the Carboniferous Period. Later, about 100 million years, a structure similar to the current neocortex would first appear in small mammals (Rakic, 2009). The ancestral neocortex expanded in size, allowing for larger neurons found in humans. More importantly, it gained convolutions: allowing for more neurons and hence, more connections (Florio and Huttner, 2014).

The neocortex's structure comprises of six cellular layers and envelops the 'primitive brain'. The outer part of the neocortex is made up of gray matter and the inner part of white matter. Gray matter is composed of cell bodies, whereas the white

matter is composed of axonal projections (Florio and Huttner, 2014). The neocortex is a functionally rich structure. The pioneering anatomical studies from Brodmann (1909) resulted in maps of the neocortex whose areas were divided based on their cytoarchitectonic profile. Specific functions were assigned to different cortical areas, comprising of motor planning and execution, sensory processing, and associative functions. Despite over 100 years of extensive research, a clear and detailed description of the neocortex's connectivity and function remains desired.

1.2.1 Cortical cellular architecture

The neocortex is composed of two major classes of cells: neurons and glia. In the cortex, pyramidal neurons are excitatory neurons and represent the majority of neurons (around 80%). Interneurons are inhibitory neurons and constitute the other 20% of cortical neurons (for review, see Harris and Shepherd 2015). Various glia types are found in the cortex, such as astrocites and microglia. In fact, they comprise 50% of all the cells found in the neocortex(Herculano-Houzel, 2009). Glial cells are key players in many cortical functions and developmental stages, such as ion buffering and neurotransmitter turnover (for review, see Florio and Huttner 2014). For the purpose of this thesis, this section will focus on the description of pyramidal and interneurons.

Pyramidal neurons are found across all six layers of the cortex. They have a similar biochemical profile but can vary substantially in morphology. Neurons in each layer can be divided according to their projection target. There are three main classes of cortical neurons. Neurons that project to subcortical structures, also known as pyramidal tract (PT) neurons, are restricted to layer 5 (L5). Neurons that project to the thalamus, or corticothalamic (CT), are confined to layer 6 (L6). Lastly, neurons that project within the cortex, or intratelencelephalic (IT), are found across all six cortical layers (for review, see Harris and Shepherd 2015).

Interneurons are also distributed across all cortical layers. In the mouse, advanced molecular tools allowed for classification according to their genetic profile. There are three major classes of interneurons: parvalbumin-expressing (PV), somatostatin-expressing (SOM), and vasoactive intestinal peptide-expressing (VIP). SOM and PV neurons are spread throughout the six cortical layers, but VIP neurons are confined in the superficial layers. In terms of connectivity, interneurons form local connections. In particular, PV and SOM neurons mostly contact pyramidal neurons. SOM neurons also synapse back to PV neurons, thus being capable of promoting inhibition and disinhibition in the cortex. VIP neurons mostly act as disinhibitors because of their contacts with SOM and PV neurons (Pfeffer et al. 2013, for review, see Harris and Shepherd 2015).

1.3 Cortical hierarchy

The concept of hierarchy is essential for understanding the anatomical and functional organization of the cortex. The pioneering work from Hubel and Wiesel (1962) first showed evidence of a cortical hierarchy. In this study, the RF size of neurons was shown to vary across many cortical areas. Specifically, the RF size of neurons in frontal areas was larger than in posterior areas. Furthermore, their description of the forward model also suggested a hierarchical organization - at least at the feature level (Vezoli et al., 2021). These findings inspired connectivity studies that described the canonical laminar organization of feedforward and feedback connections (Rockland and Pandya 1979, for review, see Vezoli et al. 2021). Next, the hierarchical model proposed by Felleman and Van Essen (1991) cemented the cortical hierarchy in monkeys, which ranked the pairwise relationship between cortical areas based on their laminar origin and termination of projections.

The mouse cortex is also hierarchically organized. As in monkeys, feedforward inputs terminated preferentially in L4 of the target area and feedback inputs in superficial and deep layers. In an anatomical study, Harris et al. (2019) measured the projection distribution of different areas, layers, and cell types in the mouse and assigned a hierarchical score to all visual areas based on their connectivity pattern. For the visual areas, they proposed a hierarchy in which the extremes are LGN (bottom) and the anteromedial area (AM). Such hierarchical structure was further linked to the cortical function in a following study that showed that different functional measures of hierarchical processing, such as response latency and RF size, systematically changed across the visual regions probed (Siegle et al., 2021). Although the hierarchy found in mice is shallower than in monkeys (Harris et al., 2019), the homology in this organization suggests some cortical functions might be conserved between rodents and primates.

1.3.1 Laminar specificity of feedforward and feedback projections

Feedforward and feedback connections have a distinct laminar organization in the cortex (Felleman and Van Essen, 1991; Rockland and Pandya, 1979). Incoming projections arrive in the cortex at superficial, middle, and deep layers (Orange and brown arrows, left side, Fig.1.1B). Most of the feedforward projections terminate in middle layers, primarily in layer 4 (L4). Superficial and deep layers, such as L1, L5, and L6, are primarily targeted by feedback projections (Fig.1.1C) (Felleman and Van Essen, 1991; Harris et al., 2019; Rockland and Pandya, 1979).

Local connections within the cortical layers are also organized in a distinct manner (Gray arrows, Fig.1.1B). L2/3 neurons mainly contact other neurons within L2/3, forming horizontal connections. L2/3 also contacts neurons in L5. Most L4 neurons project to L2/3 and L5. Lastly, L5 neurons mainly project to neurons in L2/3 and L6 (Harris et al. 2019, see pictured in Niell and Scanziani 2021).

The cortex sends its outputs from L2/3, L5, and L6 (Orange and brown arrows, right side, Fig.1.1B). The output of L2/3 compose feedforward projections to other cortical areas. The output of L5 is composed of IT and PT neurons. IT neurons send projections to other cortical areas, making up feedforward and feedback inputs. PT neurons send projections to subcortical areas. Lastly, the output of L6 is composed of CT neurons that project to the thalamus and IT neurons that project to other cortical areas (Harris et al. 2019, for review, see Harris and Shepherd 2015).

1.4 The mouse primary visual cortex

V1 is located in the dorsal part of the posterior cortex, and it can be identified by the robust input from LGN. It is one of the most studied cortical regions, mostly because of its importance to visual perception in humans and monkeys. V1 has been used as a model to understand canonical cortical properties and computations in monkeys (Livingstone, 1998), cats (Hubel and Wiesel, 1962), and, more recently, mice (for review, see Niell and Scanziani 2021). Several neuronal properties differ between the visual system of the mouse and primates or carnivores. At the most basic level, mice have poor visual acuity due to the lack of a fovea (for review, see Niell and Scanziani 2021). However, several anatomical and functional similarities suggest that the core computations implemented by the primary visual cortex are conserved across these species.

One example of a conserved neuronal property of monkeys, cats, and mice is the preference of V1 neurons for edges of light and motion direction (Niell and Stryker, 2008). As described in cats (Hubel and Wiesel, 1962), orientation selectivity arises in V1 neurons of the mouse through the proper alignment of LGN RFs (Lien and Scanziani, 2013). Direction selectivity has also been shown to emerge with similar mechanisms, but it requires the alignment of temporal and spatial dimensions (Lien and Scanziani, 2018). However, although a minority, a more significant number of neurons in the mouse LGN already shows a preference for edges compared to cats and monkeys (Scholl et al., 2013). The arrangement of V1 neurons in mice is also different because of the lack of cortical columns (Hubel and Wiesel, 1959; Mountcastle, 1957). In monkeys, neurons with shared orientation or direction preference are spatially con-

fined into vertically oriented columns. In the mouse, neurons with different orientation preferences are intermingled in a' salt-and-pepper' manner (Ohki et al., 2005). Nevertheless, excitatory neurons with shared tuning properties are more likely to connect to each other (Ko et al., 2011). This connectivity motif is called 'like-to-like' and is thought to enhance certain stimulus features through recurrent processing. Orientation and direction-selectivity in V1 are instructive for behavior, specifically when mice are trained to discriminate between stimuli. For instance, the mouse's ability to discriminate directions of motion of a random dot kinetogram (RDK) is brought to chance levels after pharmacological inactivation of V1 (Marques et al. 2018b, for review, see Niell and Scanziani 2021).

Although artificial visual stimuli, such as drifting gratings and RDK, have propelled the understanding of visual processing in V1, there is a strong argument for using naturalistic stimuli to probe its function (for review, see Kayser et al. 2004). Naturalistic stimuli are closer to ethologically relevant scenes animals encounter in the wild and have temporal and spatial statistics that shape neuronal responses. Behaviorally, subjects require attention to classify classical artificial stimuli, whereas no attention is necessary to classify natural stimuli (Li et al., 2002). Furthermore, artificial stimuli, such as noise or grating stimuli, do not predict well responses to natural scenes (David et al., 2004; Felsen et al., 2005; Sharpee et al., 2006; Yeh et al., 2009), and neuronal populations seem to be selective to either artificial or natural stimuli (Vries et al., 2019). Neuronal responses to natural stimuli are sparse (Deitch et al., 2021; Froudarakis et al., 2014; Marks and Goard, 2021; Xia et al., 2021; Yoshida and Ohki, 2020) and have inspired the sparse coding hypothesis. Sparse coding is part of efficient coding theories that try to explain responses to natural stimuli considering the limited nature of neural resources, such as the number of neurons, spikes per neuron, among others. These theories propose that the visual system efficiently uses those resources to represent a visual scene. In this context, the sparse coding hypothesis proposes that sparse responses to natural stimuli represent the efficient representation of information present in natural scenes. Since a great deal of information at a natural stimulus is redundant, the resources are allocated to represent only the informative parts of the visual scene (Field, 1994).

Natural stimuli are hard to parameterize, and hence few studies have used them to characterize V1 activity, particularly in mice. Thus the knowledge about the processing of natural stimuli is scattered. In mouse V1, higher sparseness in neuronal responses facilitates with the discrimination of two natural movies (Froudarakis et al., 2014). Furthermore, the sparse activity from a few highly responsive neurons in V1 contributes the most to encoding of visual features in natural images. The reliability

of their representations is unaffected by trial-to-trial response variability (Yoshida and Ohki, 2020). Additionally, a series of recent studies continuously measured the activity of mouse V1 neurons for weeks while presenting natural movies to probe their representation longitudinally. One study showed that the tuning of individual V1 neurons to natural movies is less stable than to drifting gratings (Marks and Goard, 2021). Interestingly, the two following studies show that the relationship between the population activity patterns, or manifold, does not change despite changes in the tuning of individual V1 neurons (Deitch et al., 2021; Xia et al., 2021). These stable structures behind the population coding suggest that the representations of natural movies are stable in the long run at the population level. Lastly, such rich processes involved in encoding naturalistic stimuli in the mouse V1 are in part a result of modulations of visual stimulation outside the neuron's RF, as shown in monkeys (Vinje and Gallant, 2000, 2002). Influences from stimuli outside the classical RF on V1 responses have been a strong point in the argument for using naturalistic stimuli. That is, animals in the wild do not encounter isolated visual features in their RF but a full-field visual scene composed of many features.

The population of neurons in mouse V1 encodes a wide range of visual features, from simple to complex and non-visual features, including locomotion, variables related to navigation, arousal, and vestibular signals (see review in Niell and Scanziani 2021). Locomotion, in particular, has a profound impact on the activity of V1 neurons (Niell and Stryker 2010, see review in Busse 2020). These will be better reviewed in the introduction of Chapter 4. Such a broad range of responses suggests that V1 can integrate various kinds of information from different sources to build representations of the sensory environment and drive behaviors. Thus, representations in V1 are likely modulated by signals from other sensory and non-sensory areas. Investigating which areas, signals, and connections impart such modulations is necessary to understand better how neurons in V1 build representations.

1.5 Higher-order visual areas of the mouse

The easy identification of V1 through anatomical properties does not extend to other visual cortical areas. Two higher-order visual cortical areas (HVA) were first identified in the mouse based on transitions in the density of neurons and axons: area 18a and area 18b (Caviness, 1975). Modern methods of tracing and intrinsic signal imaging reviewed at least nine HVA in the mouse: anterior (A); anterolateral (AL); anteromedial (AM); lateralintermediate (LI); lateromedial (LM); posterior (P); posteromedial (PM); postrhinal (POR); rostrolateral (RL) (for review, see Glickfeld

and Olsen 2017). This thesis will use the nomenclature mentioned above for HVA, whose borders were defined by intrinsic signal imaging and confirmed with the Allen Mouse Common Coordinate Framework conventions.

V1 is the primary source of feedforward inputs to the HVA. HVA starts to receive innervation from V1 only after birth, at the first post-natal week (Dong et al., 2004). Feedforward V1→HVA inputs are not exclusive since HVA also receive feedforward inputs from LP (Sherman, 2016). Furthermore, V1 neurons projecting to HVA do not target all HVA homogeneously. The most robust projection from V1 targets LM, and the weakest PM (Wang et al., 2012). Moreover, most HVA-projecting V1 neurons target more than one HVA (about 75%) (Han et al., 2018). The rich functional and anatomical organization of V1→HVA pathways might be due to its late development: since it happens after birth, it might be experience-dependent (Dong et al. 2004, for review, see Glickfeld and Olsen 2017).

The output of HVA target cortical and subcortical regions. The cortical targets comprise extravisual cortical areas, such as the retrosplenial cortex and temporal association cortex. In primates, information is directed through the ventral and dorsal streams. The ventral stream, or the 'what pathway', is involved in object recognition functions. The dorsal stream, or the 'Where pathway', is specialized in spatial processing. In the mouse, areas LM, LI, P, and POR are thought to compose the monkey-analogous ventral stream. The dorsal stream analogous is proposed as areas AL, RL, PM, AM, and A. However, the mouse's dorsal and ventral streams are less clear than in monkeys (for review, see Glickfeld and Olsen 2017).

HVA can be specialized in different functions, such as spatial-temporal encoding. For instance, neurons in PM prefer visual stimuli moving at slow speeds, while neurons in AL and RL prefer fast speeds (Andermann et al., 2011; Marshel et al., 2011; Tohmi et al., 2014), but neurons in LM, AM, and LI prefer medium speeds (Marshel et al., 2011; Tohmi et al., 2014). Such functional specializations of HVA might be inherited from the specific distribution of information to each HVA by V1 neurons. Indeed, Glickfeld et al. (2013) have shown that V1→PM projections preferred visual stimulus moving at slow speed while V1→LM projections preferred medium speed. Thus, specializations of neuronal properties in each HVA hint that some types of information are transmitted in specific streams in the mouse visual system (for review, see Glickfeld and Olsen 2017 and Niell and Scanziani 2021).

Responses from neurons in the mouse HVA can be complex. Neurons along the various HVA have been shown to encode complex visual stimuli, such as natural images and movies (Vries et al., 2019). Other types of rich encoding have also been described in the HVA, such as mixed selectivity. Neurons with mixed selectivity can

code for various parameters, such as stimulus from different sensory modalities. For instance, Olcese et al. (2013) has show that RL neurons can integrate visual and somatosensory signals. Furthermore, neurons in POR respond to visual objects and their spatial location (Furtak et al., 2012). HVA neurons also code for variables relevant to complex behaviors. Funamizu et al. (2016) showed that the activity of PM neurons in mice performing a virtual navigation task likely represents predictions (for review, see Glickfeld and Olsen 2017). The complex signals in HVA neurons pose the question that their feedback projections to V1 might carry vital information to shape the activity of V1 neurons.

1.6 Feedback connections

Feedforward projections to higher-order areas are reciprocal: neurons in higher stages of the cortical hierarchy send descending inputs to lower areas, also known as feedback projections, which carry a variety of rich signals back to lower areas (Felleman and Van Essen, 1991; Rockland and Pandya, 1979). Even though the role of feedforward projections in visual processing is far better understood than feedback projections, anatomical data shows that feedback inputs can be denser than their feedforward counterparts (Van Horn et al., 2000), hinting feedback inputs play a central role in the computation of sensory signals.

Feedback inputs in V1 can be classified into three main categories: cortico-cortical, thalamo-cortical, and neuromodulatory projections. Cortico-cortical feedback originates from other cortical areas, such as HVA, whereas thalamo-cortical feedback from LP. These projections are mainly excitatory and, in V1, connect to pyramidal neurons and interneurons. In primates, cortico-cortical feedback preferentially innervates L1 and L5, while thalamo-cortical feedback is confined to L1. In rodent V1, cortico-cortical and thalamo-cortical feedback innervate L1, L5, and L6. The third type of feedback is neuromodulatory, such as cholinergic, noradrenergic, and serotoninergic inputs from the basal forebrain, locus coeruleus, and raphe nuclei, respectively. Feedback projections of neuromodulators target all V1 layers in primates and rodents (for review, see Pennartz et al. 2019). Due to the experimental work presented in this thesis, this introduction will focus on cortico-cortical and thalamo-cortical feedback projections.

How do feedback projections act upon neurons in V1? Feedback inputs are part of about 90% of L1 synapses, contacting interneurons and distal tuft dendrites of pyramidal neurons. One described mechanism through which feedback inputs control the firing of L5 pyramidal neurons is the *backpropagation-activated Ca2+ spike firing.*

The input of feedback to the tuft dendrites results in calcium action potentials in dendrites that, in turn, produce depolarization along the axon which generates a burst of axonal spikes (for review, see Larkum 2013). In fact, dendritic calcium spikes can produce more axonal spikes than inputs in the pyramidal neuron's somata (Larkum et al., 2004). In this way, feedback inputs can steer the firing of V1 neurons. Nonetheless, the complex connectivity between feedback inputs and the various components of L1 and L5 indicates that other mechanisms may underlie feedback modulations of downstream V1 neurons.

1.6.1 Cortico-thalamo-cortical pathway

Cortico-cortical and thalamo-cortical feedback are part of an intricate innervation pattern between V1, HVA, and LP. Excitatory neurons in the thalamus project to many brain areas and their projections can be classified into two classes: *drivers* or *modulators* (Halassa and Sherman, 2019). Projections from the type *driver* compose the first-order thalamic nuclei, such as LGN. Their synapses can strongly modify the physiology of the neuron they contact, e.g. by producing large excitatory postsynaptic potentials. Moreover, *drivers* receive their driving inputs from the periphery, such as the retina. Projections from the type *modulators* compose the second-order thalamic nuclei, such as LP. They form weaker contacts that have mild effects on the postsynaptic neuron. The driving input of *modulators* originate in the cortex (for review, see Halassa and Sherman 2019; Murray Sherman and Guillery 2011; Sherman 2016). In the case of LP, the driving input originates from axonal branches of cortical L5 neurons projecting to subcortical structures (Bourassa and Deschenes, 1995). In turn, LP drives HVA through feedforward projections reaching L4 neurons. LP also roots feedback projections to superficial and deep layers of V1. Therefore, LP acts as a hub connecting V1 and HVA: it can influence the activity of V1 neurons directly through direct thalamo-cortical feedback projections or indirectly by driving HVA, which then send cortico-cortical projections back to V1 (for review, see Pennartz et al. 2019).

Silencing LP affects the activity of neurons in the visual cortex. For instance, pharmacological inactivation of the cat LP changed responses in V1 and HVA (De Souza et al., 2020). In mice, evidence suggests that LP projections shape the tuning properties of neurons in the HVA. Tohmi et al. (2014) found that the tuning preference to the stimulus speed of neurons in the HVA did not change after aspiration of V1. However, lesions in the superior colliculus altered the preferred velocity of neurons in the HVA. Because the HVA connect to the superior colliculus through LP, some tuning properties of HVA neuronal responses must be inherited from LP. Thus, this observation

suggests that HVA→V1 feedback inputs can potentially carry signals transmitted by feedforward inputs from LP→HVA.

Although thalamo-cortical feedback seems to be a key modulator of V1 activity (De Souza et al., 2020) and to have a distinct role compared to cortico-cortical feedback in cortical processing Sherman 2016, isolating the effects of these feedback pathways in the activity of V1 neurons is experimentally challenging. Many studies have resorted to inactivating HVA. However, by doing so, both cortico-cortical and thalamo-cortical feedback inputs are manipulated, and effects can not be explicitly assigned to either of these projections. Thus, further studies that carefully control the manipulation of each of these pathways are necessary to pinpoint which signals are conveyed and how they influence the computation of V1 neurons.

1.6.2 Sources of feedback input to the mouse V1

A wide range of brain areas sends feedback projections to V1. In the mouse, two studies measured the sources of feedback to V1 using advanced molecular and imaging tools coupled with robust systems for automated quantification of cell bodies and axons. In particular, they measured whether a brain area is a source of feedback projections to V1 and estimated how much it contributes to the total amount of feedback innervation in V1.

Leinweber et al. (2017) used a transsynaptic rabies tracing strategy to quantify the density of presynaptic neurons across different areas in the mouse brain that send projections to V1. This strategy is based on the capacity of rabies viruses to jump a synapse and travel retrogradely in a neuron. Specifically, this study combined a co-injection of an adeno-associated (AAV) virus into V1, coding for rabies' G protein and the TVA receptor, and an EnvA-coated rabies virus. They found presynaptic neurons labeled in many cortical and subcortical areas. Surprisingly, this study found that 14% of presynaptic labeled neurons were in the retrosplenial cortex, crowning it as the single area that contributes the most feedback to V1. However, all the HVA combined represented 20% of presynaptic labeled neurons and hence, together, represent the primary source of feedback to V1.

In a similar experiment, Morimoto et al. (2021) injected cholera toxin subunit B (CTB) in the mouse V1 and quantified the density of presynaptic neurons across the mouse brain. CTB enters axon terminals and travels retrogradely, labeling neuronal cell bodies. They found over 50% of presynaptic labeled neurons in the combined HVA. The area LM was the single area with the most contribution to feedback innervation in V1. Interestingly, the distribution of HVA →V1 inputs was not uniform across V1: medial HVA preferentially targeted medial V1, whereas lateral HVA mainly targeted

lateral V1. The bias in feedback coverage suggests that different portions of the visual field are summoned during visual processing according to ethological demands.

The extensive contribution of HVA to feedback innervation in V1 hints that these cortico-cortical connections might have a central role in the computations performed by V1 neurons. Nevertheless, their contribution to visual and non-visual processing information in V1 is poorly understood.

1.6.3 Fine organization of HVA feedback inputs in V1

A few studies have investigated the anatomical and functional organizational rules of HVA feedback inputs in V1. Knowledge of such rules helps constrain models of feedback function, leading to better predictions for their computational role in complex brain functions. For instance, anatomical evidence shows that HVA inputs terminate at specific and confined areas within the superficial and deep layers of V1 in monkeys (Federer et al., 2021) and mice (Ji et al., 2015). Hence, feedback projections in V1 do not contact all regions in these layers equally. In monkeys, neurons in V1 send parallel information streams to V2 through feedforward projections. Thus, a 'patchy' feedback organization has an evident functional prediction: feedback inputs target functionally specific domains in V1 and maintain stream specificity like feedforward pathways. In mice, feedback inputs from AL and PM form interleaved patches in L1. Whereas AL feedback patches are found in V1 regions with a high concentration of acetylcholine receptors, PM patches matched regions with a low concentration of these receptors. Interestingly, neurons in these V1 regions were shown to encode distinct spatial-temporal features (Ji et al., 2015). This observation hints at a modular organization of feedback projections in the mouse V1 since the encoding of distinct spatial-temporal features is also segregated in their reciprocal V1→AL and V1→PM feedforward inputs (Glickfeld et al., 2013).

Neurons in V1 and HVA form loops with cellular and laminar specificity. Young et al. (2021) mapped the connection strength of ascending and cortico-cortical descending inputs to V1 neurons. In particular, this study separated effects on V1 neurons that send reciprocal projections to the source of those inputs (looped neurons) or not (non-looped). This study found that the strength of feedforward and HVA feedback innervation was larger to looped infragranular IT neurons than to looped neurons projecting to subcortical areas. Loops between neurons in V1 and HVA could be the circuit basis of selective recurrent interactions illustrated in many models of cortical function. Interestingly, the selectivity of HVA feedback inputs for apical dendrites of looped infragranular neurons was stronger than for perisomatic dendrites, suggesting apical dendrites might be involved in recurrent computations.

HVA→V1 inputs are functionally specific. Using calcium imaging, Marques et al. (2018a) showed that LM→V1 feedback inputs target, on average, regions in V1 representing the same visual field location as V1 neurons. Notably, a significant fraction of LM→V1 feedback inputs responded to portions of space distant from the RF center of V1 neurons, demonstrating that feedback inputs carry distal visual information to V1 neurons. This observation is crucial since feedback from HVA has been implicated in modulations of V1 activity by visual information outside their RF (Keller et al., 2020b; Nassi et al., 2013; Nurminen et al., 2018; Vangeneugden et al., 2019). Furthermore, LM→V1 feedback inputs were shown to convey information about the orientation and direction of the stimulus to V1.

In summary, various brain areas send feedback projections to V1, yet HVA are, collectively, the primary source of feedback inputs to V1. Most cortico-cortical projections are excitatory and terminate in L1, L5, and L6. In these layers, they modulate the activity of V1 neurons by contacting interneurons, pyramidal neurons, and their apical dendrites. Recent studies have proposed that HVA→V1 inputs are organized in parallel streams, form loops, and are functionally specific. Although recent advances have helped clarify the organizational rules and signals encoded by HVA→V1 projections, there is little causal evidence on whether and how cortico-cortical feedback inputs influence the visual and non-visual representations built by V1 neurons.

1.7 Theories of cortico-cortical feedback function

Feedback projections have been proposed to be key players in some general theories of neural processing and cortical function. A basic intuition of these theories will be provided in this section.

1.7.1 Predictive coding

The core computation of the brain in predictive coding is to make inferences about the world (Friston, 2005; Rao and Ballard, 1999). In this framework, the brain builds a model of the external world. As animals experience the world, their brain constantly updates such model by comparing the current sensory stimulus with the prediction internally generated. Thus, for the upcoming sensory stimulus, better predictions will be generated and outcomes less uncertain (for review, see Keller and Mrsic-Flogel 2018).

Feedback connections are thought to carry predictions in the predictive processing theories. Cortico-cortical projections specifically communicate predictions encoded by their source areas to V1 neurons. Indeed, evidence suggests feedback projections from

ACC carry motor predictions of optic flow to the mouse V1 (Leinweber et al., 2017). The fact that HVA receive inputs from many parts of the brain and the code for a wide variety of signals reinforces a putative role in predictive processing.

HVA feedback has yet to be formally investigated in the predictive coding framework. One attractive hypothesis is that V1 neurons could use contextual signals to update their responses to a given visual stimulus. Some types of contextual modulations have already been shown to be dependent on signals from HVA (Keller et al., 2020b; Kirchberger et al., 2021; Nassi et al., 2013; Vangeneugden et al., 2019) and their direct feedback inputs in V1 (Nurminen et al., 2018). Theoretically, HVA cortico-cortical inputs in V1 were proposed to carry predictions about the lower-level representations in a neural network similar to the cortical hierarchy (Rao and Ballard, 1999).

1.7.2 Reinforcement learning

The constantly changing daily life situations require animals to have flexible and adaptive behaviors, the creation and expression of which requires cortical plasticity. How does one experience modify specific synapses in the brain? In reinforcement learning theories, the simultaneous firing of two connected neurons can change synaptic weights depending on action outcomes (for review, see Roelfsema and Holtmaat 2018).

Cortico-cortical feedback inputs have been proposed to act as 'taggers' in this framework. For instance, if the outcome of an action is more positive than expected, cortico-cortical feedback tags the synapses responsive to such outcome. These are later potentiated by neuromodulators, increasing the probability of the positive outcome to happen again in future actions. On the other hand, synapses are weakened if outcomes are worst than expected (for review, see Roelfsema and Holtmaat 2018).

A small body of evidence supports the participation of HVA $\rightarrow$V1 inputs gating cortical plasticity. In the monkey V1, feedback inputs activate N-methyl-D-aspartate (NMDA) receptors, increasing the representation of behaviorally relevant stimuli (Self et al., 2012). In mice, stimulus selectivity of V1 neurons is enhanced by NMDAR-dependent calcium events (Smith et al., 2013). Nonetheless, further studies are needed to formally test the role of cortico-cortical feedback inputs in reinforcement learning.

1.7.3 Error backpropagation

The architecture of deep neural networks has a remarkable similarity with that of the visual cortex's canonical hierarchical organization. In fact, these models are widely used for tasks involving 'visual processing', like image classification (for review, see Ricci and Serre 2020). However, tuning a large number of parameters is a challenging

task. One of the most popular methods used to adjust weights during training is error backpropagation algorithms. These algorithms present labeled data to minimize the classification error on the training data (for review, see Kreiman and Serre 2020).

Feedback inputs carry teaching signals in error backpropagation algorithms. Acting in many layers of the network, error signals are transmitted by feedback inputs to modify synaptic weights of bottom-up, feedforward inputs. In particular, feedback inputs target apical dendrites of lower-level neurons (Lillicrap et al., 2016).

The 'credit assignment problem' is one of the big constraints for the implementation of backpropagation in organic systems. During learning, neurons are assigned credit for their contribution to the outcome. Assigning credit correctly in a hierarchical neural network is hard because of its size, the complexity of signals, and integration of credit signals with other inputs. In sum, the credit assignment problem arises from the difficulty of synaptic plasticity mechanisms to find the correct synapses to target.

Segregation of inputs to separated dendritic compartments has been proposed to solve the 'credit assignment problem'. For instance, feedforward signals would only target basal dendrites, whereas feedback signals would target the apical dendrites (for review, see Richards and Lillicrap 2019). Evidence supporting backpropagation models has been shown in the mouse. Young et al. (2021) have shown that apical dendrites are selectively innervated by cortico-cortical feedback.

1.8 Functional correlates of HVA feedback in V1

Activity from HVA modulates responses of V1 neurons. The most basic form of modulation that top-down signals from HVA can exert is at the magnitude of the V1 neuron's firing rate. The pioneering study from Sandell and Schiller (1982) showed that most of the recorded neurons in area 17 of the anesthetized squirrel monkey became unresponsive to visual stimulation after cooling of area 18, a homolog of V2. Such excitatory effect of top-down signals from HVA in V1 was also observed when area 18, area 21a (V4) or postero-temporal visual (PTV) cortex was silenced in the anaesthetised cat (Bardy et al., 2006, 2009; Huang et al., 2007, 2004; Mignard and Malpeli, 1991; Wang et al., 2010, 2000). In monkeys, the effects of top-down silencing were more diverse. For instance, cooling of the middle-temporal area (MT) (Hupe et al., 1998; Hupé et al., 2001) reduced the visually-evoked activity of V1 neurons, but pharmacological inhibition of V2 did not have a consistent effect on the firing rate of V1 neurons (Bullier et al., 1996). However, cooling V2 and V3 increased V1 activity (Nassi et al., 2013). Conflicting results were also found in the mouse: pharmacological inhibition of PPC (which likely includes A, AM, and RL) led to

an increase of visually-evoked activity in V1 (Hishida et al., 2019), but optogenetic inhibition of AL or PM resulted in an overall decrease of V1 responses (Oude Lohuis et al., 2021). Furthermore, there is evidence that direct feedback inputs promote the changes in the firing rate of V1 neurons to V1 (Nurminen et al., 2018). Thus, it remains unclear whether the net effect of HVA top-down signals over V1 is excitatory or inhibitory. The large variability in effects can be assigned to the vast experimental differences between studies, such as species, inactivation method, visual area silenced, visual stimuli presented, number of recorded neurons, and animal state.

What is the functional relevance of HVA modulations of V1 activity? Top-down signals from HVA has been related to many functions. In this section, I review the evidence for the main known functions of HVA feedback in V1. Evidence for functional correlates mainly originates from physiological recordings and studies that silenced HVA. For the purpose of this thesis, it is essential to note that inhibiting the activity of HVA perturbs modulations of direct cortico-cortical feedback inputs in V1 and feedback from areas that receive inputs from HVA, such as LP and frontal cortical areas. So far, only one study has explicitly silenced direct HVA inputs in V1 and could assign effects specifically to those projections (Nurminen et al., 2018). It remains largely unknown through which circuit top-down signals from HVA exert their modulations in the mouse V1.

1.8.1 Visual perception

HVA are a key element in the neuronal circuits underlying visual perception. Percepts are thought to arise from visual information processing at the cortical hierarchy and instruct behavior according to the animal's demands. In the mouse, top-down signals from HVA were shown to be necessary for the performance of three different visual perceptual tasks (Jin and Glickfeld, 2020). After optogenetic inhibition of areas LM and AL, animals needed larger deviations in orientation, or contrast, to correctly report the visual stimulus in a Go/No-Go orientation discrimination task or a Go/No-Go contrast detection task. Surprisingly, silencing area PM did not impair performance in reporting visual features. Instead, it increased incorrect reports, suggesting PM signals contribute to the processing of 'high-level' information, such as decision variables. Hence, HVA inputs in V1 could mediate behavioral effects through modulation of features encoded by V1 neurons.

A few studies have demonstrated that HVA modulate the tuning properties of V1 neurons. In fact, the first study that measured the effects of cooling area 18 in the visually-evoked activity of V1 neurons reported two neurons that increased responses to the preferred and null direction of motion elicited by moving bars (Sandell and

Schiller, 1982). Nevertheless, V1 neurons kept their motion preference, i.e., their preferred direction. Similarly, cooling V2 and V3 in the rhesus monkey did not change the tuning preference of V1 neurons. However, orientation-selective neurons selectively increased their response to orientations orthogonal to the preferred (Nassi et al., 2013). In the cat, the tuning preference of V1 neurons was unchanged after cooling area 21a or PVT. However, some neurons sharpened their tuning curves, while others broadened (Huang et al., 2007; Wang et al., 2000). In another study, the silencing of area 21a flattened orientation tuning curves (Wang et al., 2007).

Manipulating HVA has diverse effects on the tuning properties of neurons in the mouse V1. Optogenetic silencing of LM resulted in the selective reduction of responses to the preferred orientation in L2/3 pyramidal neurons (Pafundo et al., 2016). A similar reduction in responses to specific spatial frequencies was also observed when optogenetic inactivating AL→V1 or PM→V1 projecting neurons (Huh et al., 2018). Interestingly, neurons in V1 responded less to spatial frequencies that matched the preferred spatial frequency of the feedback source. In another study, optogenetic inhibition of AL or PM caused neurons in V1 to reduce their responses to bars moving at non-preferred motions (Oude Lohuis et al., 2021). However, after a cortical incision between PPC (likely A, AM and RL) and the visual cortex, neurons in V1 increased their responses indiscriminantly to all presented motion directions (Hishida et al., 2019). Hence, while some studies suggest feedback increases orientation-selectivity (Hishida et al., 2019; Pafundo et al., 2016) others suggest the opposite (Oude Lohuis et al., 2021).

Representation of complex visual information by V1 neurons is also dependent on HVA top-down signals. A recent study investigated the perception of Kanizsa illusory contours in the mouse (Pak et al., 2020). Kanizsa illusory contours do not stimulate neurons' RF in the early visual cortex, yet they evoke responses in neurons in these areas. Consequently, the perception of that stimuli is thought to arise from recurrent processing. In this study, Kanizsa square drives responses in V1 neurons, and mice learn to discriminate between Kanizsa-type illusory bars of different orientations. Optogenetic silencing of LM reduced the responses evoked by the Kanizsa square, suggesting LM top-down signals mediate illusory contour perception in mice.

1.8.2 Contextual modulations

Perception of a visual stimulus and the underlying neuronal activity depend not only on the visual information in the RF but also on visual features surrounding the stimulus and behavioral variables associated with the moment. For instance, a light beam projecting the filled contour of a bat into the night skies sparks a specific percept

- especially during a bank robbery. As beautifully put by Schwartz et al. (2007): 'No sensory stimulus is an island unto itself'. In the visual system, context can be defined as the visual scene surrounding a particular visual stimulus. Hence, perception of a visual stimulus can depend on the spatial and temporal components in which a stimulus is embedded.

The most studied form of contextual modulation is surround suppression. In the case of V1, neurons have a stimulus size that best drive their activity, which covers most of their RF. As visual stimuli expand outside their RF, i.e., a larger stimulus, responses decrease. The decrease in activity caused by surround stimulation is called surround suppression. Because of their large RF and fast conductance, feedback from HVA were proposed to mediate this phenomenon (Angelucci et al., 2017). Also, feedback projections were shown to convey distal information to V1 neurons (Marques et al., 2018a). Indeed, in the rhesus monkey, cooling areas V2 and V3 reduced surround suppression of V1 neurons. This was observed by the increase in response magnitude to larger patches of drifting gratings. Furthermore, evidence suggests that, in primates, V2's effects on surround suppression of V1 neurons occur via direct feedback projections. Nurminen et al. (2018) optogenetically silenced V2→V1 inputs in the marmoset while measuring the activity of V1 neurons elicited by expanding grating patches. Silencing cortico-cortical terminals increased the response of V1 neurons to large stimuli, reducing surround suppression. In the mouse, optogenetic inhibition of lateral HVA (mainly LM) also increased the response of V1 neurons to large stimuli (Keller et al., 2020b; Vangeneugden et al., 2019). However, it is still unknown if the circuitry through which HVA modulate surround suppression is conserved in primates and rodents.

Not every surround modulation causes suppression of V1 activity. Stimulation of the surround has been shown to induce responses of V1 neurons when no visual stimulus is present in the RF. In the mouse, this response was dependent on HVA. Specifically, L2/3 neurons decreased their responses to the stimulation of the surround alone when multiple HVA were simultaneously inhibited with optogenetics. The same effect was observed when animals were in an anaesthetized state, in which top-down signals are thought to be suppressed (Keller et al., 2020a). Responses elicited solely by the surround were proposed to underlie perceptual competition.

Another form of contextual modulation is figure-ground segregation. This phenomenon allows objects to 'pop-out', leading their perception to be segregated from their background. Figures elicit a strong and fast response followed by late background suppression (Kirchberger et al., 2021; Poort et al., 2016). Hence, during the later phase of the neuronal response, figures evoked more robust responses than back-

grounds, a phenomenon known as figure-ground modulation. Extracellular recordings in primates show that figure-ground segregation correlates with excitatory activity in superficial and deeper layers of V1 (Self et al., 2013), suggesting a contribution of feedback projections. This hypothesis was tested in a recent study which showed that HVA are the source of figure-ground modulation of V1 neurons. In this study, mice were presented with a visual stimulus composed of a patch of oriented gratings (figure) surrounded by gratings in a different orientation (background). Upon simultaneous optogenetic inhibition of multiple HVA (PM, AM, A, LM, RL, and AL), neurons in the mouse V1 responded less to the figure at the late phase of the response, reducing figure-ground modulation. Behaviorally, inhibition of activity during the late phase of V1 resulted in worst performances at reporting figure locations in the background (Kirchberger et al., 2021).

Finally, contextual modulations are diverse, and for some types, there is evidence that top-down signals from HVA mediate them. Some modulations are dependent on the features covering the RF and surround, such as orientation. For instance, an iso-oriented stimulus (RF and surround) elicits a more significant surround suppression than a stimulus in which the surround is composed of gratings with orientation orthogonal to the RF (Keller et al., 2020a). Since a big part of feedback projections from HVA are tuned to orientation (Marques et al., 2018a), and most feedback from LP to V1 is orientation untuned (Roth et al., 2016), direct cortico-cortical inputs from HVA could be the major anatomical subtract for contextual modulations (Pennartz et al., 2019).

1.9 Cortico-cortical feedback projections and the representations of V1 neurons

The current best computational models can execute visual tasks using a pure feedforward architecture, such as image classification. In biological systems, recent theories have proposed that signals beyond the visual information within the RF can influence visual processing (Keller and Mrsic-Flogel, 2018; Rao and Ballard, 1999). These signals are thought to modulate visual information since the early stages of visual processing and are thought to be conveyed by feedback connections (Schwartz et al., 2007). Feedback connections originate in higher areas of the cortical hierarchy and project back to areas in lower stages. Even though they are more abundant than feedforward projections (Van Horn et al., 2000), little is known about the role of feedback projections in visual processing.

Feedback inputs from HVA to V1 are, collectively, the main source of feedback connections to V1 (Leinweber et al., 2017; Morimoto et al., 2021). Hence HVA→V1 inputs are a good candidate for understanding whether and how cortico-cortical feedback projections modulate representations in V1 neurons. Furthermore, many studies have related top-down signals from HVA to modulations of V1 neurons, such as in their tuning properties (Hishida et al., 2019; Huh et al., 2018; Oude Lohuis et al., 2021; Pafundo et al., 2016), surround suppression (Keller et al., 2020b; Nassi et al., 2013; Vangeneugden et al., 2019), surround facilitation (Keller et al., 2020b) and figure-ground modulations (Kirchberger et al., 2021). However, it is still an open question if HVA modulates neurons in V1 through direct cortico-cortical projections or indirectly, e.g., via thalamo-cortical projections.

This thesis aimed to broaden our understanding of the role of direct HVA→V1 feedback inputs in shaping the visual and non-visual representations of V1 neurons. Experiments presented in the following chapters took advantage of the mouse as a model system, utilizing genetic and molecular tools to specifically label and inhibit HVA→V1 feedback inputs while simultaneously recording the activity of a large number of L2/3 V1 neurons in the awake mouse. For extra insights, a comprehensive batch of visual stimuli was presented to the animal. State modulations of V1 activity were also examined by recording the mouse's running speed.

- In **Chapter 2**, I described the experimental strategy to measure the effects in V1 of silencing HVA→V1 feedback inputs.
- In **Chapter 3**, I described how HVA→V1 feedback inputs influence the tuning properties of V1 neurons to drifting gratings, natural images, and natural movies.
- In **Chapter 4**, I described how HVA→V1 feedback inputs influence state modulations of V1 neurons in the dark and during visual stimulation.
- In **Chapter 5**, I discussed the implications of our experimental strategy and main findings..

Chapter 2

A chemogenetic approach to selectively silence direct HVA $\rightarrow$V1 feedback terminals

2.1 Author Contribution

GF performed all *in vivo* imaging experiments unless noted and analysis described in the text. Margarida Baeta performed surgeries for axonal imaging experiments, and Beatriz Moura performed all the experiments and analyses for *ex vivo* experiments. Marina Fridman assisted in axonal imaging, initial analysis codes, and her expertise in data analysis.

2.2 Introduction

Uncovering the neuronal populations responsible for specific computations, behaviors, and cognitive processes has been one of the big challenges in neuroscience. Patients with brain injury and lesion experiments provided the first functional insights, such as the case study of Phineas Gage that led to the association of frontal lobes with personality, emotions, and social interaction (Filho, 2020). Nonetheless, the development of methods to reversibly perturb neuronal activity significantly drove major scientific leaps. These methods include cooling, pharmacological agents, optogenetics, and chemogenetics. Cooling and pharmacological agents were pioneers in studies that assessed the effects of suppression of HVAs in V1 neurons in monkeys and cats (Bardy et al., 2006, 2009; Bullier et al., 1996; Huang et al., 2007, 2004; Hupe et al., 1998; Hupé et al., 2001; Mignard and Malpeli, 1991; Nassi et al., 2013;

Sandell and Schiller, 1982; Wang et al., 2010, 2000) yet they are not precise and specific. Recent studies have used more versatile techniques, such as optogenetics and chemogenetics (Keller et al., 2020a,a; Kirchberger et al., 2021; Nurminen et al., 2018; Oude Lohuis et al., 2021; Pafundo et al., 2016; Pak et al., 2020; Vangeneugden et al., 2019). These techniques allow manipulation of neuronal activity of genetically defined neuronal populations, and subcellular compartments, with high temporal and spatial precision (Wiegert et al., 2017).

Chemogenetics is a method by which proteins are engineered to bind to new chemical actuators (see reviewed in Roth 2016). The most widely used are Designed Receptors Exclusively Activated by Designer Drugs (DREADDs) (Armbruster et al., 2007; Armbruster and Roth, 2005). DREADDs are modified G protein-coupled receptors (GPCRs) that can facilitate or suppress neuronal activity upon activation by a biologically inert agonist. One type of inhibitory DREADD is the mutant human M4 muscarinic receptor (hM4D(Gi)), which engages in G_i signaling cascade upon activation by clozapine- N-oxide (CNO). After CNO activation, neuronal activity is inhibited via two mechanisms: (1) hyperpolarization via activation of G protein inwardly rectifying potassium channels (GIRKs) (Armbruster et al., 2007) and (2) inhibition of presynaptic release of neurotransmitters (Stachniak et al. 2014, see reviewed in Roth 2016).

One key feature of hM4D(Gi) is its effects on the release of neurotransmitters at axon terminals because a local injection of CNO enables suppression of activity in neuronal projections. Terminal hM4D(Gi)-mediated silencing was first described by Stachniak et al. (2014) and Mahler et al. (2014) in *ex vivo* brain slices. In the first study, CNO perfusion decreased presynaptic release probability in pairs of synaptically connected neurons, whose presynaptic neurons were injected with a current and expressed hM4D(Gi). Similarly, Mahler et al. (2014) found that adding CNO to the bath caused a lower frequency of spontaneous postsynaptic events in ventral tegmental area (VTA) neurons of rats in which ventral pallidum→VTA projections expressed hM4D(Gi). A series of recent studies (Doron et al., 2020; Takahashi et al., 2020, 2021) have provided additional evidence that hM4D(Gi) can suppress activity in neuronal projections. They have shown that CNO causes a reduction in the light-evoked excitatory postsynaptic currents in mouse brain slices which had projections co-expressing hM4D(Gi) and channelrhodopsin-2 (ChR2). Finally, in all of the studies mentioned above, changes in animal behavior after local injection of CNO suggested that hM4D(Gi)-expressing projections were also silenced *in vivo*. Nevertheless, a direct measurement of terminal silencing by hM4D(Gi) *in vivo* has never been done because recording activity in terminals is technically challenging.

On the other hand, a disadvantage of suppressing neuronal activity with hM4D(Gi) is its low temporal resolution - the effects range from minutes to hours. Consequently, many studies have used optogenetics instead, which offers millisecond precision control of neuronal activity (Nurminen et al., 2018; Zhang et al., 2014). However, there are concerns regarding its usage for both excitation and inhibition of neuronal projections. First, excitation of ChR2-expressing terminals with light may generate antidromic spikes (Grossman et al., 2013; Sato et al., 2014), and the effects attributed to those projections might be due to activation of neuronal projections elsewhere. Second, evidence that opsins can inhibit projections is controversial. For instance, it has been reported that the inhibitory opsin archaerhodopsin (eArch3.0) increases spontaneous neurotransmission (Mahn et al., 2016). Also, chloride pumps, such as halorhodopsin (eNpHr3.0), might alter the chloride gradient after prolonged inhibition, potentially altering the membrane excitability (Raimondo et al., 2012). Two recently engineered opsins were shown to silence terminals of long-range projections in the mouse brain: targeting-enhanced mosquito homolog of the vertebrate encephalopsin (eOPN3) (Mahn et al., 2021) and parapinopsin (PPO) (Copits et al., 2021). eOPN3 is a mosquito-derived rhodopsin that can inhibit action potentials for minutes when exposed to blue light. PPO is a photoswitchable opsin found at the lamprey pineal gland that can be activated or turned o by UV/blue light or amber light, respectively. Both eOPN3 and PPO are coupled to $G_{i/o}$ signaling cascades and suppress synaptic transmission when in an active state.

Finally, this thesis's central question is to understand the contributions of direct HVA→V1 feedback projections to V1 representations. We approached this question by inhibiting terminals in V1, originating from multiple feedback sources, with hM4D(Gi) and local CNO injections while recording V1 neuronal activity in the awake mouse. In this chapter, we establish our experimental strategy to measure modulations of direct HVA→V1 feedback in V1 representations. We validated our strategy by showing: (1) specific label of multiple HVAs with hM4D(Gi), (2) evidence for hM4D(Gi)-mediated silencing of LM→V1 projections in *ex vivo* brain slices, and (3) evidence for hM4D(Gi)-mediated silencing of LM→V1 projections *in vivo*. Additionally, we show evidence for hM4D(Gi)-mediated facilitation of activity in neuronal somata *in vivo* after systemic injection of CNO.

2.3 Results

2.3.1 Protocol to measure contributions of direct HVA→V1 feedback projections to V1 representations

We developed a protocol to measure the contributions of direct HVA→V1 feedback projections to V1 representations. This protocol aimed to acquire a comprehensive dataset that allows the comparison of responses of a large population of V1 neurons to a broad set of visual stimuli with or without the influence of direct HVA→V1 feedback projections. To simultaneously silence direct HVA→V1 feedback projections and measure responses of V1 neurons, transgenic mice expressing GCaMP6s in the cortex and hM4D(Gi) in the HVAs, namely LM, AL, RL, AM, PM, underwent two consecutive days of 2-photon calcium imaging. This experimental group will be mentioned as hM4D(Gi)-FB (Fig.2.1A, left). On the first day, mice were injected in V1 with aCSF immediately before the imaging session (Baseline, Fig.2.1A, left). The next day, mice were injected in V1 with a CNO solution leading to HVA hM4D(Gi)-expressing axons to be silenced (CNO, Fig.2.1A, left). Another experimental group was composed of mice with no expression of hM4D(Gi) and underwent similar procedures to control for mechanical damage of axons and off-target effects of CNO (Ctrl,Fig.2.1A, right). After brain injections, mice were head-fixed under a 2-photon microscope, and a batch of different visual stimuli was shown to their right eye while running speed was measured using a linear treadmill (Fig.2.1B). Injections in V1 were done through small holes in the glass imaging window (Fig.2.1C), placed over the monocular zone, and close to the imaging location of V1 (within 200 μm of the center of the imaging location). We matched the 2-photon FOVs across imaging days, and identified neurons present on both days by their morphological features (Fig.2.1D). In summary, this protocol allowed us to investigate the influences of direct HVA→V1 feedback projections on a substantial number of V1 neurons for various visual stimuli and state modulations of V1 activity.

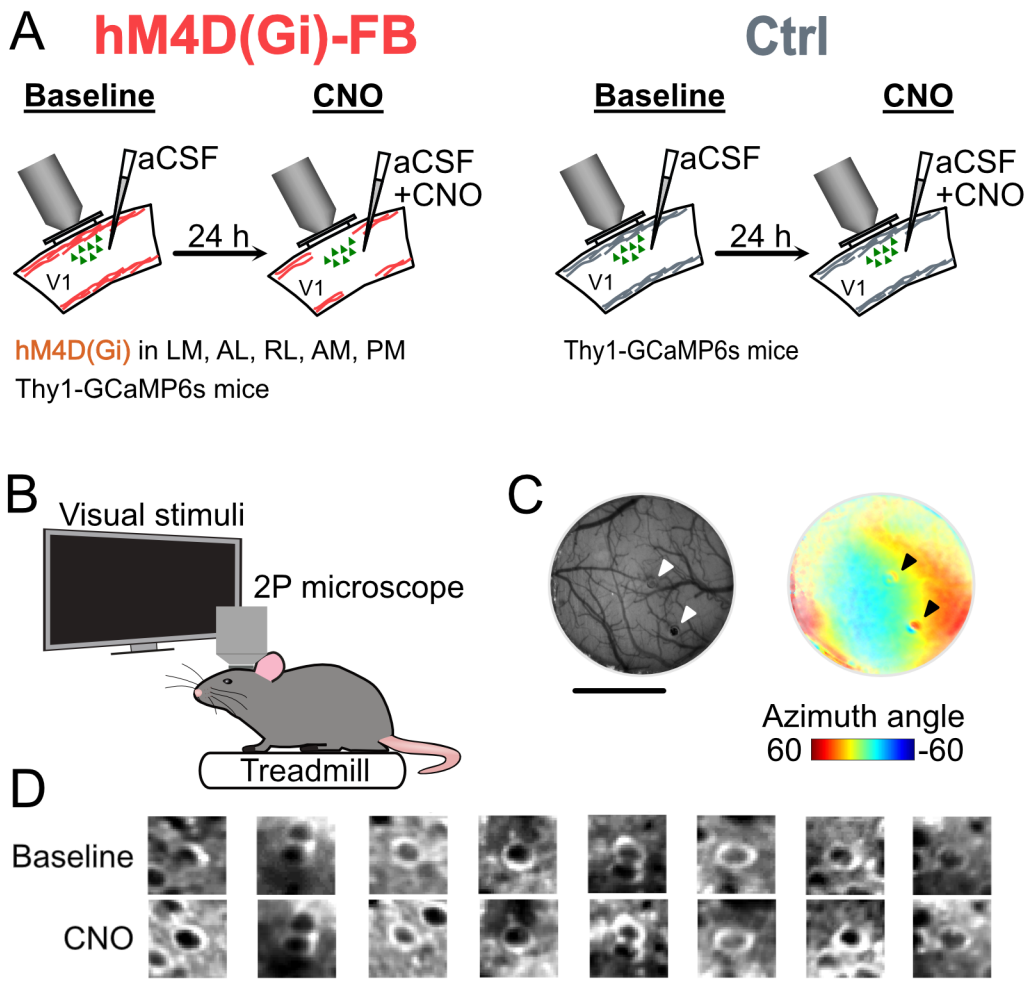

Figure 2.1: Experimental paradigm
(A) Experimental design. Left, Thy1-GCaMP6s mice expressing hM4D(Gi) at HVAs undergo two days of consecutive 2-photon imaging immediately after an injection of aCSF or CNO in V1 (hM4D(Gi)-FB group). Right, Thy1-GCaMP6s control mice are subjected to the same procedures (Ctrl group).(B) Experimental setup. Mouse is head-fixed under a 2-photon microscope. A monitor presents visual stimuli to the mouse's right eye. Running is measured using a linear treadmill.(C) Left, example implanted custom made imaging window over V1. Arrows indicate holes to allow local injections. Right, retinotopic map (azimuth) of V1. Windows are implanted so that holes are positioned over the V1 monocular zone (mint green). Scale bar = 2mm.(D) Example tracked neurons across imaging days. 2-photon imaging FOV was matched across two days of consecutive imaging and neurons present on both days were identified.

2.3.2 Expression of hM4D(Gi) is confined to HVAs

In order to label feedback projections in V1 with hM4D(Gi), we injected a mCherry-tagged anterograde virus encoding hM4D(Gi) in the main HVAs of the mouse, namely LM, AL, RL, AM, and PM. The skull was made transparent, and intrinsic signal imaging was performed to get a retinotopic map of the visual cor-

tex. We manually identified the centers of the HVAs based on the visual field sign map, calculated as the sine between the azimuth and elevation retinotopic gradients (Fig.2.2A, left). We used an image from brain vessels simultaneously taken to locate the sites for viral injections (Fig.2.2A, right). To validate that the expression of hM4D(Gi) was confined to HVAs, mice were perfused, and we registered images of brain slices counterstained with DAPI to the Allen Brain Atlas (ABA) using semi-automatic software (Yates et al., 2019). We found mCherry expression in all areas targeted by virus injections (Fig.2.2B), which we confirmed by quantifying the mean fluorescence for each HVA defined by the ABA (Fig.2.2C). We also found expression in smaller nearby HVA, such as LI, POR, A. This does not pose a problem because we are interested in labeling most of the feedback projecting to V1. Moreover, in this quantification, V1 labeling is not zero because feedback axons labeled with mCherry also contributed to the measured fluorescence in V1, and we observed small labeling of neurons at V1 borders with HVA, mainly at the binocular zone. To control the spread of virus injections to neighboring areas, we measured the fluorescence in the retrosplenial cortex (RSP), an adjacent area to the medial HVA. We found minimal labeling in RSP. Anterograde viruses also travel retrogradely in neurons to a lesser extent (Kaspar et al., 2002) and pose a concern in experiments in which projections are manipulated. Therefore, we visually checked V1 slices for mCherry-positive neurons, excluding animals in which those were present. To further control retrograde labeling, we visually checked slices containing LGN. If many neurons were labeled in V1, we expected to see their axons in LGN. However, we observed minimal labeling of axons in LGN and a dense axonal projection in the pulvinar (LP), an area innervated by HVAs (Fig.2.2D). Therefore, in our protocol, expression of hM4D(Gi) is present and confined to the majority of the mouse HVAs suggesting an extensive amount of feedback projections in V1 could be silenced.

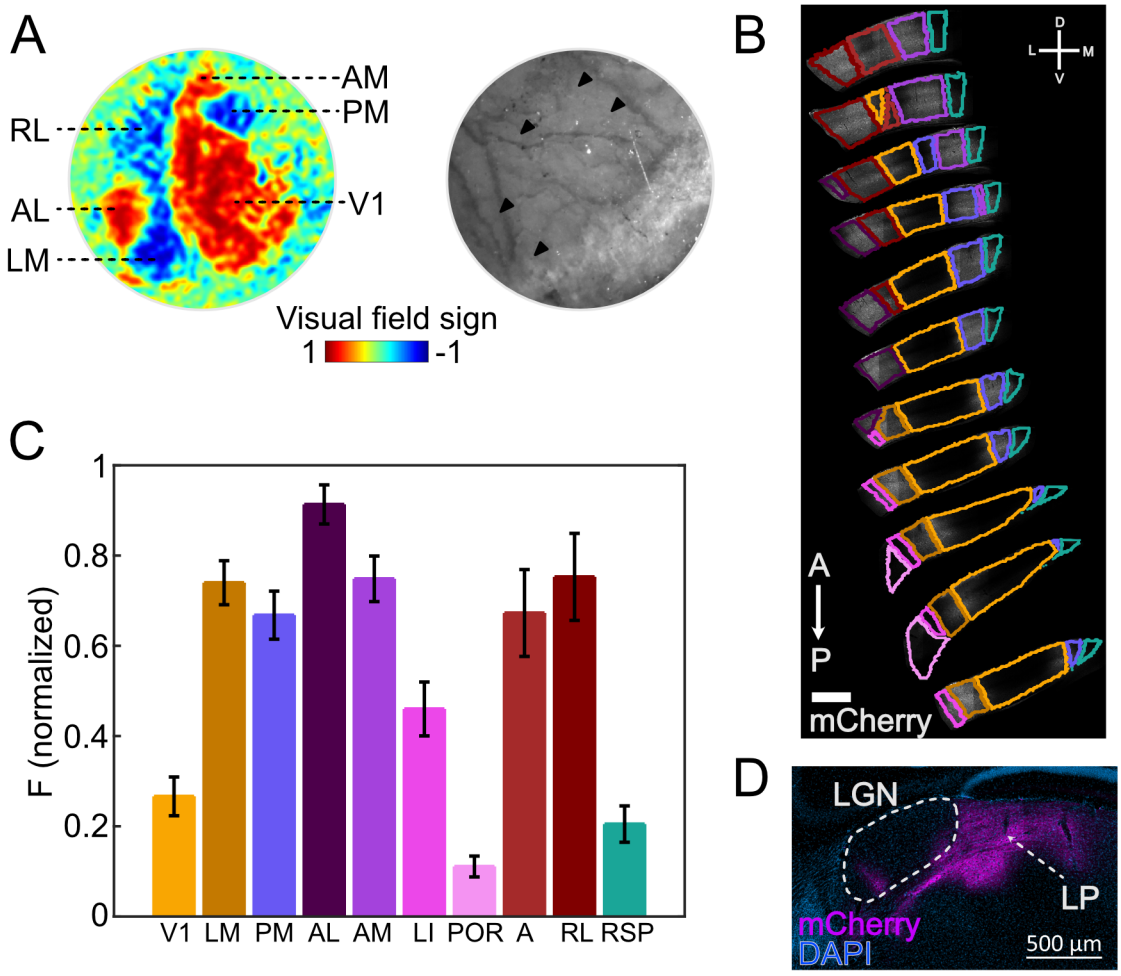

Figure 2.2: HVAs viral targeting and quantification of hM4D(Gi) expression
(A) Intrinsic-guided viral injections. Left, example visual field sign acquired with intrinsic imaging through the clear skull preparation. Right, corresponding image of vessels. Black arrows indicate injection sites.(B) Example ABA-aligned images of coronal brain slices. Colors indicate areas quantified in (C). Scale bar = 1mm.(C) Fluorescence quantification of brain areas. Bars indicate mean fluorescence across 4 animals. Error bars indicate SEM.(D) Example labelling of thalamic axons. Minimal labelling in LGN indicate minimal labelling in V1 Abbreviations: lateromedial, LM; anterolateral, AL; rostrolateral, RL; anteromedial, AM; posteromedial, PM; primary visual cortex, V1; laterointermediate, LI; posteromedial, POR; anterior, A; retrospleneal cortex, RSP

2.3.3 CNO activation of hM4Di(Gi) in LM→V1 feedback axons reduces light-evoked responses in *ex vivo* V1 slices

When activated by CNO, hM4D(Gi) were shown to suppress activity in synapses (Mahler et al., 2014; Stachniak et al., 2014) and reduce light-evoked excitatory postsynaptic currents (Doron et al., 2020; Takahashi et al., 2020, 2021) in *ex vivo* brain

slices experiments. Extending the technique used by the later studies to LM→V1 projections, we investigated whether hM4Di(Gi) activation in axons with CNO could reduce light-evoked responses in *ex vivo* brain slices. We injected mice with a mixture of viruses carrying hM4D(Gi) and channelrhodopsin (ChR2) in LM to label LM→V1 feedback projections. Next, brains were sliced, and V1 neurons were recorded using patch-clamp while delivering blue light to stimulate feedback axons. Slices containing the virus injection site were removed to avoid stimulation of LM somata. We recorded V1 neuronal responses to the blue light stimulation before (Baseline) (Fig.2.3A, left) and after adding CNO (CNO) (Fig.2.3A, right) to the recording bath. We found that neurons reduced their response to blue light stimulation when CNO was present in the bath (Fig.2.3B). We quantified the responses to all recorded cells in both conditions and normalized them by their activity without CNO (Fig.2.3C). We found that neurons reduced, on average, about 28% of their responses to blue light stimulation in the presence of CNO (n=9 neurons). Thus this shows that CNO activation of hM4D(Gi) inhibits HVA→V1 axons.

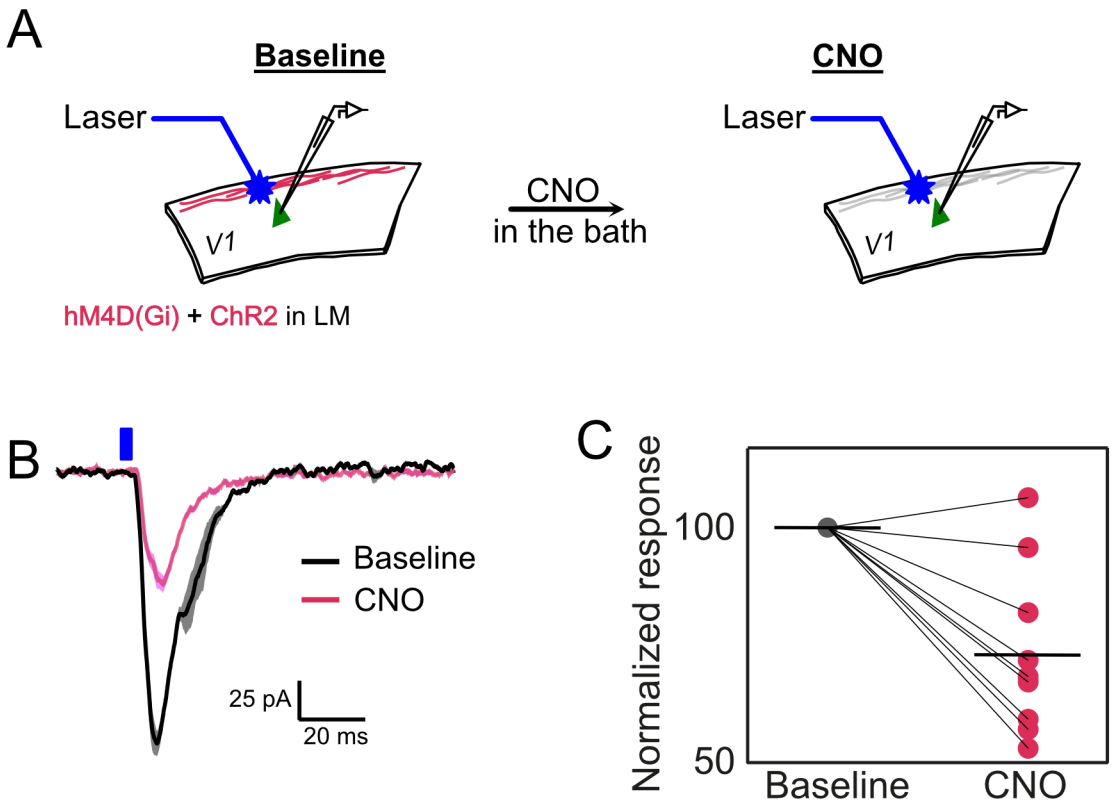

Figure 2.3: Responses to blue light stimulation is reduced in the presence of CNO (A) Experimental paradigm. Voltage clamp recordings of V1 neurons were performed in animals expressing ChR2 and hM4D(Gi) in LM neurons. Neuronal responses to blue light pulses were recorded in the absence (baseline) or presence of CNO (CNO).(B) Example mean trace of one recorded neuron. Mean of 5 trials. Shaded area indicate standard deviation.(C) Cells' responses to blue light stimulation normalised by baseline response. Each point corresponds to a recorded neuron. Black bar indicate mean across neurons.

2.3.4 Measuring hM4D(Gi)-mediated inhibition of LM→V1 feedback *in vivo*

Our previous experiment showed that cortical feedback axons are effectively inhibited by the application of CNO in *ex vivo* brain slice preparations. To directly quantify the efficacy of this approach *in vivo*, we decided to measure whether an injection of CNO in V1 would inhibit LM→V1 feedback axons expressing hM4D(Gi). We injected mice with a mixture of viruses carrying hM4D(Gi) and GCaMP in LM, and implanted them with an imaging window with small holes over V1 to allow a local injection of aCSF or CNO. We measured the responses of LM→V1 feedback axons to drifting gratings (Fig.2.4B) in two consecutive days immediately after local injection of aCSF (Baseline) (Fig.2.4A, left) or CNO (CNO) (Fig.2.4A, right). Imaging sessions were

done on anesthetized animals to avoid movement confounds because of animal running and grooming. We imaged three animals and a total of four session pairs, in which we observed co-expression of hM4D(Gi) and GCaMP in LM neurons (Fig.2.4C) and feedback axons in V1 both in histology (Fig.2.4D) and 2-photon images (Fig.2.4E). Imaging was performed over the same part of V1 on both days, resulting in a similar but not equal population of axons. We observed that LM→V1 axons were less bright in the average fluorescence per session after a CNO injection than during Baseline (Fig.2.4E), suggesting a local injection of CNO activates hM4D(Gi), which inhibits direct LM→V1 axons *in vivo*.

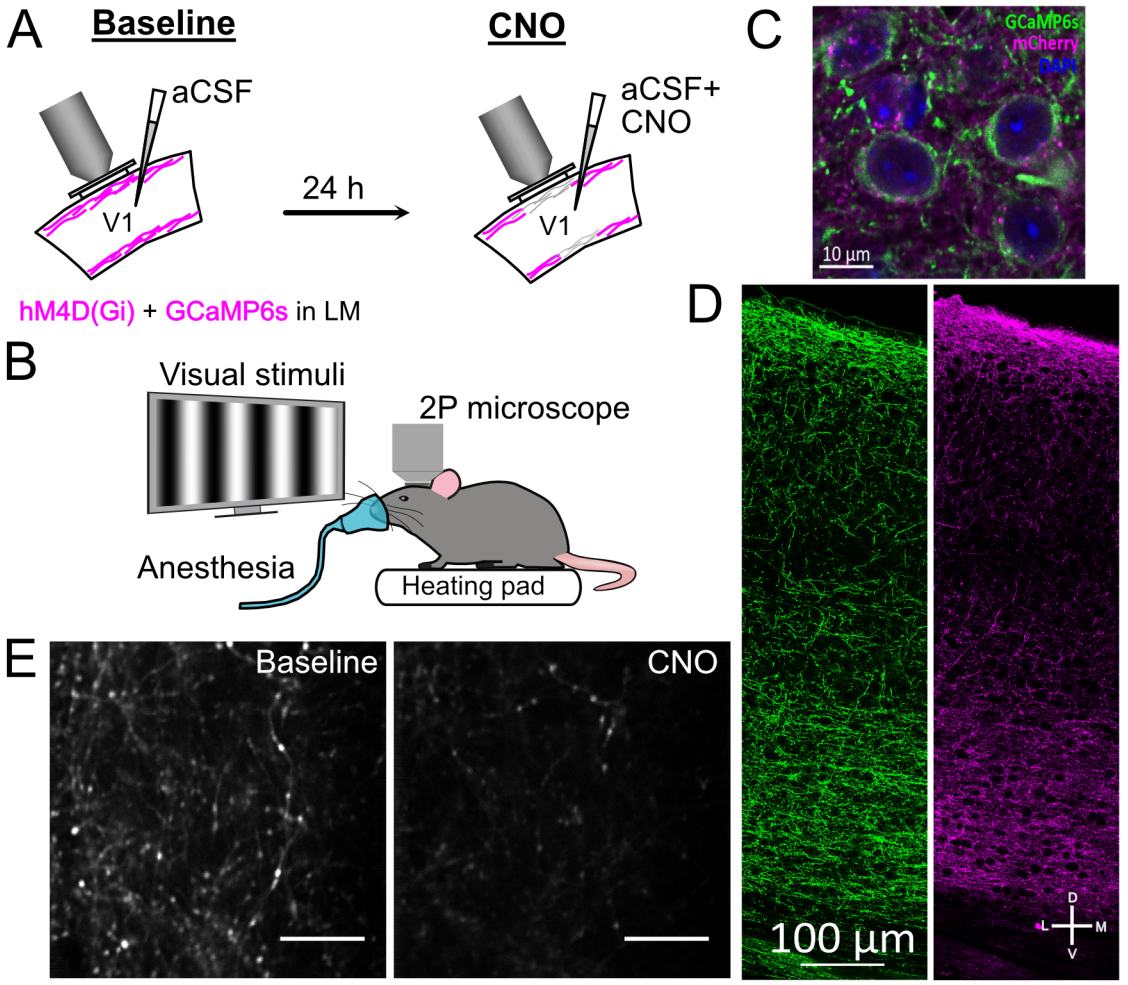

Figure 2.4: Silencing LM→V1 feedback axons *in vivo*
(A) Experimental design. Calcium imaging of LM→V1 feedback axons were performed in animals expressing GCaMP6s and hM4D(Gi) in LM neurons. Axonal responses to visual stimulation were recorded after a local injection of aCSF (baseline) or CNO (CNO).(B) Experimental setup. Anaesthetised mouse is head-fixed under a 2-photon microscope. A monitor presents visual stimuli to the mouse's right eye.(C) Example double-labelled neurons in LM. (D) Example feedback axons in V1. Left, GCaMP labelling. Right, mCherry labelling. (E) Example 2-photon FOVs. Left, baseline. Right, CNO. Both images were acquired with equal laser power. Scale bar = 20 μm.

2.3.5 CNO activation of hM4Di(Gi) in LM→V1 feedback axons reduces visual responses *in vivo*

Following the hint that CNO activation of hM4D(Gi) *in vivo* reduces visual responses in direct LM→V1 axons, we decided to measure whether a local injection of CNO reduces the activity of single putative feedback synapses in V1. We manually drew ROIs around putative presynaptic sites (n $_{Baseline}$ = 2092, n $_{CNO}$ = 1484, all

sessions) and calculated the mean response to all trials of the preferred drifting grating (the stimulus that elicited the maximum response) (Fig.2.5A). We found that a local injection of CNO reduced the average bouton visual response by about 33% (t-test, p=1.1x10^{-42}). We also observed a similar reduction (around 35%) across sessions (Fig.2.5C) (paired t-test, p=0.0478, n=4 sessions). We compared the activity during visual stimulation and the period preceding it (gray screen) to identify visually-responsive (VR) boutons. Boutons whose activity was significantly different using a paired t-test were considered VR. We observed a significant reduction in the number of VR boutons when CNO was present in the brain (Fig.2.5D) (paired t-test, p=0.0228, n=4 sessions). Therefore our data has shown that a local injection of CNO reduces the visual evoked-activity of LM→V1 hM4D(Gi)-expressing presynaptic boutons and reduces the number of boutons responsive to visual stimulation.

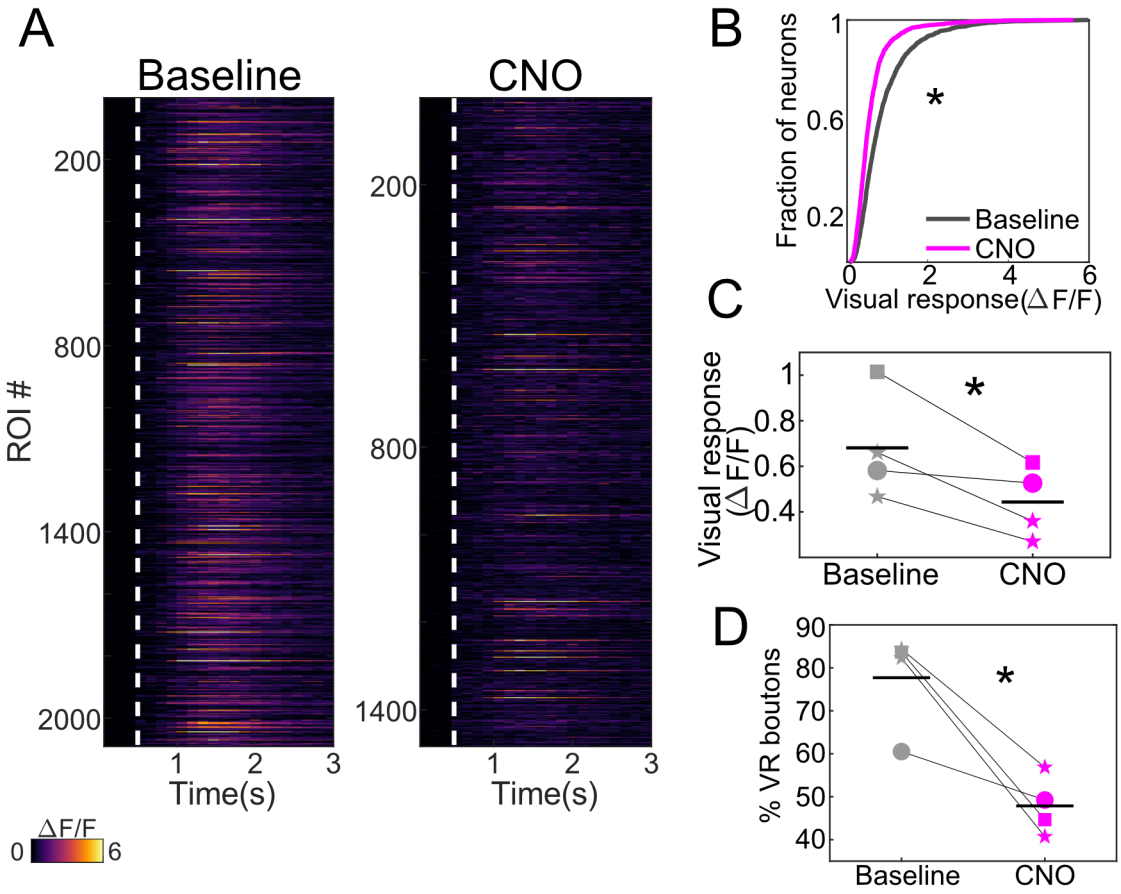

Figure 2.5: Visual responses and number of VR boutons are reduced with a local injection of CNO
(A) Single bouton mean traces. For each bouton the mean response to the grating that elicited the highest response is plotted. White line indicate the time stimulus starts to play.(B) Distribution of visual responses to preferred grating. t-test, p=1.1x10^{-42}), n baseline = 2092, n CNO = 1484.(C) Comparison of visual responses across sessions. Each point indicate the mean response for all boutons within a session. Bars indicate mean across sessions. Paired t-test, p=0.0478, N = 4 sessions, 3 animals. (D) Percentage of visually-response boutons across sessions. Circles indicate number of visually-responsive boutons for each session, black bar the mean for all sessions. Paired t-test, p=0.0228.

2.3.6 Measuring effects of hM4D(Gi) activation by systemic delivery of CNO in somatas

HVAs can modulate V1 neurons through direct (HVA→V1) or indirect (HVA→LP→V1) feedback projections. One could disentangle HVA modulations in V1 representations from these two pathways in our protocol: while a local injection of CNO silences HVA→V1 terminals, a systemic injection of CNO would inhibit hM4D(Gi)- expressing neurons, silencing both HVA→V1 and HVA→LP. With that in mind, we tested

whether a systemic injection of CNO would silence hM4D(Gi) expressing neurons in the areas AL and RL. Transgenic mice expressing GCaMP in the cortex were injected with a virus carrying hM4D(Gi) in LM, AL, RL, AM, and PM and implanted with an imaging window over the visual cortex. We imaged neurons in AL or RL after systemic injection of aCSF (Fig.2.6A, left) or CNO (Fig.2.6A, right) while presenting drifting gratings to awake mice (Fig.2.6B). On both imaging days, we identified neurons expressing hM4D(Gi) in the FOV (Fig. 2.6C). Imaging was performed over the same location across days, rendering similar FOVs. Surprisingly, we observed that many neurons in V1 were brighter in the average fluorescence per session after a systemic injection of CNO (Fig.2.6D). This finding suggests that, in this preparation, hM4D(Gi) expressing neurons increase their activity to visual stimuli after a systemic CNO injection.

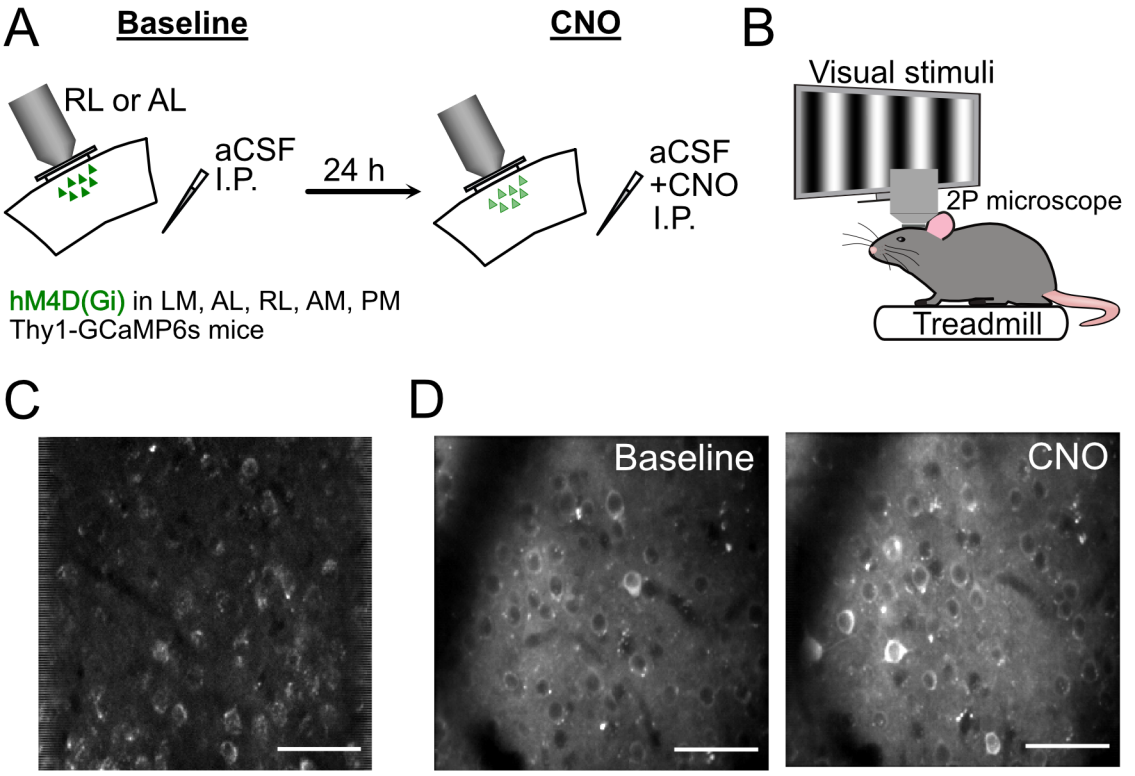

Figure 2.6: Effects of hM4D(Gi) activation in somatas of areas AL and RL
(A) Experimental design. Calcium imaging of AL or RL hM4D(Gi)-expressing neurons was performed after a systemic injection of aCSF or CNO. (B) Experimental setup. Mouse is head-fixed under a 2-photon microscope. A monitor presents visual stimuli to the mouse's right eye. (C) Example 2-photon FOV with hM4D(Gi)-expressing neurons (mCherry). Scale bar = 50 μm. (D) Example 2-photon FOVs. Left, baseline. Right, CNO. Scale bar = 50 μm.

2.3.7 Systemic injection of CNO facilitates visual responses of hM4Di(Gi)-expressing neurons

Next, we quantified the visual responses of individual V1 neurons on both imaging days. We manually drew ROIs around putative neurons ($n_{Baseline}$ = 412, n_{CNO} = 411, all sessions) and calculated the mean response to all trials of the preferred drifting grating (the stimulus that elicited the maximum response) (Fig.2.7A). We found that, on average, neurons increased their response by around 70% after a systemic injection of CNO (Fig.2.7B) (t-test, p=5.7x10^{-7}). We also observed similar facilitation across sessions, around 68% (Fig.2.7C) (paired t-test, p=0.07, n=4 sessions). Moreover, we identified VR neurons in both sessions as previously described for the bouton population. We observed an increase of around 25% in the number of VR neurons after CNO injection (paired t-test, p=0.0728, n=4 sessions) (Fig. 2.7D). Although very puzzling, our data has shown that a systemic injection of CNO facilitates visual responses of AL or RL hM4D(Gi)- expressing neurons.

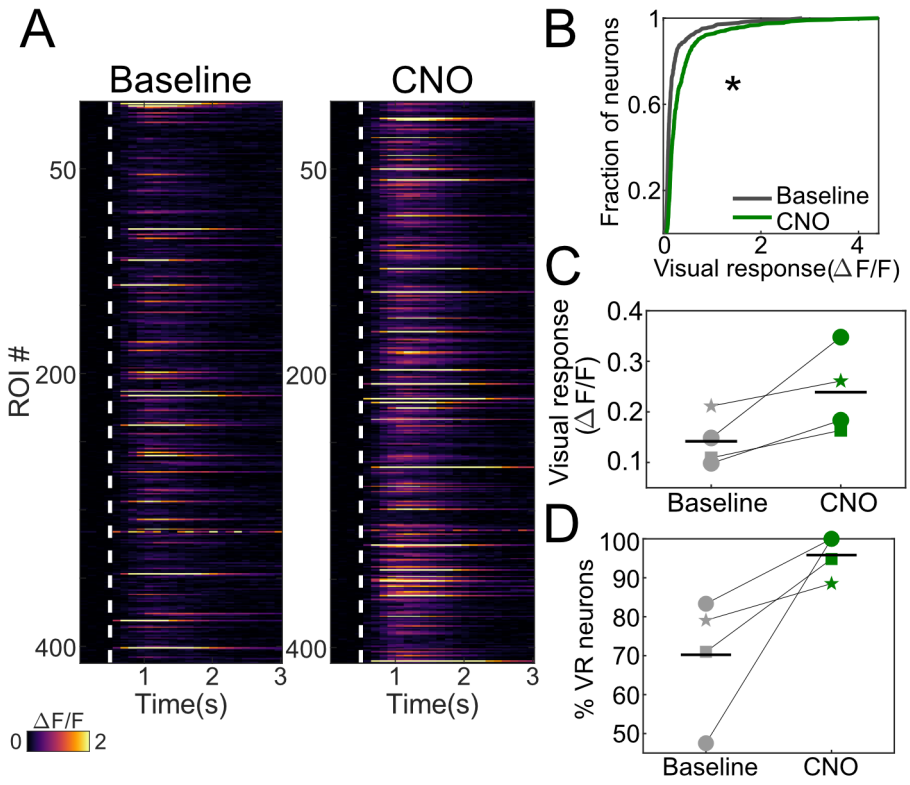

Figure 2.7: Visual responses and number of VR neurons are increased after a systemic injection of CNO
(A) Single neuron mean traces. For each neuron the mean response to the grating that elicited the highest response is plotted. White line indicate the time stimulus starts to play.(B) Distribution of visual responses to preferred grating. t-test, p=5.7x10^{-7}), n baseline = 412, n CNO = 411.(C) Comparison of visual responses across sessions. Each point indicate a mean response for all boutons within a session. Bars indicate mean across sessions. Paired t-test, p=0.07, N = 4 sessions, 3 animals. (D) Percentage of visually-response boutons across sessions. Circles indicate number of visually-responsive boutons for each session, black bar the mean for all sessions. Paired t-test, p=0.0728.

2.4 Discussion and conclusions

In this project, we asked how feedback projections from HVAs influence representations in V1. We developed a protocol to selectively silence direct HVA→V1 feedback projections to investigate their role in shaping V1 representations. This protocol consisted of labeling the majority of the mouse HVAs with hM4D(Gi) and recording V1 neurons on two consecutive days. A batch of visual stimuli was presented to awake mice under a 2-photon microscope. On the first day of imaging ('Baseline'), animals received an injection of aCSF in V1. In contrast, CNO was injected on the second day of imaging ('CNO'), leading to suppression of activity in hM4D(Gi)-expressing

feedback projections. We validated this manipulation in *ex vivo* brain slices, extending results from other studies in the literature to LM projections. We also demonstrated that cortical feedback is suppressed *in vivo* after a local injection of CNO. Surprisingly, neurons in areas labeled with hM4D(Gi) showed facilitation in responses after a systemic injection of CNO.

2.4.1 Tackling top-down modulations in V1: experimental approach

V1 receives feedback innervation from many other areas at multiple higher hierarchical levels (Felleman and Van Essen, 1991; Harris et al., 2019; Siegle et al., 2021). However, top-down influences in V1 information processing have been mostly investigated by manipulating one source of feedback projections at a time (Hupe et al., 1998; Hupé et al., 2001; Nassi et al., 2013; Oude Lohuis et al., 2021; Pafundo et al., 2016; Sandell and Schiller, 1982; Wang et al., 2010) or its direct feedback projections in V1 (Nurminen et al., 2018). By contrast, our experimental approach simultaneously silenced projections in V1 from many sources of feedback, aiming to find universal principles of top-down modulations in V1 processing. Evidence pointing to feedback from different areas (Huh et al., 2018) or modalities (Shen et al., 2020) carrying specific information raises concern for our experimental approach. However, these specific area modulations were not in the lens of our study, whose results can only be interpreted as a net effect of top-down from multiple HVAs.

Another critical difference in our experimental approach is that our dataset comprises hundreds of simultaneously recorded V1 neurons with and without the influence of direct feedback projections ('Baseline' and 'CNO' imaging days, respectively). This design allowed us to measure top-down influences on individual neurons over time. We achieved this by combining 2-photon imaging with V1 injections of aCSF or CNO through the imaging window, whereas previous studies have mainly used electrophysiology. One experimental trade o between recording neurons with 2-photon imaging and extracellular electrophysiology is that the first allows simultaneous recording of hundreds of neurons and tracking of somas across multiple days. However, the latter gives simultaneous access to cells across multiple cortical layers. In our study, only L2/3 V1 neurons were recorded because of light-induced artifacts from dense labeling of pan-neuronal GCaMP6s transgenic mouse used. Moreover, in our recordings, mice were exposed to two consecutive days of visual stimulation, which could lead to adaptation of V1 visual responses (Weber et al., 2019) and confound the interpretation of our results. We controlled for that by having animals experience the visual stimuli a similar number of times and using mice without hM4D(Gi) expression as controls

(Ctrl group). Lastly, mice from the Ctrl group were also used to control the potential damage of brain injections of aCSF and CNO.

Finally, behavioral states, such as running, are known to modulate V1 activity (Niell and Stryker, 2010) and the activity of HVA (Christensen and Pillow, 2017; Shimaoka et al., 2018). Previous studies that manipulated sources of V1 feedback recorded animals in different states, such as anesthetized (Hupe et al., 1998; Hupé et al., 2001; Nurminen et al., 2018; Oude Lohuis et al., 2021; Pafundo et al., 2016; Sandell and Schiller, 1982; Wang et al., 2010) and awake (Nassi et al., 2013; Oude Lohuis et al., 2021) yet no work so far has looked into top-down influences on running modulations of V1 activity. In our protocol, mice speed was recorded, allowing for comparisons of spontaneous or visually-driven activity in both stationary and running states.

2.4.2 Suppression of activity in neuronal projections

A single study investigated whether direct feedback projections modulate V1 (Nurminen et al., 2018) mainly because suppressing activity in neuronal projections is still challenging. Previous studies have described conflicting results using optogenetics (Mahn et al., 2016). However, *ex vivo* evidence has put DREADDs as the state-of-the-art technology to achieve such inhibition (Stachniak et al., 2014). In this chapter, we have reproduced inhibition previously observed in *ex vivo* preparations (Doron et al., 2020; Takahashi et al., 2020, 2021): the presence of CNO at the recording bath led V1 neurons to reduce their light-evoked activity in brain slices which LM→V1 were co-labeled with ChR2 and hM4D(Gi).

Inspired by our *ex vivo* results, we tested, for the first time, whether a CNO injection in V1 would cause inhibition of LM→V1 activity *in vivo*. Among other activity metrics, we observed a suppression of about 33% in the visually-evoked activity across the presynaptic bouton population, similar to the response change observed in *ex vivo* (around 28%). One possible scenario for this small suppression is the low co-infection rate of LM neurons by viruses carrying GCaMP6s and hM4D(Gi), resulting from competition to infect cells. If most LM neurons were exclusively infected with GCaMP6s or hM4D(Gi), activity measured at projections would primarily represent those not affected by CNO, leading to underestimation of silencing levels. In our histological data we observed that although many neurons in LM were double-labeled(GCaMP6s and hM4D(Gi)), many were not. We believe knowing the amount of suppression is highly relevant for interpreting our results because it can inform us of the strength of modulations by direct feedback projections on V1 representations.

In our experiments, diffusion of CNO from V1 to neighboring areas could inhibit activity in hM4D(Gi)-expressing neurons in HVAs, misleading our interpretations of effects to direct feedback projections. The length of CNO spread depends on the tissue, CNO isoform and molecular weight, medium pH, among other factors. Evidence from Stachniak et al. (2014) suggests that CNO diffuses less than 500μm in the brain: behavioral effects were not observed when CNO was injected through brain cannulas implanted over 500μm away from the targeted area. In another study, CNO spread was inferred from brain slice fluorescence of an injected dye. They observed minimal fluorescence over 600μm away from its injection site (Doron et al., 2020). Therefore, considering that V1's shorter axis is around 2.5mm and that our CNO injections were aimed at its center, CNO diffusion to HVAs is unlikely to happen in our preparation. Additional experiments could control CNO diffusion by injecting CNO in V1 and measuring activity in the HVAs.

At last, recently engineered opsins, eOPN3 (Mahn et al., 2021) and PPO (Copits et al., 2021), have been shown to inhibit activity in long-range cortical projections. Both can suppress neuronal activity by similar intracellular mechanisms that hM4D(Gi) use, but their main advantage is light activation. New studies will profit immensely from this new technology because of their higher temporal precision than hM4D(Gi), which allows trial-to-trial manipulation of neuronal activity.

2.4.3 Unexpected hM4D(Gi)-mediated facilitation of neuronal activity

Previous studies have described suppression of neuronal activity in neurons of hM4D(Gi)-expressing areas after a local (Mahler et al., 2014) and systemic (Yaeger et al., 2019) injection of CNO. However, we observed a 70% increase in the amplitude of visually-evoked activity of neurons after systemic CNO injection in our preparation.

One big difference between previous studies is that hM4D(Gi) were expressed in one brain area, whereas we labeled multiple areas with that receptor. Thus, our study's facilitation of neuronal responses could result from an inter-areal network effect resulting in disinhibition. Additionally, intra-areal circuit effects have been proposed by other authors that observed conflicting effects of DREADDs manipulations (Chang et al., 2015; Vazey and Aston-Jones, 2014). In both studies, it has been proposed that neurons with absence/low expression of DREADDs that are strongly modulated by neurons with high DREADD penetrance showed excitation instead of inhibition, and vice-versa, after CNO was delivered systemically. However, our recordings showed similar facilitation of responses when exclusively mCherry+ neurons, identified in the 2-photon FOV, were included in the analysis (data not shown).

Furthermore, we have also hypothesized that the observed increase in visual responses could be a result of disrupting the balance of excitation and inhibition (E-I balance). E-I balance has been defined as the relative invariant ratio of excitatory and inhibitory inputs a neuron receives. Biases towards excitation or inhibition are counteracted to restore E-I balance in a circuit (Sohal and Rubenstein, 2019). In our experiment, a prolonged (>2 hours) and extensive (multiple areas) suppression of excitatory events would drive the circuit to adjust and down-regulate inhibitory events. In this context, neurons would respond more to the visual stimulation, therefore becoming less selective to gratings. However, no change in orientation selectivity between neurons present in both 'Baseline' and 'CNO' imaging days was observed (data not shown).

Finally, one of the motivations behind these experiments was to compare direct versus indirect HVA modulations in V1 representations. However, given that activity in HVA was facilitated instead of inhibited, comparing the effects of such manipulation to silencing of direct HVA→V1 feedback would not be complementary and further experiments were not conducted.

2.5 Materials and Methods

2.5.1 Animals

All procedures were reviewed and approved by the Champalimaud Centre for the Unknown Ethics Committee and performed in accordance with the Portuguese Direcção Geral de Veterinária. For *ex vivo* experiments, wild type C57BL/6J mice were used and aged 21-27 days at the beginning of the experiments. Mice were housed with their littermates in a 12-12 hour light–dark cycle. For *in vivo* functional imaging of axons, wild type C57BL/6J mice were used. For *in vivo* functional imaging of somas, heterozygous male mice expressing GCaMP6s in the cortex (*C57BL/6J-Tg(Thy1-GCaMP6s)GP4.3Dkim/J*) were used. For all *in vivo* experiments, mice aged from P56 to P182 at the beginning of experiments. Mice were housed with their littermates in a 12-12 hour reversed light–dark cycle.

2.5.2 Targeting of HVA

All mice used for the hM4D(Gi)-FB group and mice that received systemic CNO injections underwent the following procedures, in order: (1) clear skull preparation, (2) intrinsic signal imaging and (3) virus injection and window implantation. Details for each step are described bellow.

2.5.3 Clear skull preparation

Animals were anaesthetized with isoflurane (induced: 5%; sustained 1-1.5%; O2 flow: 1L/min) and injected with bupivacaine (0.15ml, 0.05%, injected under the scalp), buprenorphine (0.1mg/kg, subcutaneously), dexamathasone (2mg/kg; subcutaneously) and Cefovecin (6mg/kg; subcutaneously) to supply local and general analgesia, control inflammation and to prevent post-operative infections, respectively. Eyes were kept moist using ophthalmic ointment (Vitaminoftalmina A). While under anesthesia, body temperature was maintained at 37°C using a heating pad (Supertech). A circular cut was made on the scalp exposing the skull. After cleaning the connective tissue, a layer of cynoacrylate was applied uniformly into the skull followed by a thin layer of clear dental cement. A custom-designed circular head-post was fixed to the skull over V1 with black dental cement. Next, the clear dental cement located inside the head-post well was polished using dental drills and a layer of transparent nail polish applied (Guo et al., 2014).

2.5.4 Viral injections and imaging window implantation

Animals were anaesthetized with isoflurane (induced: 5%; sustained 1-1.5%; O2 flow: 1L/min) and injected with bupivacaine (0.15ml, 0.05%, injected under the scalp), buprenorphine (0.1mg/kg, subcutaneously), dexamathasone (2mg/kg; subcutaneously) and Cefovecin (6mg/kg; subcutaneously) to supply local and general analgesia, control inflammation and to prevent post-operative infections, respectively. Eyes were kept moist using ophthalmic ointment (Vitaminoftalmina A). While under anesthesia, body temperature was maintained at 37°C using a heating pad (Supertech). Virus were injected using a polished pulled glass pipette with an opening of 10-15µm. Mineral oil was applied at the back of the pipette prior to insertion of a plunger, which was controlled by a hydraulic manipulator (Narashige, MO10).

For mice that underwent 'Clear skull preparation' (hM4D(Gi)-FB group and mice that received systemic CNO injections), the skull surface was exposed by removing the dental cement layer within the head-post well with a dental drill. 30-40 nL of *AAV5-CaMKIIa-hM4D(Gi)-mCherry* (Addgene, catalog 50477-AAV5) was injected in LM, AM, RL, AL and PM (left hemisphere, 0.35 mm in depth). Retinotopic maps and brain vessels obtained from intrinsic signal imaging were used to define the injection sites. For the Ctrl group and mice used for axonal imaging, a circular cut was made on the scalp exposing the skull and connective tissue was cleaned. For *in vivo* functional imaging of axons, mice were injected with 100nL of a mix (1:1) of *AAV5-CaMKIIa-hM4D(Gi)-mCherry* and *AAV1-nSyn-GCaMP6s* in LM (3.55mm posterior and -3.65

lateral to bregma, 0.4mm in depth). Mice from the Ctrl group were not injected with viruses.

Next, a circular craniotomy (4mm) was drilled in the bone over the left visual cortex using a dental drill. The dura mater was kept undamaged. We built a custom-designed imaging window from two layers of glass attached with a UV-curable optical glue (Norland Optical Adhesive 61). For mice that received a V1 injection of CNO, the top glass had a torus shape with an outer diameter of 5mm and inner diameter of 3mm. The bottom layer of glass was shaped as a circle with outer diameter of 4 mm and two circular holes of 0.15 mm allowing intracerebral injection of solutions. For mice that received a systemic injection of CNO, top and bottom glass layers were circles with 4mm and 3mm, respectively. The window was carefully placed over the craniotomy and attached to the skull with cynoacrylate and black dental cement. Next, animals that did not undergo 'Clear skull preparation' had a custom-designed circular iron head-post fixed to the skull with black dental cement.

For all mice used for *ex vivo* experiments, surgeries were performed under anesthesia (37.5 mg/kg ketamine, 0.5 mg/kg medetomidine, I.P.). Eyes were kept moist using ophthalmic ointment (Vitaminoftalmina A). While under anesthesia, body temperature was maintained at 37°C using a heating pad (Supertech). 50nL of a mix (1:0.5:0.5) of *AAV-2/1-CAG-Channelrhodopsin-2-Venus*, *AAV5-CaMKIIa-hM4D(Gi)-mCherry* and PBS 1x was injected in LM (1.5mm anterior of transverse sinus, -3.5mm lateral to midline, 0.8 mm in depth).

2.5.5 Intrinsic signal imaging

Retinotopic maps of the visual cortex were acquired using intrinsic signal imaging (Kalatsky and Stryker, 2003; Marshel et al., 2011). Imaging was performed at the 'clear skull preparation' (Guo et al., 2014) or the glass imaging window. Mice were anesthetized with isoflurane (induced: 5%; sustained 1-1.5%; O2 flow: 1L/min) and injected with chlorprothixene (1mg/kg, intramuscularly) (Kalatsky and Stryker, 2003). Eyes were kept moist using silicone oil (Sigma-Aldrich) while not perturbing the animal's vision. While under anesthesia, body temperature was maintained at 37°C using a heating pad (Supertech). We used a Retiga QIClick camera (QImaging) controlled using Ephus (Suter et al., 2010) to record intrinsic signals at 5Hz. High magnification zoom lens (Thorlabs) focused at the skull or brain surface under the glass imaging window. We illuminated the surface of the skull or imaging window with a 620nm red LED while recording the hemodynamic responses to a drifting bar stimulus being presented to the mouse's right eye. The drifting bar crossed the screen 80 (clear skull preparation) or 40 (imaging window) times for each of the four cardinal

directions (12s period, 20° width, masking an alternating checkerboard pattern at 5 Hz). At the end of the experiment, a picture of the blood vessels was taken using a 535nm green LED.

2.5.6 Drugs preparation and injections

For intracerebral injections, mice were lightly anaesthetized with isoflurane (induced: 5%; sustained 0.5%; O2 flow: 0.5L/min) and injected with dexamathasone (2mg/kg; subcutaneously) to prevent bleeding. Eyes were kept moist using ophthalmic ointment (Vitaminoftalmina A). Temperature of animals under anesthesia was maintained at 37°C using a heating pad (Supertech). Solutions were injected using a polished pulled glass pipette with an opening of 10-15µm. Mineral oil was applied at the back of the pipette prior to insertion of a plunger, which was controlled by a hydraulic manipulator (Narashige, MO10). Mice were injected with 100 nL of aCSF (125mM NaCl, 5mM KCl, 10M glucose, 10mM Hepes, 2mM $CaCl_2$, 2mM $MgSO_4$) or CNO diluted in aCSF (300 µM) at 200-300 µm in depth (Stachniak et al., 2014). Animals were taken to the imaging setup immediately after the injections and recording started after animals recovered from anaesthesia (around 15-30 min). All CNO solutions were made fresh on the day of the injection.

For I.P. injections, mice were injected with aCSF with 1% DMSO or 10mg/kg of CNO diluted in aCSF with 1% DMSO. DMSO was added to help homogenize the mixture. There was an interval of 2 hours between the I.P. injection and beginning of functional imaging. This time window has been shown to be a enough for the activation of DREADDs receptors when CNO is delivered systemically (Yaeger et al., 2019). All CNO solutions were made fresh on the day of injection.

For *ex vivo* experiments, a stock solution of 10mM CNO in aCSF was prepared and frozen. At the day of the recordings, an aliquot was defrosted (room temperature) and added to the aCSF recording bath. The final concentration in the aCSF bath was 10uM. This concentration has been shown to silence axons in a similar preparation (Doron et al., 2020).

2.5.7 Two-photon calcium imaging

For *in vivo* functional imaging, we used a custom microscope (based on the MIMMS design, Janelia Research Campus, https://www.janelia.org/open-science/mimms) equipped with a resonant scanner. GCaMP6 was excited using a Ti:sapphire laser (Chameleon Ultra II, Coherent) tuned at 920nm. mCherry was excited using an ultrafast fiber laser (Fidelity-2, Coherent) tuned at 1070nm. We used GaAsP photomultiplier tubes (10770PB-40, Hamamatsu) and a 16x (0.8 NA) objective lens

(Nikon). We performed volumetric imaging by scanning in the axial direction with a piezo actuator (Physik Instrumente). Data from the time of the piezo flyback was discarded. Rubber rings in torus shape were glued to the headpost to form a imaging a well. Imaging well was shielded from light from the monitor with a custom-made conical shield attached to the objective lens. The microscope was controlled using ScanImage (Vidrio; Pologruto et al., 2003). The objective was perpendicularly aligned to the surface of the imaging window and kept for the two consecutive days of imaging. Imaging of calcium indicators began 3 weeks after viral injections and lasted for another 3 weeks.

For functional imaging of somas, seven planes separated by 30µm were acquired at sampling rate of 8.32Hz per plane. Each FOV had 200×200µm (256×256 pixels). The first field of view was placed 150–180µm below the dura. Imaging areas were located over areas RL or AL and defined based on intrinsic signal imaging maps and vessels. For 2 sessions, only one plane was acquired at 60Hz and data was downsampled to match other sessions sampling rate.

For functional imaging of axons, mice were head-fixed and lightly anesthetized with isoflurane (induced:5%, sustained:1%, O_2 flow: 1L/min) and injected with chlorprothixene (1 mg/kg, intramuscular) to reduce movement artifacts. Temperature of animals under anesthesia was maintained at 37°C using a heating pad (Supertech). Four planes separated by 10µm were acquired at sampling rate of 7.5Hz per plane. Each FOV had 80×80µm (512×512 pixels). Axons were imaged 20–100µm below the dura. Imaging areas were located over monocular primary visual cortex and defined based on intrinsic signal imaging maps and vessels.

2.5.8 Visual stimuli

Visual stimuli were presented on a LED (BenQ XL2411Z 24") monitor positioned 20cm from the mouse. Monitor was positioned to provide stimulation to the mouse's right eye and about 45° to the mouse's head axis. We used Matlab and Psychophysics Toolbox (Brainard, 1997) to generate the batch of visual stimuli.

For the results presented in this chapter, animals were presented with full-screen, full-contrast drifting gratings. Gratings moved in one of eight directions (cardinals and obliques). For functional imaging of axons, gratings had a spatial frequency of 0.04 cpd and a temporal frequency of 1 Hz. For functional imaging of somas, gratings had a spatial frequency of 0.02 or 0.04 cpd and temporal frequency of 0.5 or 1 Hz. Each grating type (combination of direction, spatial frequency and temporal frequency) was repeated 20 times. The structure of the trials was as follows: 0.5s of gray screen, 0.5s of visual stimulation, 2s of gray screen.

To avoid light contamination from the monitor during imaging, monitor was on when laser was off and vice-versa.

2.5.9 Running speed measurement

Mice speed was measured with a linear treadmill coupled to a magnetic analog rotary encoder (MAE3, US Digital). Rotation of the linear treadmill was recorded and digitalized using Bpod and Analog Input Module (SamWorks, www.sanworks.io).

2.5.10 Acute brain slices and electrophysiology

14–20 days after surgery (P35–P47), mice were decapitated under deep anesthesia (isoflurane), brains were dissected and sectioned in 300-µm-thick coronal slices. Slices were kept in aCSF aerated with 95%O2 /5%CO2 at room temperature until the electrophysiology recordings. Electrophysiological recordings were performed under a microscope with the slices submerged in ACSF, aerated with 95% O2/5% CO2, with 3-((R)-2-carboxypiperazin-4-yl)-propyl-1-phosphonic acid (CPP, 5µM). CPP was added to the bath to block nonlinear NMDA conductances within the postsynaptic compartment. Cells were recorded in voltage clamp (-70 mV) mode at depths between 30 and 80µm. V1 was identified by the presence of fluorescent axons. Photostimulation was performed with short light pulses of 1 ms with a 10s interval between pulses (with power ranging from 0.1 to 1.1µW) and delivered by a blue laser (473 nm, Cobolt Laser) over the cell body of the recorded cell. After 20 pulses, CNO solution was pipetted to the ACSF bath. The measurements were repeated at least 40 times after adding CNO to the bath. depending on the quality of the recording and the cell's durability.

2.5.11 Histology

Up to one week after the end of imaging sessions, mice were deeply anaesthetized and transcardially perfused with 4% paraformaldehyde in 0.1 M phosphate buffer, pH 7.4. Brains were sliced into 50µm coronal sections. We performed immunohistochemistry to boost GCaMP6s and mCherry signals. GCaMP6s signal was boosted with a polyclonal anti-GFP antibody (ThermoFisher, A-6455) and an Alexa Fluor 488-conjugated secondary antibody (ThermoFisher, A-11008). mCherry signal was boosted with a polyclonal anti-mCherry antibody (abcam, ab167453) and an Alexa Fluor 594-conjugated secondary antibody (ThermoFisher, A-11037). DAPI was used as counterstain. We imaged all brain slices that contained cortical structures using a

slide scanner with a 10× objective (Axio Scan.Z1, Zeiss). Some brain slices were also imaged with a confocal microscope with a 40× objective (LSM 710, Zeiss).

2.5.12 Data analysis

Pre-processing of calcium imaging data

For each imaging session, we selected a trial with visible structure and averaged all frames from the trial. All recorded frames in the imaging session were registered to this average image using a cross-correlation based fast algorithm (Guizar-Sicairos et al., 2008). We drew doughnut shaped regions of interest (ROIs) over somatas or circles ROIs over boutons in the mean projection of the registered session (Chen et al., 2013). Fluorescence of a ROI was estimated by averaging its pixel values. ROI's baseline fluorescence, Fo, was calculated using the mean fluorescence during the 0.5s prior to stimulus presentation (gray screen). Baseline fluorescence was used to calculate Δ F/F as follows:

$$\Delta F/F = \frac{F - Fo}{Fo}$$

Tracking of neurons across days

Neurons present in both days of imaging were identified using ROIMatchPub (source code: www.github.com/ransona/ROIMatchPub). This program uses the mean projection of the registered sessions and user input landmarks and landmarks given by the user to identify ROIs position overlaying in both days. After that, ROIs are manually curated based on their anatomical features to confirm neuron's identity.

Analysis running speed

For each trial, running speed was calculated and a trial was classified as 'running trial' if the animal speed was over 1cm/s for more than 10% of the trial.

Analysis of electrophysiology data

Response to the blue laser was computed as the mean cell response (pA) to the first 20 stimulations (baseline) and the last 15 stimulations (CNO). Only cells with stable ratio Rm/Rs were included in the analysis to guarantee cells were healthy.

Analysis of histology data

Images of brain slices were aligned to the Allen Brain Atlas (www.portal.brain-map.org) using the counterstaining labelling (DAPI), first with a course registration process followed by a fine curation by the user(Yates et al., 2019). Masks were created from aligned brain areas and used to calculate the mean fluorescence of simultaneous images taken of mCherry marker.

Statistical analyses

To define visually-responsive neurons/boutons, we calculated the mean raw fluorescence value (F trace) for each trial during stimulus presentation plus 1.7s (to account for GCaMP slow decay) and 0.5s prior to it (gray screen). These distributions were compared using a paired t-test and α set to 0.05. F traces were used instead of $\Delta F/F$ because the gray screen period was used as Fo. For awake recordings, running trials were discarded from the analysis. Most comparisons between groups were done using t-test and α was set to 0.05. When not mentioned, t-test were unpaired. Numbers of mice, sessions, cells and/or boutons are stated in the text.

Numbers of mice and cells are stated in the text.

Chapter 3

The role of direct HVA $\rightarrow$V1 feedback connections in V1 visual representations

3.1 Author Contribution

GF performed all experiments and analyses described in the text. Marina Fridman contributed with primary codes and her expertise in data analysis.

3.2 Introduction

The visual system is remarkable at building elaborate representations of the world. Visual scene representations are thought to arise in the cortex, a hierarchical brain structure (Felleman and Van Essen, 1991; Harris et al., 2019; Siegle et al., 2021). Cortical areas send visual information up the hierarchy through feedforward connections, and neurons in each sequential hierarchical stage extract more complex features and encode more significant portions of space (Siegle et al., 2021). This architecture and logic make up the feedforward model. It is deployed in neural network models that are widely and successfully used for image classification (Ricci and Serre, 2020), a central task of the visual system. Although neglected in such models, descending feedback connections are prevalent along the cortical hierarchy and have a fine anatomical structure. One prominent thought is that feedback connections convey contextual signals to lower-order neurons, influencing the perception of a visual stimulus. Thus, contextual modulations seem to be fundamental to visual processing since information from the context can provide meaning to visual scenes. Furthermore, they are

thought to underlie many perceptual processes, such as detecting borders and objects and figure-ground segregation (Angelucci et al., 2017; Phillips et al., 2015). Such rich innervation hence poses the question of how feedback connections contribute to building representations of visual scenes.

Evidence indicates that feedback connections modulate the tuning of neurons in lower-order areas. In the mouse, most studies have focused on how top-down modulations shape V1 responses to edges and motion, yet the results were diverse. One set of studies showed that silencing areas that are sources of V1 feedback causes a depression of V1 responses to their preferred stimuli. In one study, silencing LM suppressed responses of V1 L2/3 neurons to gratings of the preferred orientation (Pafundo et al., 2016). Another study showed that inhibiting the anterior cingulate cortex (ACC) reduced V1 responses to the preferred motion-direction angle (Zhang et al., 2014). Moreover, silencing areas AL or PM caused suppression of responses at the spatial frequencies that matched the preferred frequency from the feedback source (Huh et al., 2018). On the other hand, Oude Lohuis et al. (2021) have found a general reduction of V1 responses to drifting gratings upon AL or PM inhibition, particularly at directions of motion eliciting smaller responses (non-preferred stimulus). These studies inhibited higher-order areas resulting in manipulation of direct cortico-cortical feedback and indirect feedback pathways. Therefore, the contributions of direct cortico-cortical feedback to responses of the mouse V1 remain unclear.

Direct cortico-cortical feedback has been implicated in contextual modulations of V1 responses. Contextual modulations are diverse (Phillips et al., 2015) and can originate from the scene surrounding a visual stimulus. Surround modulations are thought to arise in V1 from higher-order area inputs. Nurminen et al. (2018) investigated the contributions of direct V2→V1 feedback on surround suppression of V1 neurons in marmosets. Surround suppression is the reduction of neuronal activity elicited by a large stimulus that extends beyond the neuron's receptive field (surround) compared to the response elicited by a stimulus presented only within the neuron's receptive field. In this study, inhibition of direct V2→V1 feedback caused a reduction of surround suppression in V1 neurons. In the mouse, silencing lateral HVA has also reduced surround suppression (Vangeneugden et al., 2019). Surround modulations can also facilitate V1 responses, particularly when the visual features within and surrounding the receptive field differ. A disinhibitory circuit involving activation of different classes of interneurons has been proposed to mediate surround suppression and facilitation in the mouse (Keller et al., 2020a). Furthermore, a recent study has shown that stimulation of surround alone drives V1 L2/3 neurons, which is mediated by HVA (Keller

et al., 2020b). Thus, among other anatomical substrates, feedback connections from HVA mediate surround effects on V1 responses.

In order to expand our knowledge of the contributions of direct cortico-cortical feedback on visual representations, we examined the effects of inhibiting direct HVA→V1 feedback in V1 responses to drifting gratings, natural images, and natural movies in the awake non-behaving mouse. In this study, we demonstrated that direct cortico-cortical feedback modulates the tuning of V1 neurons to drifting gratings and natural movies, but not to natural images. Our findings suggest that the modulation of direct HVA→V1 feedback depends on the surround, particularly on the stimulus spatial-temporal correlations. Finally, we demonstrated that direct cortico-cortical feedback participates in mechanisms to build visual representations in V1 neurons.

3.3 Results

3.3.1 Protocol to measure modulations of direct HVA→V1 feedback in V1 L2/3 responses to drifting gratings, natural movies and natural images

To investigate the role of direct HVAV1 feedback in V1 representations of drifting gratings, natural movies, and natural images, we silenced direct cortico-cortical feedback projections from HVAs and measured responses of V1 neurons, as described in the previous chapter. Mice expressing hM4D(Gi) in the HVAs underwent two consecutive days of 2-photon calcium imaging immediately after a V1 injection of aCSF or CNO (hM4D(Gi)-FB, Fig.3.1A, left) in the left hemisphere. To control for CNO off-target effects and mechanical damage of the injection, mice with no expression of hM4D(Gi) underwent similar procedures (Ctrl, Fig.3.1A, right). After brain injections, mice were head-fixed under a 2-photon microscope, and a batch of visual stimuli was shown to their right eye while running speed was measured using a linear treadmill (Fig.3.1B, left). V1 neurons at the vicinity of the injection site ($<200\mu$m) were repeatedly imaged across the two days of imaging (Baseline and CNO imaging days, Fig.3.1A). The batch of visual stimuli consisted of drifting gratings, natural movies, and natural images. The set of drifting gratings consisted of two spatial (0.02 and 0.04 cpd) and temporal (0.5 and 1 Hz) frequencies and eight motion directions (cardinal and obliques). The set of natural images was composed of 75 black and white images from the van Hateren image set (Van Hateren and Van der Schaaf, 1998). As for the natural movie, mice were presented with a black and white 30s clip from the movie Nineteen Eighty-Four (directed by Michael Radford, 20th Century Fox, 1984). After pre-processing 2-photon images, we calculated the normalized fluorescence ($\Delta F/F0$,

Fig.3.1B, right) for each putative neuron (ROI). Next, we deconvolved the $\Delta F/F0$ into events (Event, Fig.3.1B, right) to avoid contamination of decaying GCaMP6s traces on several trials. We observed neurons responding to the visual stimuli presented (Fig.3.1B) and quantified the number of neurons whose activity was modulated by each visual stimulus independently (One-Way ANOVA, groups were grating types (combinations of direction, temporal and spatial frequency), or natural images IDs, or movie epochs (movie presentation was split in 1s bins)). Only neurons present on both days of imaging (Baseline/CNO) whose activity was modulated by the visual stimulus were included in the following analyses. Specifically, we included 331 neurons (hM4D(Gi)-FB group) and 509 neurons (Ctrl group) for the drifting gratings protocol, 363 neurons (hM4D(Gi)-FB group) and 446 neurons(Ctrl group) for the natural movies, and 698 neurons(hM4D(Gi)-FB group) and 930 neurons (Ctrl group) for natural images. To control for state modulations of neuronal responses, only periods in which the animal was stationary were included in the analyses, except for the natural movies protocol because of the low number of trials. In the next analysis, we made two important conceptual distinctions: (1) we defined tuning preference as the visual stimulus that drives maximal responses of a given neuron, and (2) neuronal tuning as the profile of neuronal responses to a given set of stimuli. Lastly, for fluidity in reading, we made two types of statistical comparisons. First, between the Baseline and CNO imaging days of the hM4D(Gi)-FB group to evaluate whether direct feedback modulated variables. Second, between hM4D(Gi)-FB and Ctrl groups to reject CNO off-target effects and mechanical damage.

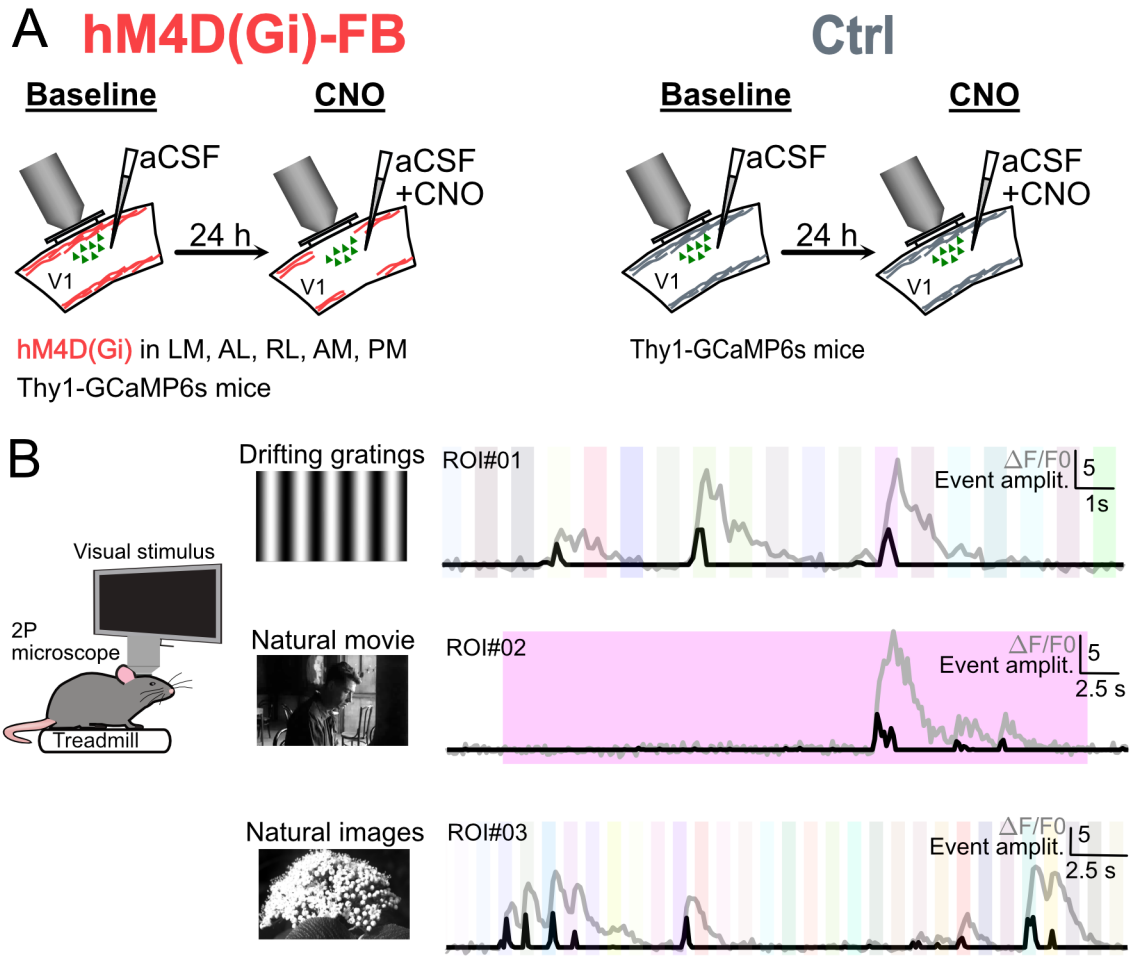

Figure 3.1: Experimental description and example traces
(A) Experimental groups. V1 was imaged on two consecutive days immediately after a local injection of aCSF (Baseline) or aCSF+CNO (CNO) in animals expressing hMD4(Gi) receptors in LM, AL, RL, AM and PM (Left, hM4D(Gi)-FB group). Control animals with no expression of hMD4(Gi) receptors were submitted to the same procedures (Right, Ctrl group). (B) Setup description and example responses. Left, mice were head-fixed under a two-photon microscope and allowed to run freely on a treadmill. Right, drifting gratings (top), natural movie (middle) and natural images (bottom) were presented to the animal's eye contralateral to the imaging hemisphere. Putative neurons (ROIs) were identified and $\Delta F/F0$ (gray line) calculated. $\Delta F/F$ traces were deconvolved into events (black line). Shaded areas mark visual stimulation. Colors indicate drifting grating types (combinations of direction, temporal and spatial frequency) or image IDs.

3.3.2 Tuning preference of V1 neurons to drifting gratings is not determined by HVA→V1 feedback

A neuron's tuning preference is defined as the stimulus that elicits the largest response. The orientation or direction preference of V1 L4 neurons is thought to be

determined by the arrangement of geniculate inputs (Hubel and Wiesel, 1962; Lien and Scanziani, 2013, 2018). Thus, we wondered whether such preference is modulated by direct HVA→V1 feedback. For each neuron, we calculated the tuning curve as the average activity for each motion direction angle of gratings for the combination of temporal and spatial frequencies that elicited the maximal response on Baseline and CNO imaging days. Upon visual inspection, we found neurons kept their preferred orientation and direction after silencing direct cortico-cortical feedback (Fig.3.2A). Next, we measured whether V1 tuning preference would remain unchanged at the population level after direct feedback silencing by calculating the preferred orientation and direction angle for each neuron at Baseline and CNO imaging days. We found that neurons kept their preferred orientation (hM4D(Gi)-FB group, Baseline vs. CNO, Watson- Williams test, p=1) (Fig.3.2B, left) and direction (hM4D(Gi)-FB group, Baseline vs. CNO, Watson-Williams test, p=1) (Fig.3.2B, right) after silencing direct HVA→V1 feedback. We inspected whether the tuning preference stability was due to direct feedback silencing by comparing the preferred orientation and direction angle between hM4D(Gi)-FB and Ctrl groups. We calculated the absolute difference between the preferred angles in Baseline and CNO imaging days for all neurons in each group (Δ preferred orientation or direction = |preferred $^{\circ}{}_{CNO}$ - preferred $^{\circ}{}_{Baseline}$|). We found no difference in the distributions of Δ preferred orientation (hM4D(Gi)-FB vs Ctrl group, Multi-sample test for equal median directions, p=0.23) (Fig.3.2C) or Δ preferred direction (hM4D(Gi)-FB vs Ctrl group, Multi-sample test for equal median directions, p=0.06) (Fig.3.2D). Thus, the tuning preference of V1 neurons to drifting gratings is not determined by direct HVA→V1 feedback.

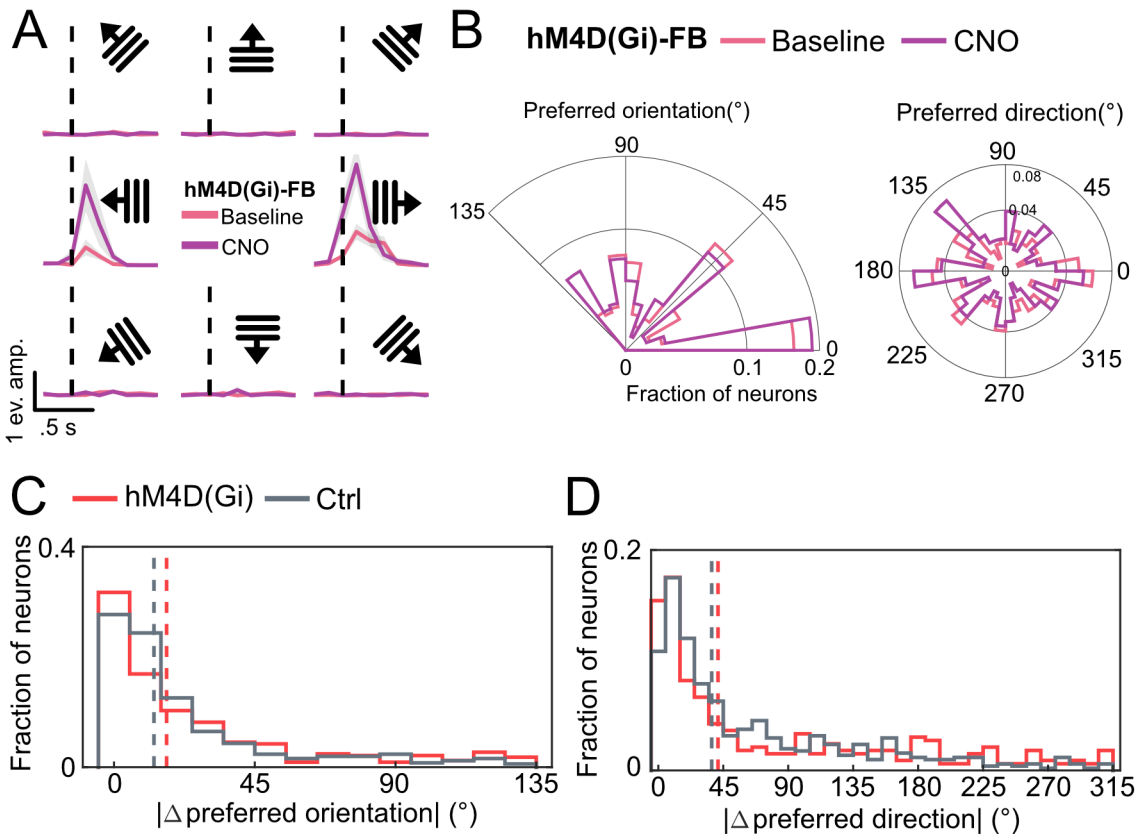

Figure 3.2: Silencing of direct HVA→V1 feedback does not modulate V1 preferred orientation or direction
(A) Example tuning curve (hM4D(Gi)-FB group). Mean activity to grating directions on Baseline (gray line) and CNO (yellow line) imaging days. Shaded area indicate SEM (n=20 trials). Dashed lines denote stimulus onset. (B) Distribution of preferred orientation (left) and direction (right) angle for Baseline (light pink) and CNO (dark pink) imaging days of the hM4D(Gi)-FB group. Watson-Williams test, p=1 and 1, respectively. (C) Distribution of Δ preferred orientation angle (Δ preferred orientation = |preferred $^{\circ}_{CNO}$ - preferred $^{\circ}_{Baseline}$|) of hM4D(Gi)-FB and Ctrl groups. Multi-sample test for equal median directions, p=0.23. (C) Distribution Δ preferred direction angle (Δ preferred direction = |preferred $^{\circ}_{CNO}$ - preferred $^{\circ}_{Baseline}$|) of hM4D(Gi)-FB and Ctrl groups. Multi-sample test for equal median directions, p=0.06. Dashed lines indicate medians.

3.3.3 Silencing direct HVA→V1 feedback sharpens orientation tuning curves of V1 neurons

Next, we wondered whether direct HVA feedback could modulate V1 orientation tuning curves so that neurons' preferred orientation would remain unchanged. To investigate that, we computed the average population tuning curve. We sorted each neuron's tuning curve by their preferred orientation and normalized it by the response amplitude of the preferred orientation on the Baseline imaging day. We found that

responses to drifting gratings in the preferred orientation were selectively enhanced on the CNO day in the hM4D(Gi)-FB group (Fig.3.3A, left) (Two-Way ANOVA, grating orientations and imaging days as groups, interaction p=1.2x10^{-8}, followed by Bonferroni post-hoc p=4.9x10^{-10}). Responses were similar across orientations for the Ctrl group (Fig.3.3A, right) (Two-Way ANOVA, grating orientations and imaging days as groups, interaction p=0.87). To check for unspecific effects, we compared orientation tuning curves of hM4D(Gi)- FB and Ctrl groups. We computed the difference between the population tuning curves of Baseline and CNO imaging days (tuning curve CNO - tuning curve Baseline) for both groups (Fig.3.3B). Silencing direct HVA feedback led to a selective increase of responses to the preferred orientation (Two-Way ANOVA, grating orientation and experimental groups as groups, interaction p=1.2x10^{-9}, followed by Bonferroni post-hoc p=1.6x10^{-12}) while not changing responses to the other orientations. We also observed a similar trend across animals (Fig.3.3C) (Hierarchical bootstrap, p=0.06). To quantify how direct feedback contributes to V1 responses to drifting gratings, we computed the global orientation selectivity index (gOSI) (Mazurek et al., 2014). In this index, values closer to one indicate that neuronal responses are more orientation-selective, while values close to zero indicate neurons respond to many different orientations. Previous studies which silenced HVAs produced conflicting results: one study has shown an increase in gOSI and gDSI (Oude Lohuis et al., 2021), and another suggests a decrease in those metrics (Pafundo et al., 2016). We found that gOSI was increased on the CNO day in the hM4D(Gi)-FB group (Fig.3.3D) (Baseline and CNO imaging days, Paired t-test, p=0.0001). To check for unspecific effects of CNO and mechanical damage, we compared gOSI of hM4D(Gi)-FB and Ctrl groups (Fig.3.3E). We computed the difference between the gOSI on 'Baseline' and 'CNO' imaging days (Δ gOSI = gOSI_{CNO} - $\text{gOSI}_{Baseline}$). In this index, positive values mean responses on the CNO imaging day were more orientation-selective than on the Baseline imaging day. In contrast, negative values mean the responses are more selective on the Baseline imaging day. We found an increase in ΔgOSI (hM4D(Gi)-FB vs Ctrl group, t-test, p = 6x10^{-8}), suggesting that the increase in gOSI at CNO imaging day is not due to unspecific effects of CNO injection. We also observed this effect when considering animal variability (Fig.3.3F) (Hierarchical bootstrap, p = 0.0044). These findings show that silencing of direct HVA$\rightarrow$V1 feedback results in a selective increase of the responses of V1 neurons to drifting gratings in their preferred orientation while not affecting responses to other orientations and hence sharpening the orientation tuning curves.

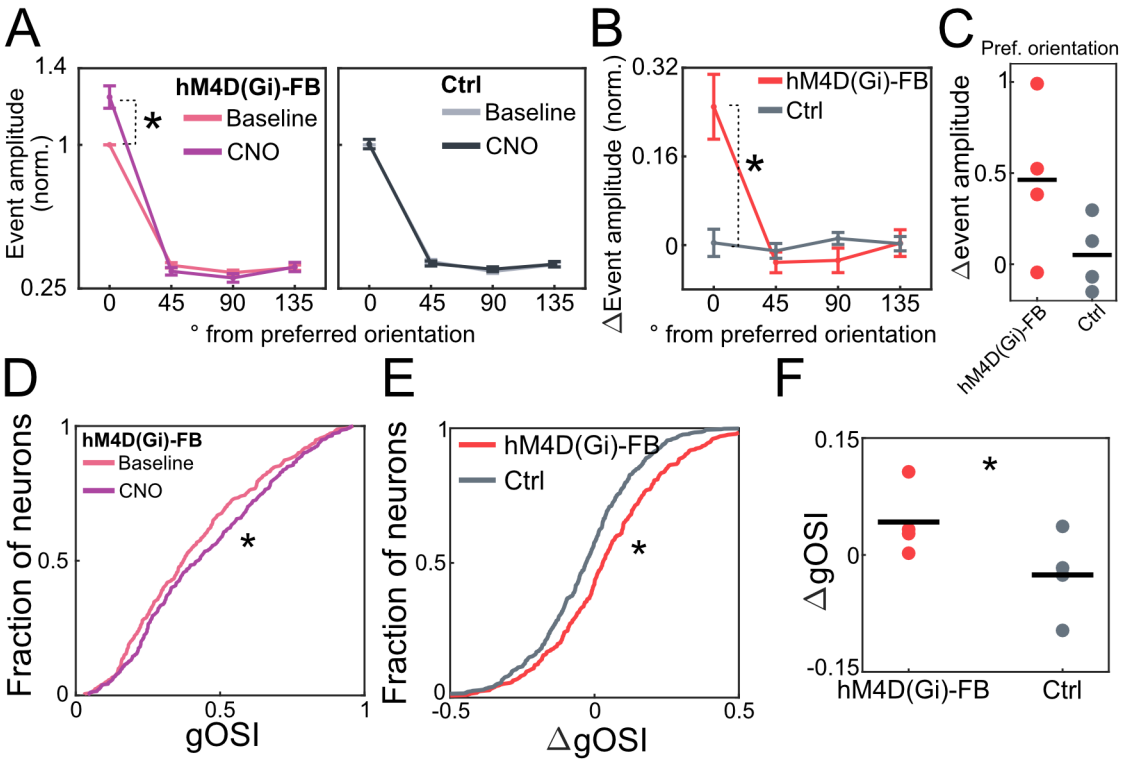

Figure 3.3: Silencing of direct HVA→V1 feedback facilitates visual responses to the preferred orientation

(A) Population tuning curves for Baseline and CNO imaging days. For each neuron, activity to each grating direction was normalised by the response amplitude to the preferred orientation defined at Baseline. Tuning curves were averaged across neurons. Error bars indicate SEM. Star indicates significance. Left, hM4D(Gi)-FB group. Two-Way ANOVA, grating orientations and imaging days as groups, interaction p=3x10^{-15}, followed by Bonferroni post-hoc p=1x10^{-18}). Right, Ctrl group. (B) Δ Population tuning curves for both groups (tuning curve $_{CNO}$ - tuning curve $_{Baseline}$). For each neuron, normalised tuning curves of CNO injection day were subtracted from Baseline. Error bars indicate SEM. Star indicates significance, Two-Way ANOVA, grating orientations and experimental groups as groups, interaction p=1x10^{-15}, followed by Bonferroni post-hoc p=1.6x10^{-59}. (C)Δ mean visual responses to preferred orientation per animal. Black lines indicate mean across animals. (D) Distributions of global orientation selectivity index (gOSI) per neuron for Baseline and CNO imaging days for the hM4D(Gi)-FB group. Star indicates significance. Paired t-test, p=0.0001. (E) Distributions of Δ global orientation selectivity index (ΔgOSI = gOSI $_{CNO}$ - gOSI $_{Baseline}$) per neuron for hM4D(Gi)-FB and Ctrl groups. Star indicates significance. t-test, p = 6x10^{-8}. (F) Mean ΔgOSI per animal. Black lines indicate mean. Star indicates significance. Hierarchical bootstrap, p=0.0044.

3.3.4 Silencing direct HVA→V1 feedback facilitates responses to the preferred direction

To investigate if the spatial-temporal structure of the visual stimulus could influence the observed sharpening of the orientation tuning curves, we examined V1

responses to all grating motion directions after silencing direct cortico-cortical feedback. We computed the average population tuning curve by sorting each neuron's tuning curve by their preferred direction and normalizing it by the response amplitude of the preferred direction at the Baseline imaging day (Fig.3.4A). We found that responses to drifting gratings moving in the preferred direction were selectively enhanced on the CNO day in the hM4D(Gi)-FB group (Fig.3.4A, left) (Two-Way ANOVA, grating directions and imaging days as groups, interaction p=3x10^{-15}, followed by Bonferroni post-hoc p=1x10^{-18}). Next, we checked for unspecific effects by comparing direction tuning curves of hM4D(Gi)-FB and Ctrl groups (Fig.3.4B). We computed the difference between the population tuning curves of 'Baseline' and 'CNO' imaging days (tuning curve $_{CNO}$ - tuning curve $_{Baseline}$) for both experimental groups. We found that silencing direct feedback increased about 17% in the responses to the preferred direction (Two-Way ANOVA, main factors: grating directions and experimental groups, interaction p=1x10^{-15}, followed by Bonferroni post-hoc p=1.6x10^{-59}). We also observed a small but non-significant increase in responses in the anti-preferred direction (180°). We observed similar trends across animals (Fig.3.4D) at the change in average activity to the preferred and anti-preferred grating direction (Hierarchical bootstrap, p=0.05 and 0.23, respectively). Next, we computed the global direction selectivity index (gDSI) (Mazurek et al., 2014). In this index, values closer to one indicate neuronal responses are more direction-selective, while values close to zero indicate neurons respond to many different directions of motion. Surprisingly, while inhibiting direct HVA feedback inputs in V1 increases V1 responses to gratings moving in the preferred direction of motion, it does not result in a robust increase in gDSI (Fig.3.4C) (Baseline and CNO imaging days, Paired t-test, p=0.24). This is probably due to the fact that our manipulation also result in a small increase in response to the anti-preferred direction. Therefore, direct HVA→V1 feedback modulates V1 tuning by selectively suppressing activity to the preferred direction, thus highlighting the temporal structure of the visual stimulus is fundamental for direct cortico-cortical modulations in V1.

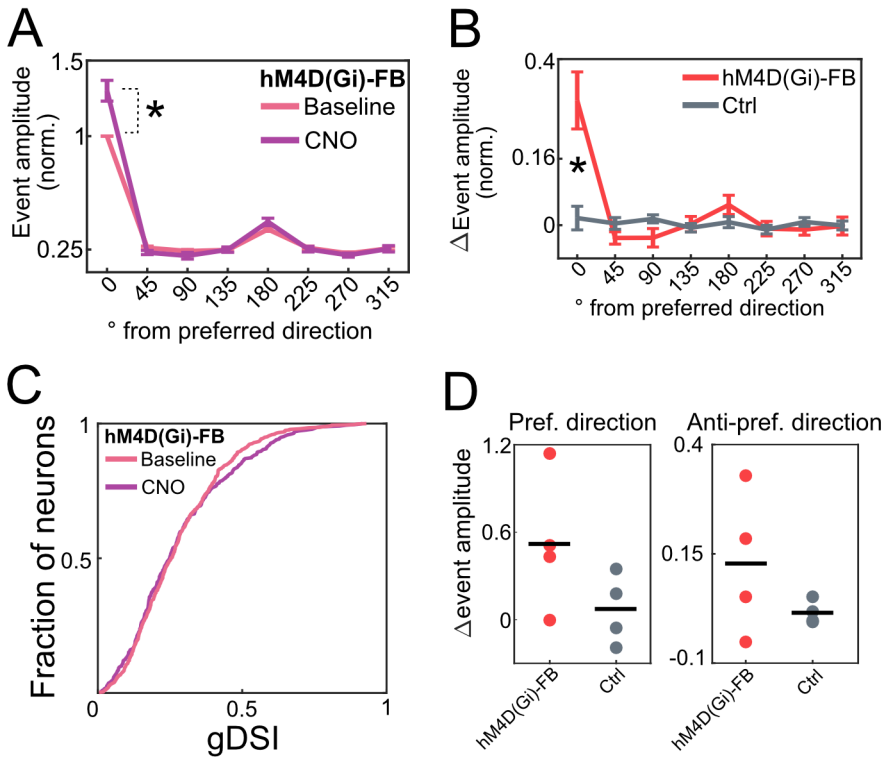

Figure 3.4: Silencing of direct HVA→V1 feedback facilitates visual responses to the preferred direction
(A) Population tuning curves for neurons in the Baseline and CNO imaging days of the hM4D(Gi)-FB group. For each neuron, activity to each grating direction was normalised by the response amplitude to the preferred direction defined at Baseline. Tuning curves were averaged across neurons. Error bars indicate SEM. Star indicates significance, Two-Way ANOVA, grating directions and imaging days as groups, interaction p=3x10^{-15}, followed by Bonferroni post-hoc p=1x10^{-18}). (B) Δ Population tuning curves for both groups (tuning curve $_{CNO}$ - tuning curve $_{Baseline}$). Error bars indicate SEM. Star indicates significance, Two-Way ANOVA, grating directions and experimental groups as groups, interaction p=1x10^{-15}, followed by Bonferroni post-hoc p=1.6x10^{-59}. (C) Distribution of global direction selectivity index (gDSI) per neuron for Baseline and CNO imaging days for the hM4D(Gi)-FB group. (D)Δ mean visual responses to preferred direction (left) and anti-preferred direction (right) per animal. Black lines indicate mean across animals.

3.3.5 V1 neurons change their tuning to natural movies upon silencing of direct HVA→V1 feedback

Following our previous finding that direct feedback modulates the tuning of V1 neurons to gratings, we wondered whether those projections would also modulate V1 responses to more complex stimuli, such as natural movies and natural images. We examined this by comparing the tuning curves to natural movies of Baseline and CNO imaging days for each experimental group. Tuning curves of natural movies were obtained by averaging activity across presentations of a 30s movie clip. We found many

neurons that responded during different periods of the movie for the Baseline and CNO imaging days (Fig.3.5A). To quantify how dissimilar were the tuning curves across the two imaging days, we measured the cosine similarity of the tuning curve vectors of Baseline and CNO imaging days. Cosine similarity is a distance metric which measures the cosine of the angle between two vectors in a multidimensional space. If tuning curves are similar between Baseline and CNO imaging days, cosine similarity values would be closer to 1 (Fig.3.5A, bottom), whereas values closer to 0 would mean a change in tuning (Fig.3.5A, top). We found a significant reduction in cosine similarity values of tuning curves of natural movies after silencing direct HVA→V1 feedback (Fig.3.5B) (hM4D(Gi)-FB vs Ctrl group, t-test, p=0.0001). This effect was also true when considering animal variability (Fig.3.5C) (Hierarchical bootstrap, p=0.01). Therefore, direct HVA→V1 feedback shapes the tuning of V1 neurons to natural movies. Specifically, V1 neurons respond to different movie epochs upon direct cortico-cortical feedback silencing.

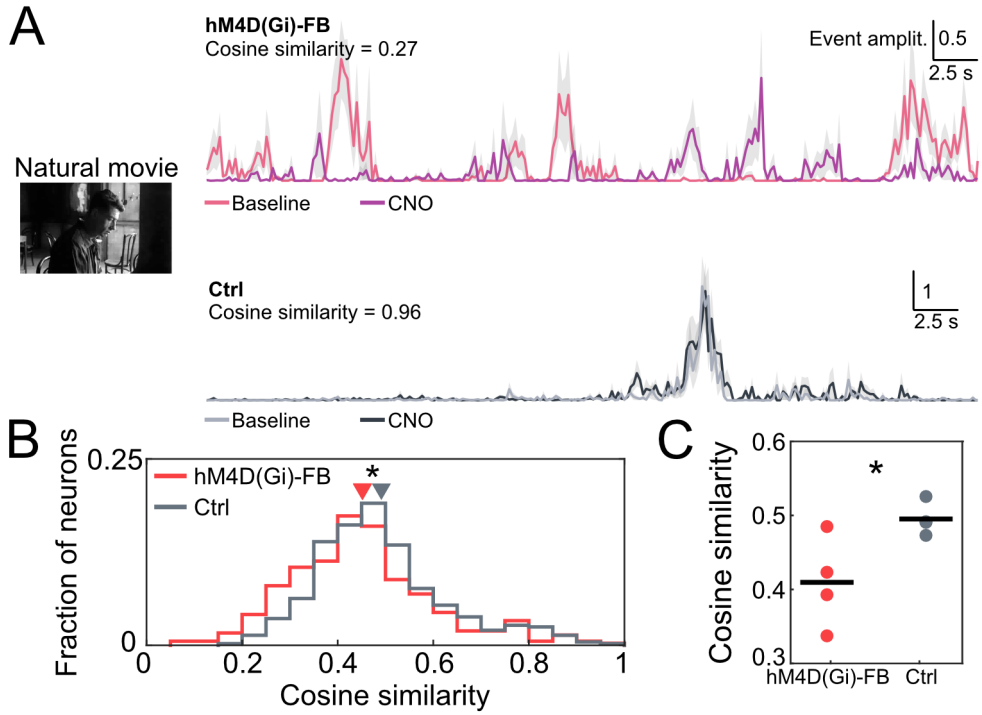

Figure 3.5: V1 tuning curves of natural movies change after direct feedback silencing
(A) Example natural movie tuning curves of two V1 neurons. Top, neuron from hM4D(Gi)-FB group. Bottom, neuron from Ctrl group. Each trace corresponds to the mean event amplitude across all trials for the entire movie presentation. Shaded areas represents standard deviation. (B) Left, distribution of cosine similarity values of natural movies tuning curves for both hM4D(Gi)-FB and Ctrl groups. For each neuron, cosine similarity was calculated between the tuning curve vectors of Baseline and CNO imaging days. Arrows indicate means, star indicates significance. t-test, p=0.0001. Right, distribution of cosine similarity per animal. Black lines indicate mean across animals, star indicates significance. Hierarchical bootstrap, p=0.01.

3.3.6 Silencing direct HVA→V1 feedback does not affect the tuning of V1 neurons to static natural images

Next, we wondered how relevant are the spatial-temporal statistics present in naturalistic stimuli for the observed tuning modulations of V1 responses to natural movies by direct cortico-cortical feedback. Suppose cortico-cortical modulations are dependent solely on spatial correlations present in the naturalistic stimulus. In that case, we expect the tuning of V1 neurons to static natural images to change upon direct HVA→V1 feedback silencing. However, if spatial-temporal correlations are fundamental, tuning curves of natural images would remain the same. To investigate that, we compared the tuning curves of natural images of neurons of Baseline and CNO imaging days for each experimental group using cosine similarity, as described before.

Tuning curves of natural images were obtained by averaging the activity in all trials of different images presented. We found that silencing direct feedback did not affect the cosine similarity values of tuning curves of natural images (Fig.3.6A) (hM4D(Gi)-FB vs. Ctrl group, t-test, p=0.5, and hierarchical bootstrap, p=0.4). This result was also verified across animals (Fig.3.6B). Therefore, these results indicate that the tuning of V1 neurons to naturalistic stimuli is modulated by direct cortico-cortical feedback and such modulation depends on spatial-temporal correlations present in the visual stimulus.

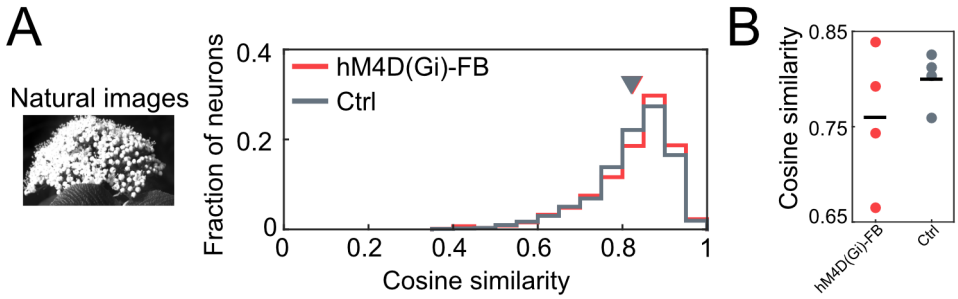

Figure 3.6: V1 tuning curves of natural images are stable after direct feedback silencing
(A) Distributions of cosine similarity values of tuning curves of natural images for both hM4D(Gi)-FB and Ctrl groups. For each neuron, cosine similarity was calculated between the tuning curve vectors of Baseline and CNO imaging days. Arrows indicate means. (B) Distribution of cosine similarity per animal. Black lines indicate mean across animals.

3.3.7 Selectivity of V1 neurons is unaltered upon direct HVA→V1 feedback silencing

The reduction in the cosine similarity of the responses of V1 neurons to the natural movie after silencing direct HVA→V1 feedback could be due to the neurons gaining new responses to some parts of the movie without losing their previous tuning (Fig.3.7A). Alternatively, V1 neurons might gain responses to parts they were unresponsive before while also losing their previous responses. In the former, the selectivity of V1 neurons for specific frames of the movie would be reduced, while in the latter, the selectivity would be unchanged. To measure the selectivity of V1 neurons, we divided the movie into 30 epochs of 1 second each (movie epochs). For each neuron, we quantified the number of movie epochs for which neurons were significantly active by comparing the activity of each movie epoch to the activity prior to the movie presentation (gray monitor) using a t-test. Neurons in the hM4D(Gi)-FB group responded to the same number of movie epochs on the Baseline and CNO days (Fig.3.7B) (Mann–Whitney U test, p=0.08). We compared the number of movie epochs across

experimental groups by calculating the difference of the number of movie epochs between imaging days (Δ number of movie epochs = number of movie epochs$_{CNO}$ - number of movie epochs$_{Baseline}$). Positive values of the number of movie epochs reflect a reduction in selectivity, while negative values reflect an increase in selectivity. We observed no change in selectivity of V1 neurons upon silencing of direct cortico-cortical feedback (Fig.3.7C) (hM4D(Gi)-FB vs Ctrl groups, t-test, p=0.1). This result was also verified across animals (Fig.3.7D) (Hierarchical bootstrap, p=0.78). We also verified this result by measuring another metric for neuronal selectivity, the lifetime sparseness of neuronal responses. Lifetime sparseness refers to the kurtosis of the distribution of neuronal responses of a single neuron to many stimuli (Willmore et al., 2011). We compared the Δ lifetime sparseness across experimental groups by calculating the Δ lifetime sparseness (Δ lifetime sparseness = lifetime sparseness$_{CNO}$ - lifetime sparseness$_{Baseline}$). We observed no changes in lifetime sparseness upon direct cortico-cortical feedback silencing (Fig.3.7E) (hM4D(Gi)- FB vs Ctrl groups, t-test, p=0.26). Thus silencing direct HVA$\rightarrow$V1 inputs results in changes in the tuning of V1 neurons to natural movies without broadening their selectivity, indicating neurons gain responses to parts they were unresponsive and lose a fraction of their previous responses.

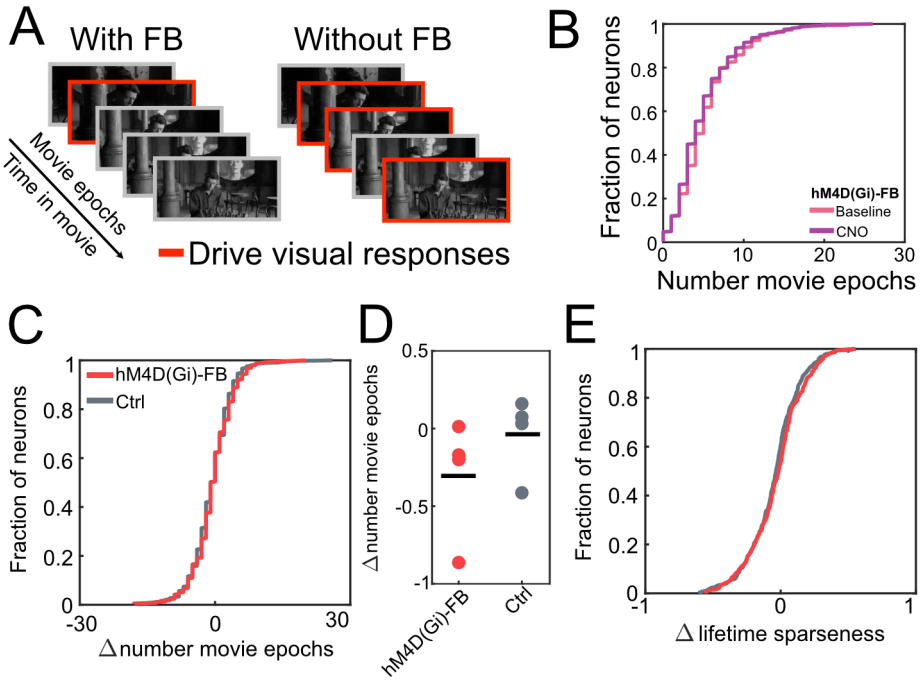

Figure 3.7: Silencing of direct HVA→V1 feedback does not change selectivity of V1 neurons
(A) Toy model showing how direct HVA→V1 inputs can contribute to an increase in selectivity to natural movie stimuli. When direct feedback is functional, a specific part of the movie (movie epoch) drives visual responses in a neuron in V1. After feedback is removed, neurons in V1 respond to more movie epochs (decreased selectivity), resulting in a novel tuning curve. (B) Distributions of number of movie epochs that significantly drive V1 neurons in the Baseline and CNO imaging days of the hM4D(Gi)-FB group. (C) Distributions of Δ number of movie epochs (Δ number of movie epochs = number of movie epochs $_{CNO}$ - number of movie epochs $_{Baseline}$) for hM4D(Gi)-FB and Ctrl groups. (D) Δ number of movie epochs across animals for each experimental group. Black lines indicate means across animals. (E) Distributions of Δ lifetime sparseness for neurons in the hM4D(Gi)-FB and Ctrl groups.

3.3.8 Direct HVA→V1 feedback increases the diversity of representations in V1

Following our finding that neurons gain responses to novel parts of the natural movie, we asked: are responses added to similar movie parts across the neuronal population (Fig.3.8A)? This hypothesis implies that HVA→V1 feedback inputs participate in mechanisms underlying the diversification of V1 representations. To test that we measured the similarity of tuning curves across the population of V1 neurons, we computed the Pearson's correlation of the tuning curves between all pairs of neurons (signal correlations) in each imaging session. Upon visual inspection, we found that tuning curves of neurons were more correlated across the neuronal population after silencing direct cortico-cortical feedback (Fig.3.8B). We quantified the correlation of

tuning curves for all pairs in the Baseline and CNO days for the hM4D(Gi)-FB and Ctrl group. We found that the signal correlations of neurons pairs were specifically increased on the CNO day in the hM4D(Gi)-FB group (Baseline vs CNO imaging days, paired t-test, p=8x10^{-8}, n_{pairs}=10282) but not in the Ctrl group (Baseline vs CNO imaging days, paired t-test, p=0.2, n_{pairs}=17479) (data not shown). To check for unspecific effects, we compared signal correlations of neuron pairs of the hM4D(Gi)-FB and Ctrl group by calculating the difference in the correlation coefficients of neuron pairs between imaging days (Δ signal correlations = correlation coefficient $_{CNO}$ - correlation coefficient $_{Baseline}$). We found that the enhancement in signal correlations was not due to unspecific effects (Fig.3.8C) (hM4D(Gi)-FB vs Ctrl group, t-test, p=7x10^{-8}). This was also true when considering animal variability (Fig.3.8D) (Hierarchical bootstrap, p=0.0025). Thus, tuning curves of different V1 neurons become more similar after silencing direct cortico-cortical feedback, as neurons tend to gain responses to similar movie epochs.

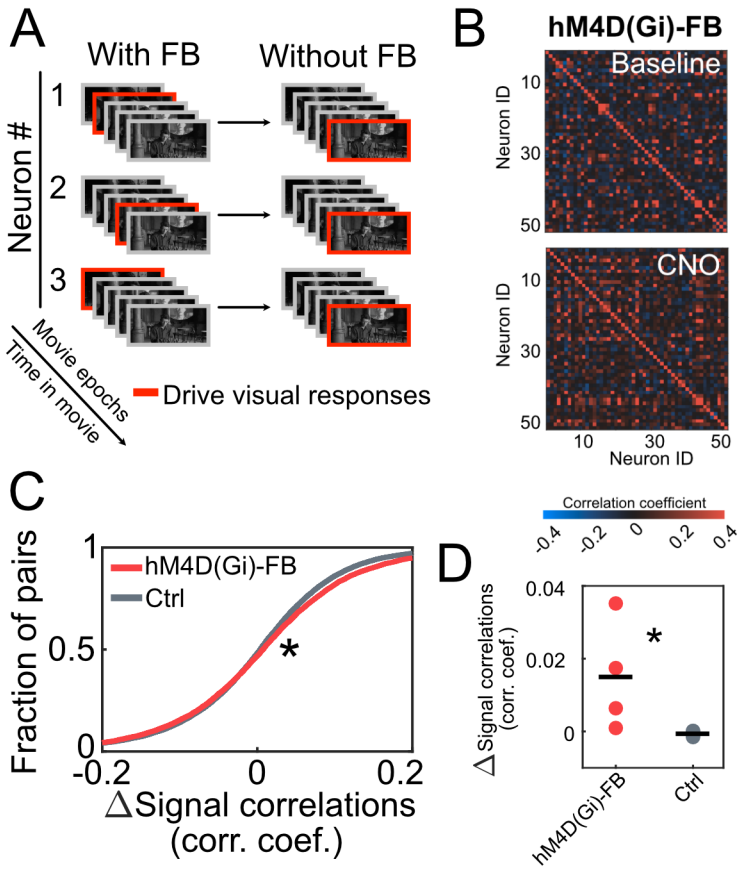

Figure 3.8: Silencing of direct HVA→V1 feedback results in an increase in signal correlations
(A) Toy model showing how direct HVA→V1 inputs can diversify representations of natural movies at the V1 population level. When direct feedback is functional, neurons have a tuning preference to particular part of the movies. After feedback is removed, neurons respond to novel and similar movie parts, making their responses become more correlated. (B) Signal correlations of example session pair. Colorbar indicates Pearson's correlation coefficient at Baseline (top) and CNO (bottom) imaging days. (C) Distributions of Δ Signal correlations (Δ Signal correlations = correlation coefficient $_{CNO}$ - correlation coefficient $_{Baseline}$). Star indicates significance. t-test, p=7x10^{-8}. (D) Δ Signal correlations across animals for each experimental group. Black lines indicate mean across animals, star indicates significance. Hierarchical bootstrap, p=0.0025.

3.3.9 Direct HVA→V1 feedback decorrelates V1 trial-to-trial fluctuations

The amount of information encoded by a neuronal population is dependent on the correlations of trial-to-trial responses. Since calcium imaging allows us to simultaneously record from hundreds of neurons, we have access to the variability in trial-by-trial responses, known as noise correlations. To investigate whether direct feedback also

modulates this aspect of stimulus encoding, we computed the noise correlations across pairs of neurons. We found imaging sessions in which silencing direct cortico- cortical feedback led to an increase in noise correlations (Fig.3.9A). We quantified the noise correlation across all neuron pairs in the Baseline and CNO days for the hM4D(Gi)-FB and Ctrl groups. We found that the noise correlations specifically increased on the CNO day in the hM4D(Gi)-FB group (Baseline vs CNO imaging days, paired t-test, p=2x10^{-64}, n_{pairs}=69020) but not in the Ctrl group (Baseline vs CNO imaging days, paired t-test, p=0.8, n_{pairs}=121970) (data not shown). We calculated the CNO-induced changes in noise correlation as the difference between imaging days (Δ Noise correlations = correlation coefficient $_{CNO}$ - correlation coefficient $_{Baseline}$) for each experimental group. We observed that increases in noise correlations were higher in the hM4D(Gi)-FB than in the Ctrl group (Fig.3.9B) (hM4D(Gi)-FB vs Ctrl group, t-test, p=2x10^{-45}), showing that the enhancement in noise correlations was not due to unspecific effects of CNO. This was also true when considering animal variability (Fig.3.9C) (Hierarchical bootstrap, p=0.0004). Therefore, direct HVA→V1 feedback modulates average tuning curves to natural movies and information encoding in a trial-to-trial fashion by decorrelating V1 activity.

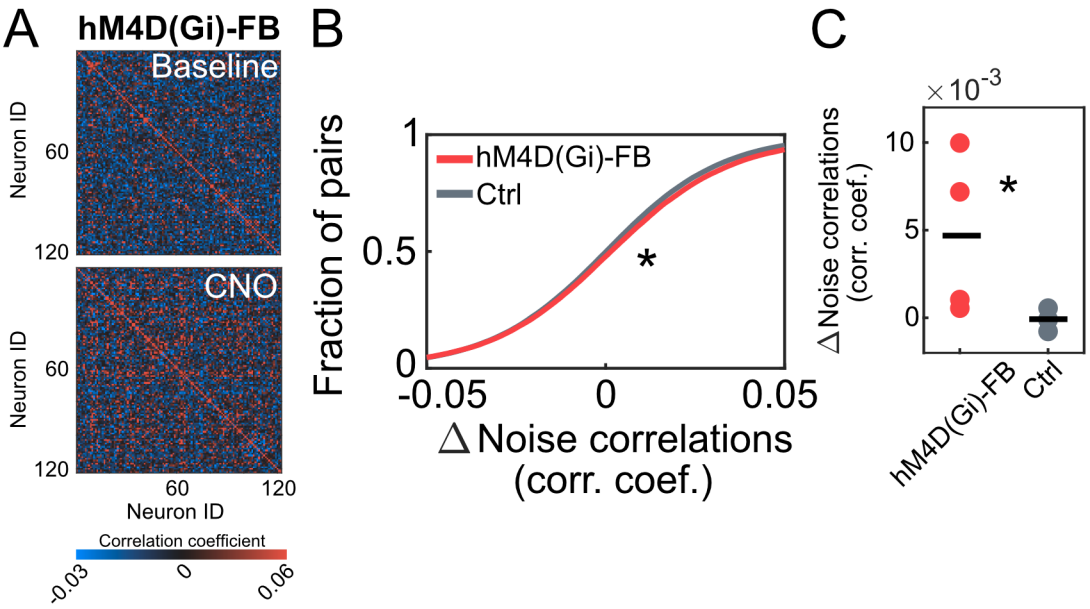

Figure 3.9: Silencing direct feedback leads to an increase in noise correlations
(A) Noise correlations of example session pair. Colorbar indicates Pearson's correlation coefficient at Baseline (top) and CNO (bottom) imaging days. (B) Distribution of Δ Noise correlations (Δ Noise correlations = correlation coefficient $_{CNO}$ - correlation coefficient $_{Baseline}$) for hM4D(Gi)-FB and Ctrl groups. Star indicates significance. t test, p=2x10^{-45}.(C) Δ Noise correlations across animals for hM4D(Gi)-FB and Ctrl groups. Black lines indicate mean across animals, star indicates significance. Hierarchical bootstrap, p=0.0004.

3.4 Discussion

In this study, we tested the contributions of direct cortico-cortical feedback from HVAs on the representations of V1 neurons of different visual stimuli. We measured V1 L2/3 responses to drifting gratings, natural images, and natural movies while suppressing the activity of direct HVA→V1 feedback in the awake non-behaving mouse. We found that suppression of direct cortico-cortical feedback affects V1 responses to drifting gratings and natural movies but not to natural images. We showed that V1 preference for moving gratings of particular orientations was unaltered upon direct feedback silencing, yet tuning for orientation became sharper due to selective enhancement of activity at the preferred direction angle. Furthermore, silencing direct HVA→V1 feedback resulted in V1 neurons responding to different parts of the natural movie. This gain in responses tended to be for similar epochs of the movie across the population of V1 neurons. Silencing direct HVA→V1 feedback also resulted in more correlated trial-to-trial fluctuations across neurons.

3.4.1 Direct cortico-cortical feedback suppresses responses to the preferred orientation

We find that the orientation and direction tuning preference of V1 neurons is maintained after silencing direct HVA→V1 feedback. This is consistent with previous studies that suppressed the activity of neurons in HVAs and reported no changes in the tuning preference of V1 neurons (Oude Lohuis et al., 2021; Pafundo et al., 2016). Neurons in layer 4 of V1 are mainly driven by feedforward connections, and their tuning preference for segments of specific orientation is thought to arise mainly from the spatial arrangement of the lateral geniculate inputs converging on V1 neurons (Hubel and Wiesel, 1962; Lien and Scanziani, 2013). Thus, the sensory cortex is the first stage of processing of orientation selectivity. Our results suggest that the orientation and direction tuning preference of L2/3 neurons, like in L4, is also driven primarily independent of feedback connections. However, while preference for specific moving gratings did not change when silencing HVA→V1 feedback inputs, tuning curves of V1 neurons became sharper. This increased selectivity mainly came through specific enhancement of responses to the preferred direction when silencing HVA→V1 feedback inputs. Thus, under normal conditions, HVA→V1 feedback inputs might selectively hamper the responses of V1 neurons to their preferred stimulus through selective inhibition.

As feedback connections are mainly excitatory, the inhibitory effects of HVA→V1 inputs on excitatory neurons have to be mediated disynaptically through inhibitory

interneurons. However, it is unclear how this inhibition of V1 responses by feedback inputs is selective for the preferred stimulus. As the strength of feedback inputs is lower than the feedforward ones, feedback connections might only be able to enhance activity in its target interneurons for the preferred stimulus. Some subpopulations of interneurons like the somatostatin-positive (SOM) (Ma et al., 2010) and subsets of L1 interneurons (Cohen-Kashi Malina et al., 2021) are orientation-selective. Thus, our results are consistent with L2/3 neurons being inhibited by co-tuned, orientation-selective interneurons that are in turn innervated by cortico-cortical feedback from HVAs. Such an arrangement would result in the observed selective increase in responsivity of L2/3 neurons for the preferred stimuli when silencing HVA→V1 feedback inputs while sparing responses to non-preferred orientations. Future experiments that combine *in vivo* recordings of interneurons and manipulations of direct cortico-cortical feedback would help access this hypothesis.

V1 responses to drifting gratings of increasing size become increasingly suppressed. This suppression depends on feedback inputs from HVA (Keller et al., 2020b; Nassi et al., 2013; Nurminen et al., 2018; Vangeneugden et al., 2019). As feedback inputs from HVAs converging onto V1 neurons are excited by positions surrounding the receptive field of the target neurons (Marques et al., 2018a), the recruitment of feedback inputs from HVAs by gratings of larger diameter is thought to mediate the reduction of V1 responses through interactions with specific interneurons (Keller et al., 2020a). The grating we presented encompassed the full extent of the monitor, corresponding to 120°in azimuth and 60°in elevation. Given its large size, the visual stimulus most likely was surround suppresing V1 responses. Thus, the increase in responses to preferred orientation observed when silencing HVA→V1 feedback inputs likely results from a release of surround suppression.

Evidence suggests that surround suppression occurs even if the stimulus presented is not in the preferred orientation of the recorded neuron. However, it is maximal when the orientation within the receptive field and surround are identical (Shushruth et al., 2012). Our study observed only small and non-significant increases in the activity to the anti-preferred direction after silencing HVA→V1 feedback inputs. Such small modulations suggest that minor effects of surround modulation to non-optimal stimuli could be hidden because of the low sensitivity of GCaMP to detect a few spikes (Chen et al., 2013). The slight increase of activity in the non-preferred direction, combined with the significant increase in the activity in the preferred direction, also contributed to the enhancement of orientation but not direction selectivity. Enhancement of orientation selectivity upon feedback silencing is consistent with another study in the mouse that silenced areas AL and PM (Oude Lohuis et al., 2021). Although that

study used moving bars that are known to recruit less surround suppression, some modulations of feedback connections on orientation tuning might be independent of surround modulation.

Finally, our results are consistent with previous observations showing that HVA are critically involved in surround suppression in the monkey (Nassi et al., 2013) and mouse (Vangeneugden et al., 2019) V1. They also show that HVA-mediated surround suppression of V1 responses is likely mediated by direct cortico-cortical inputs terminating in V1 independently of other indirect pathways, as previously shown in the marmoset (Nurminen et al., 2018). Surround modulations are essential to the visual processing of animals. In the wild, animals do not encounter a visual stimulus in isolation but embedded in a rich context (Angelucci et al., 2017). Hence, conservation of surround modulations and their circuits are expected. Our findings suggests that, at least in part, the circuit underlying surround suppression is conserved in the mouse and monkeys.

3.4.2 Tuning of V1 neurons to natural movies depends on direct cortico-cortical feedback

Neurons in V1 are known to respond sparsely to naturalistic stimuli (Deitch et al., 2021; Froudarakis et al., 2014; Xia et al., 2021; Yoshida and Ohki, 2020), which is thought to reflect the amount of redundancy present in the natural world. For example, nearby pixels tend to have similar luminance values. Hence, to make stimulus coding more efficient and less redundant, each stimulus drives robust responses in only a small number of neurons (Field, 1994). Our results agree with previous studies and show that natural movies and natural images drive sparse responses in V1 neurons, rendering them highly selective. Furthermore, we found that the tuning of V1 neurons to natural movies depends on direct cortico-cortical feedback. Silencing HVA→V1 inputs results in V1 neurons responding to different parts of the natural movie. However, added responses were not accompanied by changes in the selectivity of V1 neurons. Moreover, the increase in signal correlations upon silencing direct HVA→V1 feedback shows V1 neurons added responses to similar parts of the natural movies, turning their tuning curves more similar across the population of V1 neurons. Thus, our findings suggest that direct cortico-cortical inputs participate in mechanisms to diversify responses in V1 and thus reducing the redundancy of representations in V1 at the population level.

Stimulation of the surround of a V1 neuron's receptive field with naturalistic stimuli modulates V1 responses. For instance, it increases the selectivity of individual V1 neurons (Vinje and Gallant, 2000), results in more information transmitted with

higher efficiency (Vinje and Gallant, 2002), and decorrelates the activity of V1 neuron pairs (Vinje and Gallant, 2000). Are feedback connections the substrate of the surround-mediated sparseness of V1 responses? We observed that the selectivity of V1 neurons to natural movie epochs and lifetime sparseness was unchanged after silencing direct cortico-cortical feedback, suggesting other anatomical substrates for such phenomena. However, upon silencing direct HVA→V1 feedback, V1 tuning curves and trial-to-trial fluctuations became more correlated, suggesting direct HVA feedback inputs decorrelation mediated by surround stimulation. The observed increase in noise correlations could simply reflect the reduction of variability resulting from the removal of inputs (feedback connections) to V1 neurons. The concomitant increase in signal correlations opposes this idea since noise correlations are stronger in neuron pairs with similar tuning preferences (Cohen and Kohn, 2011). Thus, our findings suggest that direct cortico-cortical feedback conveys surround information to reduce the redundancy of V1 representations of natural movies at the population level. However, it does not participate in sparsification of responses of individual V1 neurons.

Lastly, could the statistics of the natural movies account for the differential effects of direct cortico-cortical feedback? Our data indicate that the natural vs. artificial stimulus's nature is not the sole explanation for our results because the tuning to natural images was stable after silencing direct HVA→V1 feedback. However, far more images were present in natural movies than in the set of natural images (75 images). Hence, an absence of an effect could originate from a non-optimal selection of visual features in the natural images. The stationary nature of natural images could also explain the lack of direct cortico-cortical feedback modulation in V1 responses. Natural movies have complex spatial-temporal correlations that are not present in the natural images. The fact that HVA→V1 feedback modulates V1 responses to drifting gratings, a non-stationary stimulus, reinforces this hypothesis. Further experiments that carefully manipulate spatial-temporal components of the visual stimuli combined with silencing direct cortico-cortical feedback, or simultaneous recording of HVAs, could help address this hypothesis.

3.4.3 Direct cortico-cortical feedback modulations depend on spatial-temporal correlations of the visual stimuli and surround stimulation: a toy model

How could the tuning preference of V1 neurons to natural movies be differently modulated by direct cortico-cortical feedback? The context in which the stimulus is embedded influences the tuning of V1 neurons. In the visual system, such context can be the visual scene surrounding a stimulus. Modulations from the surround are

dependent on top-down signals, such as surround suppression (Nassi et al., 2013; Nurminen et al., 2018; Vangeneugden et al., 2019) and facilitation (Keller et al., 2020b). In the mouse, stimulation of the surround alone drives responses of L2/3 neurons in the mouse V1 (Keller et al., 2020b). Moreover, surround stimulation with naturalistic stimuli has been shown to modify V1 responses (Vinje and Gallant, 2000, 2002). Cortico-cortical feedback is a suitable candidate to mediate surround modulations of V1 responses because feedback has been shown to bring distant information from the receptive field center to V1 neurons (Keller et al., 2020b; Marques et al., 2018a). Hence, we propose that the tuning preference of V1 neurons to natural movies depends on cortico-cortical feedback inputs, which are recruited by spatial-temporal correlations of surround signals.

This idea can be illustrated with a simplified example: the receptive field (RF) and surround (S) of two V1 neurons, N_1 and N_2, are stimulated with drifting gratings, natural images, and natural movies (Fig.3.10). Because N_1 and N_2 are in close anatomical proximity, they have equal RF locations and hence the same visual features within the RF. While feedforward connections provide V1 neurons with information from the RF visual features, feedback connections convey S features. In the case N_1 and N_2 are stimulated with full field gratings, the tuning preference to orientation and direction is independent of HVA feedback inputs and hence is mainly defined by feedforward connections, as demonstrated by our results. Thus the tuning preference of N_1 and N_2 when direct cortico-cortical feedback is present or absent is the same (Fig.3.10A, table), and responses reflect the features in the RF (90°).

In the second case, the RF and S of N1 and N2 are stimulated with natural images (Fig.3.10B). Natural images are composed of a complex set of spatial correlations, within the RF and between the RF and the S. The RF visual features are conveyed to N1 and N2 by feedforward inputs whose tuning preference is the natural image that contains such features, I_0. Although composed of complex spatial features, our results indicate that spatial correlations do not recruit direct cortico-cortical feedback. Hence, HVA inputs do not contribute to the tuning of V1 neurons to natural images. Therefore, the tuning preference of N_1 and N_2 in the presence or absence of HVA→V1 feedback inputs is similar (Fig.3.10B, table). It is unclear which mechanisms give rise to diverse and sparse responses of V1 neurons to natural images. Further studies could investigate whether their tuning could be inherited from geniculate inputs or result from mechanisms involving indirect feedback pathways or horizontal connections.

In the last case, the RF and S of N_1 and N_2 are stimulated with natural movies (Fig.3.10C). Unlike the natural images, the S and R are composed of complex spatial and temporal features. Spatial-temporal features are encoded by cortico-cortical

feedback projections in the mouse since they show tuning to motion (Marques et al., 2018a). In this scenario, spatial-temporal correlations between the RF and S recruit feedback inputs from HVAs, which, in turn, modify the tuning of V1 neurons. In particular, the RF visual features are conveyed to N_1 and N_2 by feedforward inputs whose tuning preference is the movie epoch which contains such features, E_0. Whereas N_1 is modulated by a set of surround spatial-temporal features (S_1), N_2 is modulated by another set of surround spatial-temporal features (S_1). Consequently, N_1 and N_2 respond to different movie parts (E_1 and E_2, respectively). In the absence of direct HVA feedback, the influences of S_1 and S_2 are removed, and thus N_1 and N_2 responses are biased towards the features encoded by feedforward connections. Therefore, N_1 and N_2 respond to a novel and similar movie epoch, E_0.

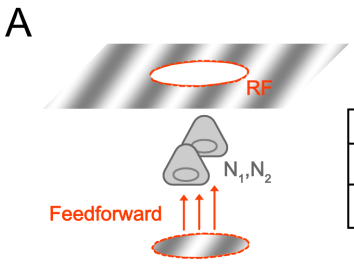

		Direct HVA Feedback	
		Present	Absent
Neuron	RF	Pref.	Pref.
N_1	90°	90°	90°
N_2	90°	0°	0°

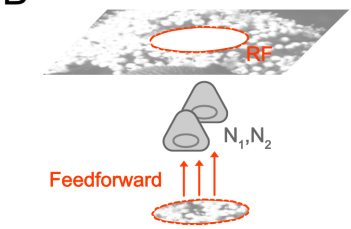

		Direct HVA Feedback	
		Present	Absent
Neuron	RF	Pref.	Pref.
N_1	I_0	I_1	I_1
N_2	I_0	I_2	I_2

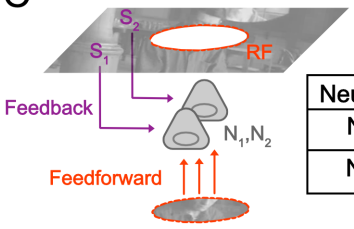

			Direct HVA Feedback	
			Present	Absent
Neuron	RF	S	Pref.	Pref.
N_1	E_0	S_1	E_1	E_0
N_2	E_0	S_2	E_2	E_0

Figure 3.10: Direct cortico-cortical feedback modulations: toy model
(A) Drifting gratings stimulate the center of the receptive field (RF) and surround (S) of neurons 1 (N_1) and 2 (N_2) in V1. Table: tuning of N_1 and N_2 in the presence or absence of direct cortico-cortical feedback. In the presence of feedback the preferred orientation of N_1 is 90° and of N_2 is 0°. Because cortico-cortical feedback is not recruited by drifting gratings, the responses of N_1 and N_2 reflects features in RF and hence tuning preference is unaltered in the absence of feedback. (B) Natural images stimulate RF and S of neurons 1 (N_1) and 2 (N_2) in V1. Table: tuning of N_1 and N_2 in the presence or absence of direct cortico-cortical feedback. In the presence of feedback the tuning preference of N_1 is I_1 and of N_2 is I_2. Because cortico-cortical feedback is not recruited by spatial correlations present in the natural images, the tuning preference of N_1 and N_2 is unaltered in the absence of feedback. (C) Natural movies stimulate RF and S of N_1 and N_2 in V1. Table: tuning of N_1 and N_2 in the presence or absence of direct cortico-cortical feedback. While preferred movie epoch (E) of N_1 is E_1 and it's response is modulated by S_1, the preferred E of N_2 is E_2 and it's response is modulated by S_2. Because of spatial-temporal correlations between RF and S, direct feedback conveys distal information from the visual scene to V1 modifying the tuning of N_1 and N_2. In the absence of feedback, the responses of N_1 and N_2 reflects features in RF and hence the tuning preference of feedfoward inputs (E_0).

3.4.4 Predictive processing and direct cortico-cortical feedback modulations

Perception is thought to be a constant and active process because the brain continuously constructs explanations for its sensory inputs. Predictive processing is a feasible candidate theory for implementing such inferences, in which feedback connections are thought to carry predictions about the stimulus (Bastos et al., 2012; Rao and Ballard, 1999). In this framework, visual features of a stimulus in the surround region can be used to estimate the visual features present in the receptive field. The predictive signals relayed by cortical feedback are compared with the incoming, bottom-up sensory information. When sensory information matches the predictive signal, sensory responses are suppressed. When the sensory information does not match the prediction, sensory inputs result in an increase in activity signaling a prediction error.

The predictive coding framework successfully explains surround suppression (Rao and Ballard, 1999) and other properties of cortical responses (Bastos et al., 2012; Leinweber et al., 2017). Our findings are also consistent with predictive coding theories. The enhancement of the responses of V1 neurons to drifting gratings when silencing direct cortico-cortical feedback is expected under the predictive coding framework. Silencing feedback inputs removes the predictive signals usually compared with bottom-up inputs, resulting in the cancellation of redundant, expected, bottom-up input during surround suppression.

Cortical feedback from HVA relays visual information from locations surrounding the receptive field of V1 neurons (Keller et al., 2020b; Marques et al., 2018a). When presented with natural movies or images, these projections are thought to signal learned expectations between the surround and center. Consistent with this, visual deprivation degrades how V1 represents natural scenes (Kowalewski et al., 2021), while visual experience shapes the influences of the surround on V1 responses to natural images (Pecka et al., 2014). Thus, according to the predictive coding framework, silencing cortical feedback inputs from HVAs should result in an increase in error signals in V1, as learned predictions from the surround, which are normally used to cancel V1 activity in the center, are reduced. However, we did not observe increased evoked activity in V1 when silencing HVA→V1 feedback when presenting natural movies or natural images to the mouse (data not shown). Adding to that, axon terminal silencing using DREADDs lasts several hours (Stachniak et al., 2014), and our recordings started more than 30 min after injecting CNO in V1. Thus, the prediction error signaling neurons in L2/3 may have already adapted to the reduction of feedback inputs, decreasing their error-related activity by the time of our measurements. Experiments

using axon silencing methods with a higher temporal resolution, like eOPN3 (Mahn et al., 2021), should allow settling this issue.

3.5 Materials and Methods

Most procedures were already described in Chapter 02. Here I describe the materials and methods specific to the results presented in this chapter.

3.5.1 Two-photon calcium imaging

We used a microscope with similar specifications as described in Chaper 02. Imaging of calcium indicators of V1 somas was also done as described in Chapter 02. Imaging position was centered in V1 monocular zone guided by intrinsic imaging and immediately beside the hole used for injection of solutions.

3.5.2 Visual stimuli

Visual stimuli was presented as described in Chapter 02. Three different sets of visual stimulus were presented in full-screen: drifting gratings, natural images and natural movies.

Mice were presented with full field, full-contrast drifting gratings. Gratings moved in one of eight directions (cardinals and obliques). Gratings had a spatial frequency of 0.02 or 0.04 cpd and a temporal frequency of 0.5 or 1Hz. Each grating type (combination of direction, spatial frequency and temporal frequency) was repeated 20 times. The structure of the trials was as follows: 0.25s of gray screen, 0.5s of visual stimulation (stimulus period), 0.25s of gray screen.

For the natural movies, we used a black and white clip (30s) from the movie Nineteen Eighty-Four (directed by Michael Radford, 20th Century Fox, 1984). This natural movie was presented 10 times. The structure of the trials was as follows: 3s of gray screen, 30s of visual stimulation (stimulus period), 2s of gray screen.

Additionally, a set of 75 natural images were presented to the animal in a full-screen, full-contrast, black and white configuration. They were selected from the Hans van Hateren's dataset of natural images (Van Hateren and Van der Schaaf, 1998) based on their power spectrum (FFT) to match known V1 neurons preferred spatial frequencies and orientations.

3.5.3 Data analysis

Pre-processing of calcium imaging data

For each imaging session, images were registered, neurons were identified and curated and F traces (soma and neuropil) extracted using the Suite2p toolbox (Pachitariu et al., 2016). Neuropil F traces were subtracted from soma F traces using 70% of the total neuropil F trace detected. After that, we calculated each ROI baseline fluorescence, F0, as the 30th percentile of the F traces using a 60s sliding window and calculated the Δ F/F as follows:

$$\Delta F/F = \frac{F - Fo}{Fo}$$

To avoid contamination of tails into following trials due to the slow decay of the GCaMP signal, we deconvolved Δ F/F traces using the standard package available at the Suite2p toolbox.

Analysis of running speed

For each trial, running speed was calculated and a trial was classified as 'running trial' if the animal speed was over 1cm/s for more than 10% of the trial. For the rest of the analysis, 'running trials' were excluded for when drifting gratings and natural images were presented. All trials were used when natural movies were presented.

Orientation and direction selectivity index

Orientation and direction selectivity indexes were computed using a global orientation selectivity index (gOSI) and a global direction selectivity index (gDSI) (Mazurek et al., 2014), as follows:

$$gOSI = \left| \frac{\sum_k R(\theta_k) exp(2i\theta_k)}{\sum_k R(\theta_k)} \right|$$

and

$$gDSI = \left| \frac{\sum_k R(\theta_k) exp(i\theta_k)}{\sum_k R(\theta_k)} \right|$$

Where R(θ_k) is the response to angle θ_k including the stimulus period of trials at the combination of temporal and spatial frequency that elicited the maximal response (preferred temporal and spatial frequency) for each neuron.

Preferred orientation and direction

Preferred orientation and direction were calculated as the angle of the circular mean for each neuron's tuning curve (Berens, 2009).

Cosine similarity

Cosine similarity (CS) was calculated as the follows:

$$CS(a,b) = \frac{a \cdot b}{|a|\,|b|}$$

Where a and b are tuning curve vectors of a given neuron for 'Baseline' and 'CNO' imaging days, respectively. For natural movies, tuning curves were obtained by averaging all trials for each 2-photon acquired frame during stimulus presentation. For natural images, tuning curves corresponded to the average response to each stimulus type.

Lifetime sparseness

Lifetime sparseness (S_l) was calculated as in Willmore et al. (2011):

$$S_l = \frac{(1 - \frac{1}{n}\frac{(\Sigma_i r_i)^2}{\Sigma_i r_i^2})}{1 - \frac{1}{n}}$$

Where r is the neuronal response to a movie epoch averaged across trials, i is index of the movie epoch and n is the number of movie epochs.

Signal and noise correlations

Signal correlations were calculated as the Pearson's correlation coefficient of tuning curves to all combinations of pairs of neurons modulated by the stimulus in an imaging session.

For noise correlations, first 'noise' was calculated by subtracting the average response to all trials from all trial responses for each neuron. After that noise correlations were calculated as the Pearson's correlation coefficient of the noise for all pairs of neurons in an imaging session.

To calculate mean correlations for each animal, correlation coefficient were first averaged for each session and after for each animal.

Statistical analyses

Neurons were defined as stimulus modulated for each stimulus type when significant at an ANOVA with α set to 0.05. ANOVA groups were set to each drifting grating types (combination of direction, temporal and spatial frequency), natural image or movie epoch (1s of movie presentation). To find movie epochs that significantly drove responses in neurons, Bonferroni posthoc was used after the ANOVA with α set to 0.05. Only frames during the stimulus presentation were used. For the rest of the analysis, 'running trials' were excluded for when drifting gratings and natural images were presented.

Comparisons of preferred orientation and direction of motion angle were done using circular statistics. To compare Baseline and CNO imaging days of hM4D(Gi)-FB group, we used Watson-Willians test, whereas to compare hM4D(Gi)-FB and Ctrl groups, we used Multi-sample test for equal median directions (Berens, 2009).

Comparisons of tuning curves were done using a 2-way ANOVA. Imaging day (Baseline and CNO) or experimental groups (hM4D(Gi)-FB and Ctrl), and orientation or direction angles were used as groups. After that we used a Bonferroni post hoc and α was set to 0.05.

For other parameters, comparisons between imaging days (Baseline and CNO) or experimental groups (hM4D(Gi)-FB and Ctrl) were done using a t-test with α set to 0.05 and neurons were pooled across all animals. When not mentioned, t-test was unpaired.

To control for variability across animals, comparisons between means across animals were done using hierarchical bootstrap (Saravanan et al., 2020). Neurons from different sessions but same animal were pooled. Data was resampled 10000 times and frequency of neurons for each animal was kept. To obtain the p-value with α set to 0.05, the joint probability distribution of the two groups was computed with each sample forming the two axes of a 2-D plot and the total density of the joint probability distribution on one side of the unity line was measured. The computed value will be called pboot in this thesis to differentiate from the p-value of standard statistical methods. Experimental groups are significantly different if pboot $\geq$0.975 or pboot$\leq$0.025.

Numbers of mice and cells are stated in the text.

Chapter 4

The role of direct HVA →V1 feedback connections in state-dependent modulations of V1

4.1 Author Contribution

GF performed all experiments and analyses described in the text. Marina Fridman contributed with primary codes and her expertise in data analysis.

4.2 Introduction

Perception of the outside world depends on the behavioral context we experience it. For instance, watching a show sitting at the bleachers or jumping at the mosh pit can steer us to perceive a song differently. Hence, an animal's behavioral state can alter the processing of sensory information and thus neuronal activity in the brain. Specific mechanisms and circuits can be recruited at different behavioral states so sensation can serve for appropriate behaviors, such as navigation, foraging, mating, rest, etc. However, neuronal circuits underlying state modulations of brain activity are still poorly understood.

As in many cortical areas (Shimaoka et al., 2018), the behavioral state has a powerful impact on the activity of V1. First demonstrated by Niell and Stryker (2010), the activity of V1 neurons was shown to be stronger when mice run than when they are stationary during visual stimulation. Additionally, the visually-evoked activity of V1

neurons is more reliable (Bennett et al., 2013) and less correlated during locomotion (Erisken et al., 2014). Some of the locomotion influences in V1 are thought to result from the interplay between the mesencephalic locomotor region (MLR), the basal forebrain and V1. During locomotion, active projections from the MLR drive cholinergic neurons in the basal forebrain (Fu et al., 2014; Lee et al., 2014). Subsequently, cholinergic inputs in V1 act on vasoactive intestinal peptide (VIP) interneurons which inhibit somatostatin (SOM) interneurons. SOM inhibition leads to disinhibition of pyramidal neurons and hence facilitation of their responses during locomotion (Fu et al., 2014) (Fu et al. 2014, see review in Busse 2020). However, this circuit model is challenged by evidence that the activity of VIP and SOM interneurons is larger during locomotion (Dipoppa et al., 2018; Pakan et al., 2016), suggesting that locomotion exerts its impact through multiple motifs of the cortical circuitry. Furthermore, Pakan et al. (2016) have shown that locomotion exerts differential effects on each component of the VIP-SOM-pyramidal circuit in darkness and during visual stimulation, suggesting that the modulation of V1 activity by locomotion is context-dependent.

Feedback connections are an adequate candidate to underlie the effects of locomotion in V1 neurons because they are thought to convey contextual information to V1. This idea is reinforced by evidence that locomotor-related signals have been observed in the main feedback sources of V1, such as the pulvinar (Roth et al., 2016), HVAs (Christensen and Pillow, 2017; Shimaoka et al., 2018), and anterior cingulate cortex (ACC) (Leinweber et al., 2017). In addition, Leinweber et al. (2017) have shown that projections from ACC activate running-modulated neurons in V1, and silencing ACC reduces V1 responses elicited by locomotion. Furthermore, locomotion exerts similar influences on the activity of V1 neurons than other processes already associated with top-down signals, such as enhancement of responses by attention (for review, see Maunsell, 2015) and feedback connections, such as surround suppression (Ayaz et al., 2013; Erisken et al., 2014).

This chapter aimed to investigate whether direct cortico-cortical feedback from HVAs participates in the modulation of V1 neuronal activity by behavioral state. We examined the effects of inhibiting direct HVA→V1 feedback in visually-evoked and spontaneous activity of the mouse's V1 neurons during locomotion and stationary periods. We found neurons modulated by locomotion both during visual stimulation and in darkness, yet the activity of V1 neurons, at the population level, is only modulated during visual stimulation. Furthermore, we showed that direct HVA→V1 feedback inhibits the facilitation of V1 visually-evoked responses induced by locomotion. Finally, we demonstrated that direct cortico-cortical feedback participates in mechanisms of state modulations of V1 activity.

4.3 Results

4.3.1 Protocol to measure modulations of direct HVA→V1 feedback on running modulations of V1 activity

Although significant evidence has been brought to light regarding the functions of interneurons and neuromodulators in modulations of V1 responses by locomotion, no study has probed the role of direct HVA feedback in this process. To investigate the role of direct HVA→V1 feedback on running modulations of the visually-evoked activity of V1 neurons, we compared the activity of V1 neurons in running and stationary periods while mice were presented with drifting gratings in the hM4D(Gi)-FB and Ctrl groups (Fig.4.1A and B, bottom). This dataset corresponds to the same neurons and animals presented in the previous chapter. We also evaluated whether direct cortico-cortical feedback modulates the activity of V1 neurons in the dark (spontaneous activity) (Fig.4.1B, top). We recorded the spontaneous activity of 783 (5 imaging session pairs in 2 animals) and 1192 (6 imaging session pairs in 4 animals) L2/3 V1 neurons, which were present on both days of imaging (Baseline/CNO) for the hM4D(Gi)-FB and Ctrl groups, respectively. We found single neurons whose activity seems to be modulated by running during visual stimulation (Fig.4.1B, bottom-right) and in darkness (Fig.4.1B, top-right).

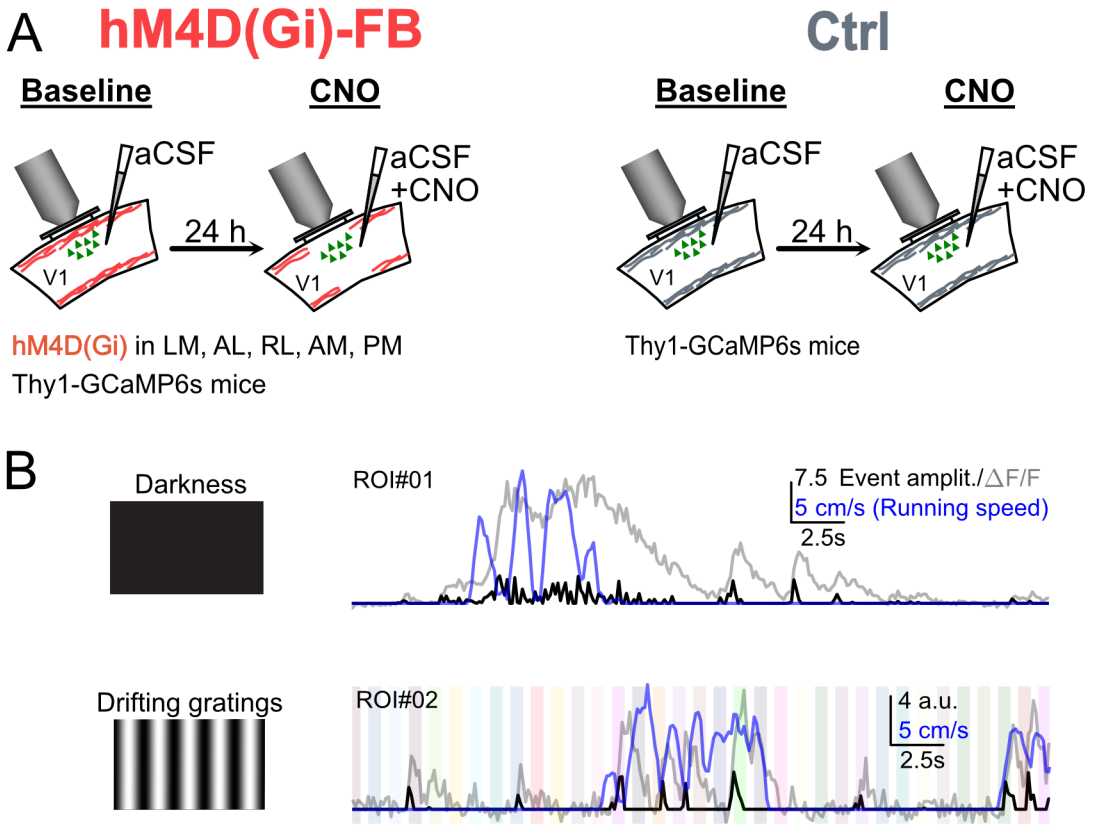

Figure 4.1: Experimental description and example traces
(A) Experimental groups. V1 was imaged in two consecutive days immediately after a local injection of aCSF (Baseline) or aCSF+CNO (CNO) in animals expressing hMD4(Gi) receptors in LM, AL, RL, AM and PM (Left, hM4D(Gi)-FB group). Control animals with no expression of hMD4(Gi) receptors were submitted to the same procedures (Right, Ctrl group). (B) Example responses. V1 activity was measured during the presentation of drifting gratings (bottom) or while the monitor was black (darkness, top) to the animal's eye contralateral to the imaging hemisphere. Putative neurons (ROIs) were identified and $\Delta F/F0$ (gray line) calculated. $\Delta F/F$ traces were deconvolved into events (black line). Mice running speed was measured and aligned to the calcium imaging data (blue line). Shaded areas mark visual stimulation. Colors indicate drifting grating types (combinations of direction, temporal and spatial frequency).

4.3.2 Spontaneous activity of V1 L2/3 neurons is not modulated by locomotion

Locomotion has been shown to increase the spontaneous activity of some V1 neurons (Niell and Stryker, 2010). To measure the effects of locomotion on spontaneous activity, we calculated the mean activity (event amplitude) for each neuron during running and stationary periods while the animal was in the dark. We found neurons that were positively modulated by locomotion on Baseline and CNO imaging days

in the hM4D(Gi)-FB and Ctrl groups (Fig. 4.2A,B). However, we observed that locomotion did not increase the response amplitude of the V1 neuronal population of the hM4D(Gi)-FB group (Paired t-test, $\text{Baseline}_{stationary}$ vs $\text{Baseline}_{running}$, p=0.95, and $\text{CNO}_{stationary}$ vs $\text{CNO}_{running}$, p=0.97). Similar results were observed for the Ctrl group (Paired t-test, $\text{Baseline}_{stationary}$ vs $\text{Baseline}_{running}$, p=0.61, $\text{CNO}_{stationary}$ vs $\text{CNO}_{running}$,p=0.07). Thus, although some neurons seem to be modulated by locomotion, locomotion and direct cortico-cortical projections do not modulate the spontaneous activity of V1 neurons in our study.

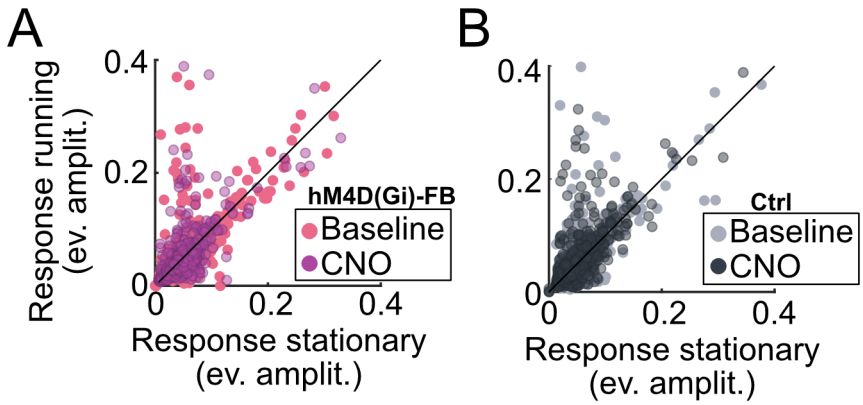

Figure 4.2: Running modulations of V1 spontaneous activity
(A) Mean spontaneous activity (event amplitude) for running and stationary periods for the hM4D(Gi)-FB group. Paired t-test, running vs stationary responses, Baseline p=0.95, CNO p=0.97, N = 783 neurons. (B) Mean spontaneous activity (event amplitude) for running and stationary periods for the Ctrl group. Paired t-test, running vs stationary, Baseline p=0.62, CNO p=0.07, N = 1192 neurons. Each circle represents one neuron.

4.3.3 Direct HVA→V1 feedback inhibits running facilitation of V1 visually-evoked responses

Running induces more robust facilitation in V1 visually-evoked responses than in spontaneous activity (Pakan et al., 2016). Thus, we wondered whether locomotion would facilitate visually-evoked responses in our dataset. Next, we asked whether direct HVA→V1 feedback could be an anatomical substrate for such modulations. First, we calculated the mean activity (event amplitude) during running and stationary trials for each neuron during visual stimulation (all grating types). We observed that locomotion positively modulated the visually-evoked activity of the majority of V1 neurons (Fig. 4.3A). On the population level, we observed that the mean event amplitude of V1 neurons was larger when animals were running in the hM4D(Gi)-FB group (Paired T-test, $\text{Baseline}_{stationary}$ vs $\text{Baseline}_{running}$, p=1.2x$10^{-16}$, and $\text{CNO}_{stationary}$ vs $\text{CNO}_{running}$, p=7.7x10^{-18}, N = 286 neurons). Similar results were observed for

the Ctrl group (Paired T-test, $\text{Baseline}_{stationary}$ vs $\text{Baseline}_{running}$, p=5.8x$10^{-28}$, and $\text{CNO}_{stationary}$ vs $\text{CNO}_{running}$, p=2.7x10^{-18}, N = 509 neurons). We quantified the effects of locomotion on visually-evoked responses by calculating the running modulation index (RMI) (RMI = $R_{running}$ - $R_{stationary}$ / $R_{running}$ + $R_{stationary}$), for each neuron on Baseline and CNO imaging days. In the RMI, positive values indicate the activity of neurons was higher during running periods, whereas negative values indicate otherwise. We found that the RMI was increased on the CNO day in the hM4D(Gi)-FB group (Paired T-test, $\text{RMI}_{Baseline}$ vs RMI_{CNO}, p=0.0073)(data not shown). To check for unspecific effects of CNO and mechanical damage, we computed the difference between the RMI on both imaging days (ΔRMI = RMI_{CNO} - $\text{RMI}_{Baseline}$). In the ΔRMI, positive values indicate locomotion modulations were increased (more activity during running periods) on the CNO imaging day, whereas negative values indicate otherwise. We found an increase in ΔRMI (T-test, hM4D(Gi)-FB vs Ctrl group, p = 0.0026), suggesting the increase in RMI at CNO imaging day is not due to unspecific effects (Fig.4.3B). This was also true when considering animal variability (Fig.4.3C) (Hierarchical bootstrap, p = 0.0021). To control for changes in running behavior across experimental groups, we compared the percentage of time running between Baseline and CNO imaging days (Fig. 4.2D). We found no difference in the percentage of time running across days at the hM4D(Gi)-FB (Paired T-test, Baseline vs CNO imaging days, p=0.1) and at the Ctrl groups (Paired T-test, Baseline vs CNO imaging days, p=0.9). The lack of behavioral changes indicates that the increase in running modulation is due to the silencing of direct HVA feedback inputs. Therefore, direct HVA→V1 feedback contributes to the modulation of locomotion on V1 neuronal visual evoked responses by suppressing their facilitation when the animal is running.

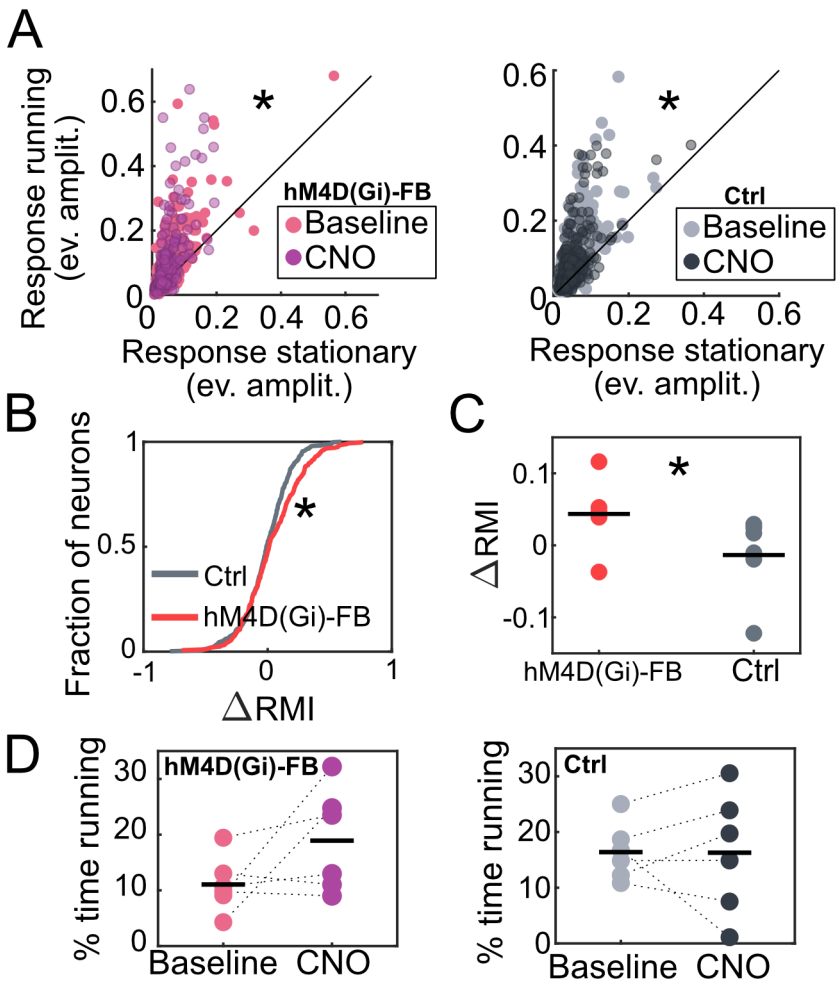

Figure 4.3: Running modulations of V1 visual evoked-activity
(A) Mean visual evoked-activity (event amplitude) for running and stationary trials. Left, No dFB group. Paired t-test running vs stationary responses, Baseline p=1.2x10^{-16}, CNO p=7.7x10^{-18}, N = 286 neurons. Right, Ctrl group. Paired t-test running vs stationary responses, Baseline p=5.8x10^{-28}, CNO p=2.7x10^{-18}, N = 509 neurons. Each circle represents one neuron.(B) Cumulative distribution of Δ running modulation index (RMI) (Δ RMI = RMI_{CNO} - $RMI_{Baseline}$) for all neurons in each group. t-test, p=0.0026.(C) Δ RMI per session pair. Hierarchical bootstrap, p=0.0021, N No dFB = 6 sessions, 3 animals. N Ctrl = 6 sessions, 4 animals. Black lines represent means across sessions.(D) Percentage of time running per imaging session pairs. Each circle represents one imaging session. Black lines represent mean across sessions. Left, No dFB group. Paired t-test, p=0.141. Right, Ctrl group. Paired t-test, p=0.977.

4.4 Discussion

Under natural conditions, animals experience the world through different behavioral contexts, and hence sensory processing can be influenced by the state of the

animal. Although interneurons and neuromodulators have been shown to underlie state-modulations in V1 neurons, other anatomical substrates have been proposed to participate as well. Our goal in this chapter was to investigate whether direct cortico-cortical feedback from HVAs participates in the modulation of V1 neuronal activity by behavioral state, specifically in locomotion modulations. We examined the effects of inhibiting direct HVA→V1 feedback in visually-evoked and spontaneous activity of the mouse's V1 neurons during locomotion and stationary periods. We found individual V1 neurons whose activity was modulated by locomotion during visual stimulation and in darkness, yet only V1's visually-evoked activity was modulated at the population level. Furthermore, we showed that direct HVA→V1 feedback inhibits locomotion-induced facilitation of V1 visually-evoked responses. Finally, we demonstrated that one of the anatomical substrates for locomotion to act upon V1 neurons is through direct cortico-cortical feedback inputs.

4.4.1 Locomotion effects on V1 activity in the dark

Locomotion has been shown to change the activity of V1 neurons in the absence of visual stimulation. The strength of this modulation is variable across different studies. Some reported locomotion-induced depolarization of V1 neurons (Polack et al., 2013), others reported neurons increasing or decreasing their activity (Ayaz et al., 2013; Niell and Stryker, 2010; Saleem et al., 2013; Vinck et al., 2015). Likewise, we found V1 neurons that increased their activity in running periods, yet we did not observe a change in the overall spontaneous activity across the population of V1 neurons.

The inconsistency of locomotion effects on the non-visual activity of V1 neurons has been proposed to result from different recording conditions across studies. Some studies used a gray monitor, and others kept the monitor black. Indeed, the activity of excitatory L2/3 V1 neurons during locomotion and presentation of gratings or grey screen was significantly higher than during darkness (Pakan et al., 2016). In our experiments, we measured V1 activity while keeping a black screen and, similar to other reports (Pakan et al., 2016), we observed fewer neurons being modulated by running during visual stimulation.

Movement has a massive impact on the spontaneous activity of V1 neurons. For instance, spontaneous behaviors, such as facial movements, can drive up to 1/3 of the V1 activity in the dark (Stringer et al., 2019), and locomotion effects on activity are widespread in the brain (Shimaoka et al., 2018). What are the sources of locomotion modulations on the non-visual activity of V1? In our study, we observed no differences in the running modulations on the activity of V1 neurons in the dark after HVA feedback inputs were silenced (data not shown). This finding suggests that HVA

feedback connections do not carry locomotion signals to V1 in the dark. Our data agree with the idea that locomotion signals in V1 serve to predict future visual events. Consequently, signals from HVA feedback inputs, which would carry visual predictions, would not be necessary without a visual stimulus.

4.4.2 Direct cortico-cortical feedback is a substrate for locomotion effects on V1 visually-evoked activity

In our study, we find that locomotion strongly modulates the visually-evoked responses of V1 neurons. This result is in line with evidence from other studies (Bennett et al., 2013; Erisken et al., 2014; Niell and Stryker, 2010; Pakan et al., 2016). In addition to modulations on the amplitude of V1 responses, locomotion also changes important features of stimulus coding, such as increased reliability of responses (Bennett et al., 2013), increased gain of orientation tuning and contrast response functions (Erisken et al., 2014; Lee et al., 2014), and reduced noise correlations (Dadarlat and Stryker, 2017; Erisken et al., 2014), among others. Such essential aspects of stimulus representation could not be accessed in our experiments because of the low yield of running trials in naive animals. Thus, running periods encompassed a range of different grating types.

Modulations of activity by locomotion are widespread across the cortex (Shimaoka et al., 2018), and hence cortical inter-areal projections are plausible to carry locomotion signals. Our study finds that HVA feedback inputs in V1 inhibit the locomotion-induced facilitation of V1 activity. The activity of HVAs has been shown to be negatively modulated by locomotion (Shimaoka et al., 2018), while the activity of most of their neurons showed a negative correlation with the mouse speed (Christensen and Pillow, 2017). Consequently, HVA feedback inputs in V1 convey locomotion signals to V1 neurons, which reduce the facilitation of visually-evoked responses in V1 by locomotion. In line with that, locomotion-induced reduction of surround suppression (Erisken et al., 2014) could be mediated by HVA feedback inputs in V1 since silencing HVAs reduces surround suppression in the mouse (Vangeneugden et al., 2019). Moreover, our data suggest that such effects are carried by direct cortico-cortical feedback in stationary periods. Surround modulations during navigation could be of utmost significance in enhancing or suppressing visual scene features according to the animal's behavioral needs.

What is the role of locomotion signals in V1? One hypothesis is that V1 signals the mismatch between the current visual stimuli and those that should have been encountered given the locomotion. In this framework, responses elicited by the mismatch of the animal speed and optic flow can be interpreted as increases in prediction

error, as in predictive coding theories. Such responses have been reported in V1 L2/3 neurons of the mouse. Moreover, ACC was shown to carry motor signals to V1 and elicit mismatch responses in V1 neurons when activated (Leinweber et al., 2017). Because feedback connections are sources of predictions in predictive coding theories, feedback from ACC is thought to carry motor-related predictions of optic flow. Because our experiments were performed without coupling animal speed and optic flow, interpretations of our results in this framework are flawed. However, we speculate whether HVA feedback inputs could convey optic flow predictions to V1 neurons since our data shows it carries locomotion signals to this area. Further experiments will help enlighten if the central role of locomotion signals from HVA terminals in V1 is to provide predictions about the visual scene during navigation.

Finally, our results demonstrate that the function of HVA feedback inputs in V1 is more than just vision. Direct cortico-cortical feedback from HVA conveys locomotion signals to V1 neurons. Locomotion signals in V1 can help animals estimate how the world is changing and allow for adaptation of visual processing mechanisms serving for fundamental behaviors, such as navigation.

4.5 Materials and Methods

Most procedures were already described in Chapter 02 and 03. Here I describe the materials and methods specific to the results presented in this chapter.

4.5.1 Visual stimuli

For the recordings done with no visual stimulation, all monitor pixel values were set to the black value, except a small white square at the corner of the monitor. Onset of the white square was detected by a photodiode and used to synchronise 2-photon images, running traces and trial times. The corner of the monitor and photodiode were covered with black tape to avoid light contamination. This protocol lasted for about 5 min.

4.5.2 Data analysis

Analysis of running speed

For recordings with no visual stimulation, the entire recording was split into periods of 1s (trials). Running speed was calculated for each trial (gratings and no visual stimulation). A trial was classified as 'running trial' if the animal speed was over 1cm/s for more than 10% of the trial.

Running modulation index

We calculated the running modulation index for each neuron as following:

$$RMI = \frac{R_{running} - R_{stationary}}{R_{running} + R_{stationary}}$$

Where R is the mean response of each neuron to all trials for the protocol without visual stimulation or all trials during stimulus presentation of drifting gratings. Only sessions with at least 5 trials per condition (running or stationary) were included.

Statistical analyses

Neurons were defined as stimulus modulated when significant at an ANOVA with α set to 0.05 and groups set to each drifting grating type (combination of direction, temporal and spatial frequency). Only frames during the stimulus presentation were used.

Comparisons between spontaneous activity or visually-evoked activity of running and stationary trials were done using a paired t-test and α was set to 0.05. When not stated, t-test was unpaired.

When neurons were pooled across all animals, comparisons between groups were done using t-test and α was set to 0.05. To control for variability between sessions, comparisons between means across sessions were done using hierarchical bootstrap (Saravanan et al., 2020). Data was resampled 10000 and frequency of neurons for each animal was kept. As in Saravanan et al. (2020) to obtain the p-value with α set to 0.05, the joint probability distribution of the two groups was computed with each sample forming the two axes of a 2-D plot and the total density of the joint probability distribution on one side of the unity line was measured. Groups are significantly different if the volume computed is $0.975 \leq p \leq 0.025$.

Numbers of mice and cells are stated in the text.

Chapter 5

General discussion and conclusion

The work presented in this thesis investigated the role of direct HVA→V1 feedback inputs in shaping the visual and non-visual representations of V1 neurons. We inhibited the activity of direct HVA→V1 feedback projections and measured the activity of V1 neurons to a comprehensive batch of visual stimuli in the awake non-behaving mouse. In this chapter, I summarize the main results of our work and present a brief general discussion highlighting future directions.

5.1 Selective inhibition of HVAs feedback terminals in V1

A single study, apart from ours, has simultaneously inhibited feedback terminals and recorded V1 activity (Nurminen et al., 2018). The challenging nature of silencing feedback axons steered the literature into investigating the role of top-down signals in V1 processing by inhibiting HVAs (Bardy et al., 2006, 2009; Bullier et al., 1996; Hishida et al., 2019; Huang et al., 2007, 2004; Hupe et al., 1998; Hupé et al., 2001; Keller et al., 2020b; Kirchberger et al., 2021; Mignard and Malpeli, 1991; Nassi et al., 2013; Oude Lohuis et al., 2021; Pafundo et al., 2016; Pak et al., 2020; Sandell and Schiller, 1982; Vangeneugden et al., 2019; Wang et al., 2010, 2000). These studies are hard to compare because of the variability in experimental conditions, such as using different species, cooling methods, and recording techniques. Perhaps the biggest confound is that inhibiting the activity of HVAs leads to manipulation of a wider circuit, making it hard to distinguish the effects of direct HVA feedback inputs and

indirect pathways. We specifically aimed to silence feedback terminals in V1 to avoid such confound.

For the first time, we show direct evidence that a local injection of CNO inhibits the activity of hDM4(Gi)-expressing boutons in vivo. Previous studies that manipulated projections with hDM4(Gi) activation and local CNO injections controlled for inhibition using ex vivo preparations and inferred behavioral changes were caused by silencing of terminals (Doron et al., 2020; Mahler et al., 2014; Stachniak et al., 2014; Takahashi et al., 2020, 2021). In our study, we measured the visually-evoked activity of LM→V1 boutons after local injections of aCSF or CNO in animals co-expressing hDM4(Gi) and GCaMP6s in LM. After a local injection of CNO, we showed (1) a reduction in the mean activity of feedback boutons (about 33%) and (2) a reduction in the number of visually-responsive boutons. Although our goal was to silence the majority of feedback inputs in V1, also by targeting multiple HVAs, we removed only 33% of the activity from direct HVA feedback inputs in V1. It is unknown how effective was the optogenetic silencing of terminals at the study of Nurminen et al. (2018), making it challenging to compare methodologies and effect sizes.

In our study, we silenced feedback inputs from many sources (PM, AM, RL, AL, LM). The motivation behind this approach was to observe larger effects by removing a big part of top-down signals. Yet, what is the weight of each area for each observed effect? Our experimental design does not aim to assign whether feedback operates specific streams of information or which information is conveyed by feedback inputs from each HVA to V1. Ideally, our results could inspire further experiments which take into account what we know from signals present in each HVA and silence direct cortico-cortical feedback inputs of individual HVAs. For instance, since areas LM and AL seem to be more relevant for processing visual features in a visual discrimination task Jin and Glickfeld (2020), it would be interesting to silence LM or AL feedback terminals to investigate their role in shaping tuning properties of V1 neurons. On the other hand, area PM has been shown to be more involved in sensory integration and decision variables Jin and Glickfeld (2020) and hence it would be plausible to have a role at state-modulations of V1 activity.

In future studies, promising newer tools, such as eOPN3 (Mahn et al., 2021) and PPO (Copits et al., 2021), would allow for more significant temporal precision of the inhibition of feedback projections. Besides the advanced precision in temporal control, eOPN3 and PPO allow for faster and high-yielding experiments granting a more extensive range of visual features and behavioral variables to be tested.

5.2 Direct HVA→V1 feedback inputs shape the visual representation of V1 neurons

For the first time in the literature, we show that direct HVA cortico-cortical feedback inputs modulate the tuning properties of V1 neurons in the mouse. Specifically, the tuning of V1 neurons to gratings and natural videos, but not to static natural images, is dependent on direct HVA→V1 feedback inputs.

In our study, the inhibition of direct HVA→V1 feedback inputs does not affect the orientation or direction tuning preference of V1 neurons. However, the orientation and direction tuning curves became sharper after silencing those inputs. Specifically, direct cortico-cortical feedback selectively inhibited responses to the preferred orientation and direction of motion. The suppression caused by direct feedback on V1 responses to gratings suggests they mediate surround suppression mediated by HVAs. Our results agree with previous studies that showed a reduction in surround suppression after silencing the lateral HVAs in the mouse (Vangeneugden et al., 2019). In monkeys, direct V2→V1 feedback inputs were shown to underlie at least part of the surround suppression observed when V2 and V3 areas are cooled (Nassi et al., 2013; Nurminen et al., 2018). Future experiments could clarify this idea by inhibiting direct HVA→V1 inputs and measuring the activity of V1 neurons while presenting expanding grating patches. Our study also proposes that direct HVA feedback inputs must contact interneurons to inhibit V1 responses to gratings. The involvement of interneurons further agrees with the idea that inhibition of V1 responses to gratings by direct HVA feedback inputs results from surround suppression. In a recent study, interneurons were shown to participate in the circuit underlying surround modulations in the mouse (Keller et al., 2020a). Hence measuring the activity of the various classes of interneurons would help clarify the connectivity motif behind direct HVA feedback modulations.

Furthermore, we found that direct HVA feedback inputs participate in mechanisms that diversify representations of naturalistic stimuli in V1. We show that the tuning curve to natural movies of a given neuron in V1 changes upon silencing direct HVA→V1 inputs. Neurons in V1 added responses to new parts of the movie while losing responses to parts that previously drove neurons. New responses were not random but to similar parts of the movie, rendering tuning curves across the V1 population more similar after direct HVA cortico-cortical feedback inhibition. Surprisingly, whereas the tuning of V1 neurons to natural movies was dependent on direct HVA feedback inputs, the tuning to natural images was not. We propose that the spatial-temporal correlations between the surround and the receptive field of V1 neu-

rons recruit direct feedback connections that modulate the tuning properties of V1 neurons. In the case of natural images, the lack of the temporal component does not engage this mechanism. To test this, one could compare V1 responses to a natural movie and to the same movie with no temporal correlations, e.g. by shuffling movie frames. Furthermore, manipulating the placement of such stimuli (full field, receptive field, or surround only) would allow for testing if the direct feedback modulations are dependent on the interaction of features in space.

Finally, our study silenced feedback inputs from many sources (PM, AM, RL, AL, LM). The motivation behind this approach was to remove a large part of top-down signals. However, given our results, what is the weight of each area for each observed effect? Unfortunately, our experimental design does not allow us to answer this question. Ideally, our findings could be informative for future experiments designed to understand if direct feedback from different HVAs participates in specific functions. For instance, probing the role of direct feedback from LM or AL in surround suppression since silencing lateral HVAs reduced surround suppression (Vangeneugden et al., 2019) and were relevant for the processing of visual features in visual discrimination tasks (Jin and Glickfeld, 2020).

5.3 Direct HVA→V1 feedback inputs influence non-visual aspects of V1 responses

The impact of locomotion on the activity of V1 neurons is powerful (Niell and Stryker, 2010). Feedback projections are a good candidate to mediate modulations of V1 activity by locomotion because many sources of feedback to V1 encode locomotor-related variables (Christensen and Pillow, 2017; Leinweber et al., 2017; Roth et al., 2016; Shimaoka et al., 2018). For the first time, we showed that direct HVA cortico-cortical feedback inputs participate in mechanisms of state-modulations of V1 neurons. In particular, we found that direct HVA→V1 feedback inputs inhibit the locomotion-induced facilitation of visually-evoked activity.

Previous studies have shown that locomotion reduces the activity of HVAs (Shimaoka et al., 2018) and that the mouse speed negatively correlates with the activity of neurons in those areas (Christensen and Pillow, 2017). We found that silencing direct HVA→V1 feedback inputs increases the facilitation of visually-evoked responses of V1 neurons by locomotion. Consequently, HVA conveys locomotion signals to V1 neurons through direct cortico-cortical feedback. Locomotion signals carried by direct HVA→V1 feedback inputs can play an essential role in the activity of V1 neurons for spatial integration and, ultimately, navigation. Future studies could explore whether

direct feedback from HVAs underlies the decrease in surround suppression during locomotion (Erisken et al., 2014).

5.4 Conclusions

The intricate anatomical connectivity and functional organization suggest that direct cortico-cortical projections have a central role in the cortical processing of visual information. In this study, we show, for the first time, that the tuning of V1 neurons to drifting gratings and natural movies is dependent on direct HVA cortico-cortical feedback inputs. We also find that direct HVA feedback inputs shape state modulations of V1 neurons. Our study suggests that direct HVA→V1 feedback inputs carry contextual information to V1 neurons and participate in mechanisms to diversify the responses of the V1 population.

References

Andermann, M. L., Kerlin, A. M., Roumis, D. K., Glickfeld, L. L., and Reid, R. C. (2011). Functional specialization of mouse higher visual cortical areas. *Neuron*, 72(6):1025–39.

Angelucci, A., Bijanzadeh, M., Nurminen, L., Federer, F., Merlin, S., and Bressloff, P. C. (2017). Circuits and Mechanisms for Surround Modulation in Visual Cortex. *Annual Review of Neuroscience*, 40(April):425–451.

Armbruster, B. N., Li, X., Pausch, M. H., Herlitze, S., and Roth, B. L. (2007). Evolving the lock to fit the key to create a family of G protein-coupled receptors potently activated by an inert ligand. *Proceedings of the National Academy of Sciences of the United States of America*, 104(12):5163–5168.

Armbruster, B. N. and Roth, B. L. (2005). Mining the receptorome. *Journal of Biological Chemistry*, 280(7):5129–5132.

Ayaz, A., Saleem, A. B., Schölvinck, M. L., and Carandini, M. (2013). Locomotion controls spatial integration in mouse visual cortex. *Current Biology*, 23(10):890–894.

Bardy, C., Huang, J. Y., Wang, C., FitzGibbon, T., and Dreher, B. (2006). 'Simplification' of responses of complex cells in cat striate cortex: Suppressive surrounds and 'feedback' inactivation. *Journal of Physiology*, 574(3):731–750.

Bardy, C., Huang, J. Y., Wang, C., FitzGibbon, T., and Dreher, B. (2009). 'Top-down' influences of ipsilateral or contralateral postero-temporal visual cortices on the extra-classical receptive fields of neurons in cat's striate cortex. *Neuroscience*, 158(2):951–968.

Bastos, A. M., Usrey, W. M., Adams, R. A., Mangun, G. R., Fries, P., and Friston, K. J. (2012). Canonical Microcircuits for Predictive Coding. *Neuron*, 76(4):695–711.

Bennett, C., Arroyo, S., and Hestrin, S. (2013). Subthreshold mechanisms underlying state-dependent modulation of visual responses. *Neuron*, 80(2):350–357.

Berens, P. (2009). CircStat: A MATLAB Toolbox for Circular Statistics. *Journal of Statistical Software*, 21(10):1–21.

Bourassa, J. and Deschenes, M. (1995). Corticothalamic projections from the primary visual cortex in rats: a single fiber study using biocytin as an anterograde tracer.

66(2):253–263.

Brainard, D. H. (1997). The Psychophysics Toolbox. *Spatial Vision*, 10(4):433–436.

Brodmann, K. (1909). Vergleichende Lokalisationslehre der Großhirnrinde in ihren Prinzipien dargestellt auf Grund des Zellenbaues. 44(0).

Bullier, J., Hupé, J. M., James, A., and Girard, P. (1996). Functional interactions between areas V1 and V2 in the monkey. *Journal of Physiology Paris*, 90(3-4):217–220.

Busse, L. (2018). The Mouse Visual System and Visual Perception. *Handbook of Behavioral Neuroscience*, 27:53–68.

Busse, L. (2020). The influence of locomotion on sensory processing and its underlying neuronal circuits. *Neuroforum*, 24(1):A41–A51.

Caviness, V. S. (1975). Architectonic map of neocortex of the normal mouse. *Journal of Comparative Neurology*, 164(2):247–263.

Chang, S. E., Todd, T. P., Bucci, D. J., and Smith, K. S. (2015). Chemogenetic manipulation of ventral pallidal neurons impairs acquisition of sign-tracking in rats. *European Journal of Neuroscience*, 42(12):3105–3116.

Chen, T. W., Wardill, T. J., Sun, Y., Pulver, S. R., Renninger, S. L., Baohan, A., Schreiter, E. R., Kerr, R. A., Orger, M. B., Jayaraman, V., Looger, L. L., Svoboda, K., and Kim, D. S. (2013). Ultrasensitive fluorescent proteins for imaging neuronal activity. *Nature*, 499(7458):295–300.

Christensen, A. J. and Pillow, J. W. (2017). Running reduces firing but improves coding in rodent higher-order visual cortex. *bioRxiv*, pages 1–14.

Cohen, M. R. and Kohn, A. (2011). Measuring and interpreting neuronal correlations. *Nature Neuroscience*, 14(7):811–819.

Cohen-Kashi Malina, K., Tsivourakis, E., Kushinsky, D., Apelblat, D., Shtiglitz, S., Zohar, E., Sokoletsky, M., Tasaka, G. i., Mizrahi, A., Lampl, I., and Spiegel, I. (2021). NDNF interneurons in layer 1 gain-modulate whole cortical columns according to an animal's behavioral state. *Neuron*, 109(13):2150–2164.

Copits, B. A., Gowrishankar, R., O'Neill, P. R., Li, J. N., Girven, K. S., Yoo, J. J., Meshik, X., Parker, K. E., Spangler, S. M., Elerding, A. J., Brown, B. J., Shirley, S. E., Ma, K. K., Vasquez, A. M., Stander, M. C., Kalyanaraman, V., Vogt, S. K., Samineni, V. K., Patriarchi, T., Tian, L., Gautam, N., Sunahara, R. K., Gereau, R. W., and Bruchas, M. R. (2021). A photoswitchable GPCR-based opsin for presynaptic inhibition. *Neuron*, 109(11):1791–1809.

Dadarlat, M. C. and Stryker, M. P. (2017). Locomotion enhances neural encoding of visual stimuli in mouse V1. *Journal of Neuroscience*, 37(14):3764–3775.

David, S. V., Vinje, W. E., and Gallant, J. L. (2004). Natural stimulus statistics alter the receptive field structure of V1 neurons. *Journal of Neuroscience*, 24(31):6991–7006.

De Souza, B. O. F., Cortes, N., and Casanova, C. (2020). Pulvinar Modulates Contrast Responses in the Visual Cortex as a Function of Cortical Hierarchy. *Cerebral Cortex*, 30(3):1068–1086.

Deitch, D., Rubin, A., and Ziv, Y. (2021). Representational drift in the mouse visual cortex. *Current Biology*, 31(19):4327–4339.

Dipoppa, M., Ranson, A., Krumin, M., Pachitariu, M., Carandini, M., and Harris, K. D. (2018). Vision and Locomotion Shape the Interactions between Neuron Types in Mouse Visual Cortex. *Neuron*, 98(3):602–615.

Dong, H., Wang, Q., Valkova, K., Gonchar, Y., and Burkhalter, A. (2004). Experience-dependent development of feedforward and feedback circuits between lower and higher areas of mouse visual cortex. *Vision research*, 44(28):3389–400.

Doron, G., Shin, J. N., Takahashi, N., Drüke, M., Bocklisch, C., Skenderi, S., Mont, L. D., Toumazou, M., Ledderose, J., Brecht, M., Naud, R., and Larkum, M. E. (2020). Perirhinal input to neocortical layer 1 controls learning. *Science*, 370(6523).

Erisken, S., Vaiceliunaite, A., Jurjut, O., Fiorini, M., Katzner, S., and Busse, L. (2014). Effects of locomotion extend throughout the mouse early visual system. *Current Biology*, 24(24):2899–2907.

Federer, F., Ta'afua, S., Merlin, S., Hassanpour, M. S., and Angelucci, A. (2021). Stream-specific feedback inputs to the primate primary visual cortex. *Nature Communications*, 12(1):1–15.

Felleman, D. J. and Van Essen, D. C. (1991). Distributed hierarchical processing in the primate cerebral cortex. *Cerebral Cortex*, 1(1):1–47.

Felsen, G., Touryan, J., Han, F., and Dan, Y. (2005). Cortical sensitivity to visual features in natural scenes. *PLoS Biology*, 3(10).

Field, D. J. (1994). What Is the Goal of Sensory Coding?

Filho, R. V. T. (2020). Phineas Gage 's great legacy. *Dement Neuropsychol*, 14(4):419–421.

Florio, M. and Huttner, W. B. (2014). Neural progenitors, neurogenesis and the evolution of the neocortex. *Development (Cambridge)*, 141(11):2182–2194.

Friston, K. (2005). A theory of cortical responses. *Philosophical Transactions of the Royal Society B: Biological Sciences*, 360(1456):815–836.

Froudarakis, E., Berens, P., Ecker, A. S., Cotton, R. J., Sinz, F. H., Yatsenko, D., Saggau, P., Bethge, M., and Tolias, A. S. (2014). Population code in mouse V1 facilitates readout of natural scenes through increased sparseness. *Nature Neuroscience*,

17(6):851–857.

Fu, Y., Tucciarone, J. M., Espinosa, J. S., Sheng, N., Darcy, D. P., Nicoll, R. A., Huang, Z. J., and Stryker, M. P. (2014). A cortical circuit for gain control by behavioral state. *Cell*, 156(6):1139–1152.

Funamizu, A., Kuhn, B., and Doya, K. (2016). Neural substrate of dynamic Bayesian inference in the cerebral cortex. *Nature Neuroscience*, 19(12):1682–1689.

Furtak, S. C., Ahmed, O. J., and Burwell, R. D. (2012). Single Neuron Activity and Theta Modulation in Postrhinal Cortex during Visual Object Discrimination. *Neuron*, 76(5):976–988.

Gilbert, C. D. and Li, W. (2013). Top-down influences on visual processing. *Nature reviews. Neuroscience*, 14(5):350–63.

Glickfeld, L. L., Andermann, M. L., Bonin, V., and Reid, R. C. (2013). Cortico-cortical projections in mouse visual cortex are functionally target specific. *Nature Neuroscience*, 16(2):219–226.

Glickfeld, L. L. and Olsen, S. R. (2017). Higher-Order Areas of the Mouse Visual Cortex. *Annual Review of Vision Science*, 3:251–273.

Grossman, N., Simiaki, V., Martinet, C., Toumazou, C., Schultz, S. R., and Nikolic, K. (2013). The spatial pattern of light determines the kinetics and modulates backpropagation of optogenetic action potentials. *Journal of Computational Neuroscience*, 34(3):477–488.

Guizar-Sicairos, M., Thurman, S. T., and Fienup, J. R. (2008). Efficient subpixel image registration algorithms. *Optics Letters*, 33(2):156.

Guo, Z. V., Li, N., Huber, D., Ophir, E., Gutnisky, D., Ting, J. T., Feng, G., and Svoboda, K. (2014). Flow of Cortical Activity Underlying a Tactile Decision in Mice. *Neuron*, 81(1):179–194.

Halassa, M. M. and Sherman, S. M. (2019). Thalamocortical Circuit Motifs: A General Framework. *Neuron*, 103(5):762–770.

Han, Y., Kebschull, J. M., Campbell, R. A., Cowan, D., Imhof, F., Zador, A. M., and Mrsic-Flogel, T. D. (2018). The logic of single-cell projections from visual cortex. *Nature*, 556(7699):51–56.

Harris, J. A., Mihalas, S., Hirokawa, K. E., Whitesell, J. D., Choi, H., Bernard, A., Bohn, P., Caldejon, S., Casal, L., Cho, A., Feiner, A., Feng, D., Gaudreault, N., Gerfen, C. R., Graddis, N., Groblewski, P. A., Henry, A. M., Ho, A., Howard, R., Knox, J. E., Kuan, L., Kuang, X., Lecoq, J., Lesnar, P., Li, Y., Luviano, J., McConoughey, S., Mortrud, M. T., Naeemi, M., Ng, L., Oh, S. W., Ouellette, B., Shen, E., Sorensen, S. A., Wakeman, W., Wang, Q., Wang, Y., Williford, A., Phillips, J. W., Jones, A. R., Koch, C., and Zeng, H. (2019). Hierarchical organization of

cortical and thalamic connectivity. *Nature*, 575(7781):195–202.

Harris, K. D. and Shepherd, G. M. (2015). The neocortical circuit: Themes and variations. *Nature Neuroscience*, 18(2):170–181.

Herculano-Houzel, S. (2009). The human brain in numbers: A linearly scaled-up primate brain. *Frontiers in Human Neuroscience*, 3(NOV):1–11.

Hishida, R., Horie, M., Tsukano, H., Tohmi, M., Yoshitake, K., Meguro, R., Takebayashi, H., Yanagawa, Y., and Shibuki, K. (2019). Feedback inhibition derived from the posterior parietal cortex regulates the neural properties of the mouse visual cortex. *European Journal of Neuroscience*, 50(6):2970–2987.

Huang, J. Y., Wang, C., and Dreher, B. (2007). The effects of reversible inactivation of postero-temporal visual cortex on neuronal activities in cat's area 17. *Brain Research*, 1138(1):111–128.

Huang, L., Chen, X., and Shou, T. (2004). Spatial frequency-dependent feedback of visual cortical area 21a modulating functional orientation column maps in areas 17 and 18 of the cat. *Brain Research*, 998(2):194–201.

Hubel, D. H. and Wiesel, T. N. (1959). Receptive fields of single neurones in the cat's striate cortex. *Journal of Physiology*, 148:574–591.

Hubel, D. H. and Wiesel, T. N. (1962). Receptive fields, binocular interaction and functional architecture in the cat's visual cortex. *The journal of physiology*, (160):106–154.

Huh, C. Y., Peach, J. P., Bennett, C., Vega, R. M., and Hestrin, S. (2018). Feature-Specific Organization of Feedback Pathways in Mouse Visual Cortex. *Current Biology*, 28(1):114–120.

Hupe, J. M., James, A., Payne, B., Lomber, S., P, G., and J, B. (1998). Cortical feedback improves discrimination between figure and background by V1, V2 and V3 neurons. *Nature*, 394(20):784–787.

Hupé, J. M., James, A. C., Girard, P., Lomber, S. G., Payne, B. R., and Bullier, J. (2001). Feedback connections act on the early part of the responses monkey visual cortex. *Journal of Neurophysiology*, 85(1):134–145.

Ji, W., Gămănuţ, R., Bista, P., D'Souza, R. D., Wang, Q., and Burkhalter, A. (2015). Modularity in the Organization of Mouse Primary Visual Cortex. *Neuron*, 87(3):632–643.

Jin, M. and Glickfeld, L. L. (2020). Mouse Higher Visual Areas Provide Both Distributed and Specialized Contributions to Visually Guided Behaviors. *Current Biology*, 30(23):4682–4692.

Kalatsky, V. A. and Stryker, M. P. (2003). New paradigm for optical imaging: Temporally encoded maps of intrinsic signal. *Neuron*, 38(4):529–545.

Kaspar, B. K., Erickson, D., Schaffer, D., Hinh, L., Gage, F. H., and Peterson, D. A. (2002). Targeted retrograde gene delivery for neuronal protection. *Molecular Therapy*, 5(1):50–56.

Kayser, C., Körding, K. P., and König, P. (2004). Processing of complex stimuli and natural scenes in the visual cortex. *Current Opinion in Neurobiology*, 14(4):468–473.

Keller, A. J., Dipoppa, M., Roth, M. M., Caudill, M. S., Ingrosso, A., Miller, K. D., and Scanziani, M. (2020a). A Disinhibitory Circuit for Contextual Modulation in Primary Visual Cortex. *Neuron*, 108(6):1181–1193.

Keller, A. J., Roth, M. M., and Scanziani, M. (2020b). Feedback generates a second receptive field in neurons of the visual cortex. *Nature*, 582(7813):545–549.

Keller, G. B. and Mrsic-Flogel, T. D. (2018). Predictive Processing: A Canonical Cortical Computation. *Neuron*, 100(2):424–435.

Kirchberger, L., Mukherjee, S., Schnabel, U. H., van Beest, E. H., Barsegyan, A., Levelt, C. N., Alexander Heimel, J., Lorteije, J. A., van der Togt, C., Self, M. W., and Roelfsema, P. R. (2021). The essential role of recurrent processing for figure-ground perception in mice. *Science Advances*, 7(27).

Ko, H., Hofer, S. B., Pichler, B., Buchanan, K. A., Sjöström, P. J., and Mrsic-Flogel, T. D. (2011). Functional specificity of local synaptic connections in neocortical networks. *Nature*, 473(7345):87–91.

Kowalewski, N. N., Kauttonen, J., Stan, P. L., Jeon, B. B., Fuchs, T., Chase, S. M., Lee, T. S., and Kuhlman, S. J. (2021). Development of Natural Scene Representation in Primary Visual Cortex Requires Early Postnatal Experience. *Current Biology*, 31(2):369–380.

Kreiman, G. and Serre, T. (2020). Beyond the feedforward sweep: feedback computations in the visual cortex. *Annals of the New York Academy of Sciences*, 1464(1):222–241.

Larkum, M. (2013). A cellular mechanism for cortical associations : an organizing principle for the cerebral cortex. *Trends in Neurosciences*, 36(3):1–11.

Larkum, M. E., Senn, W., and Lüscher, H. R. (2004). Top-down dendritic input increases the gain of layer 5 pyramidal neurons. *Cerebral Cortex*, 14(10):1059–1070.

Lee, A. M., Hoy, J. L., Bonci, A., Wilbrecht, L., Stryker, M. P., and Niell, C. M. (2014). Identification of a brainstem circuit regulating visual cortical state in parallel with locomotion. *Neuron*, 83(2):455–466.

Leinweber, M., Ward, D. R., Sobczak, J. M., Attinger, A., and Keller, G. B. (2017). A Sensorimotor Circuit in Mouse Cortex for Visual Flow Predictions. *Neuron*, 95(6):1420–1432.

Li, F. F., VanRullen, R., Koch, C., and Perona, P. (2002). Rapid natural scene categorization in the near absence of attention. *Proceedings of the National Academy of Sciences of the United States of America*, 99(14):9596–9601.

Lien, A. D. and Scanziani, M. (2013). Tuned thalamic excitation is amplified by visual cortical circuits. *Nature Neuroscience*, 16(9):1315–1323.

Lien, A. D. and Scanziani, M. (2018). Cortical direction selectivity emerges at convergence of thalamic synapses. *Nature*, 558(7708):80–86.

Lillicrap, T. P., Cownden, D., Tweed, D. B., and Akerman, C. J. (2016). Random synaptic feedback weights support error backpropagation for deep learning. *Nature Communications*, 7:1–10.

Livingstone, M. (1998). Mechanisms of direction selectivity in macaque V1. *Neuron*, 20(3):509–526.

Ma, W. P., Liu, B. H., Li, Y. T., Huang, Z. J., Zhang, L. I., and Tao, H. W. (2010). Visual representations by cortical somatostatin inhibitory neurons - Selective but with weak and delayed responses. *Journal of Neuroscience*, 30(43):14371–14379.

Mahler, S. V., Vazey, E. M., Beckley, J. T., Keistler, C. R., Mcglinchey, E. M., Kaufling, J., Wilson, S. P., Deisseroth, K., Woodward, J. J., and Aston-Jones, G. (2014). Designer receptors show role for ventral pallidum input to ventral tegmental area in cocaine seeking. *Nature Neuroscience*, 17(4):577–585.

Mahn, M., Prigge, M., Ron, S., Levy, R., and Yizhar, O. (2016). Biophysical constraints of optogenetic inhibition at presynaptic terminals. *Nature Neuroscience*, 19(4):554–556.

Mahn, M., Saraf-Sinik, I., Patil, P., Pulin, M., Bitton, E., Karalis, N., Bruentgens, F., Palgi, S., Gat, A., Dine, J., Wietek, J., Davidi, I., Levy, R., Litvin, A., Zhou, F., Sauter, K., Soba, P., Schmitz, D., Lüthi, A., Rost, B. R., Wiegert, J. S., and Yizhar, O. (2021). Efficient optogenetic silencing of neurotransmitter release with a mosquito rhodopsin. *Neuron*, 109(10):1621–1635.

Marks, T. D. and Goard, M. J. (2021). Stimulus-dependent representational drift in primary visual cortex. *Nature Communications*, 12(1):1–16.

Marques, T., Nguyen, J., Fioreze, G., and Petreanu, L. (2018a). The functional organization of cortical feedback inputs to primary visual cortex. *Nature Neuroscience*, 21(5):757–764.

Marques, T., Summers, M. T., Fioreze, G., Fridman, M., Dias, R. F., Feller, M. B., and Petreanu, L. (2018b). A Role for Mouse Primary Visual Cortex in Motion Perception. *Current Biology*, 28(11):1703–1713.

Marshel, J. H., Garrett, M. E., Nauhaus, I., and Callaway, E. M. (2011). Functional specialization of seven mouse visual cortical areas. *Neuron*, 72(6):1040–54.

Maunsell, J. H. (2015). Neuronal Mechanisms of Visual Attention. *Annual Review of Vision Science*, 1(1):373–391.

Mazurek, M., Kager, M., and Van Hooser, S. D. (2014). Robust quantification of orientation selectivity and direction selectivity. *Frontiers in Neural Circuits*, 8(August):1–17.

Mignard, M. and Malpeli, J. G. (1991). Paths of information flow through visual cortex. *Science*, 251(4998):1249–1251.

Morimoto, M. M., Uchishiba, E., and Saleem, A. B. (2021). Organization of feedback projections to mouse primary visual cortex. *iScience*, 24(5):102450.

Mountcastle, V. (1957). Modality and topographic properties of cat's somatic sensory cortex. *Journal of Neurophysiology*, 20(4):408–34.

Murray Sherman, S. and Guillery, R. W. (2011). Distinct functions for direct and transthalamic corticocortical connections. *Journal of Neurophysiology*, 106(3):1068–1077.

Nassi, J. J., Lomber, S. G., and Born, R. T. (2013). Corticocortical feedback contributes to surround suppression in V1 of the alert primate. *Journal of Neuroscience*, 33(19):8504–8517.

Niell, C. M. and Scanziani, M. (2021). How Cortical Circuits Implement Cortical Computations: Mouse Visual Cortex as a Model. *Annual Review of Neuroscience*, 44:517–546.

Niell, C. M. and Stryker, M. P. (2008). Highly selective receptive fields in mouse visual cortex. *Journal of Neuroscience*, 28(30):7520–7536.

Niell, C. M. and Stryker, M. P. (2010). Modulation of visual responses by behavioral state in mouse visual cortex. *Neuron*, 65(4):472–9.

Nurminen, L., Merlin, S., Bijanzadeh, M., Federer, F., and Angelucci, A. (2018). Top-down feedback controls spatial summation and response amplitude in primate visual cortex. *Nature Communications*, 9(1).

Ohki, K., Chung, S., Ch'ng, Y. H., Kara, P., and Reid, R. C. (2005). Functional imaging with cellular resolution reveals precise microarchitecture in visual cortex. *Nature*, 433(7026):597–603.

Olcese, U., Iurilli, G., and Medini, P. (2013). Cellular and synaptic architecture of multisensory integration in the mouse neocortex. *Neuron*, 79(3):579–593.

Oude Lohuis, M. N., Canton, A. C., Pennartz, C. M. A., and Olcese, U. (2021). Higher Order Visual Areas Enhance Stimulus Responsiveness in Mouse Primary Visual Cortex. *Cerebral Cortex*, pages 1–20.

Pachitariu, M., Stringer, C., Dipoppa, M., Schröder, S., Rossi, L. F., Dalgleish, H., Carandini, M., and Harris, K. (2016). Suite2p: beyond 10,000 neurons with stan-

dard two-photon microscopy. *bioRxiv*, page 061507.

Pafundo, D. E., Nicholas, M. A., Zhang, R., and Kuhlman, S. J. (2016). Top-Down-Mediated Facilitation in the Visual Cortex Is Gated by Subcortical Neuromodulation. *Journal of Neuroscience*, 36(10):2904–2914.

Pak, A., Ryu, E., Li, C., and Chubykin, A. A. (2020). Top-down feedback controls the cortical representation of illusory contours in mouse primary visual cortex. *Journal of Neuroscience*, 40(3):648–660.

Pakan, J. M., Lowe, S. C., Dylda, E., Keemink, S. W., Currie, S. P., Coutts, C. A., and Rochefort, N. L. (2016). Behavioral-state modulation of inhibition is context-dependent and cell type specific in mouse visual cortex. *eLife*, 5(AUGUST):1–18.

Pecka, M., Han, Y., Sader, E., and Mrsic-Flogel, T. D. (2014). Experience-Dependent Specialization of Receptive Field Surround for Selective Coding of Natural Scenes. *Neuron*, 84(2):457–469.

Pennartz, C. M., Dora, S., Muckli, L., and Lorteije, J. A. (2019). Towards a Unified View on Pathways and Functions of Neural Recurrent Processing. *Trends in Neurosciences*, 42(9):589–603.

Pfeffer, C. K., Xue, M., He, M., Huang, Z. J., and Scanziani, M. (2013). Inhibition of inhibition in visual cortex: The logic of connections between molecularly distinct interneurons. *Nature Neuroscience*, 16(8):1068–1076.

Phillips, W. A., Clark, A., and Silverstein, S. M. (2015). On the functions, mechanisms, and malfunctions of intracortical contextual modulation. *Neuroscience and Biobehavioral Reviews*, 52:1–20.

Polack, P. O., Friedman, J., and Golshani, P. (2013). Cellular mechanisms of brain state-dependent gain modulation in visual cortex. *Nature Neuroscience*, 16(9):1331–1339.

Pologruto, T. A., Sabatini, B. L., and Svoboda, K. (2003). ScanImage: Flexible software for operating laser scanning microscopes. *BioMedical Engineering Online*, 2:1–9.

Poort, J., Self, M. W., Van Vugt, B., Malkki, H., and Roelfsema, P. R. (2016). Texture Segregation Causes Early Figure Enhancement and Later Ground Suppression in Areas V1 and V4 of Visual Cortex. *Cerebral Cortex*, 26(10):3964–3976.

Preuss, T. M. (2007). Evolutionary specializations of primate brain systems. *PRIMATE ORIGINS: Adaptations and Evolution*, pages 625–675.

Raimondo, J. V., Kay, L., Ellender, T. J., and Akerman, C. J. (2012). Optogenetic silencing strategies differ in their effects on inhibitory synaptic transmission. *Nature Neuroscience*, 15(8):1102–1104.

Rakic, P. (2009). Evolution of the neocortex: A perspective from developmental biology. *Nature Reviews Neuroscience*, 10(10):724–735.

Rao, R. P. and Ballard, D. H. (1999). Predictive coding in the visual cortex: A functional interpretation of some extra-classical receptive-field effects.

Ricci, M. and Serre, T. (2020). Hierarchical Models of the Visual System. *Encyclopedia of Computational Neuroscience*, pages 1–14.

Richards, B. A. and Lillicrap, T. P. (2019). Dendritic solutions to the credit assignment problem. *Current Opinion in Neurobiology*, 54:28–36.

Rockland, K. S. and Pandya, D. N. (1979). Laminar origins and terminations of cortical connections of the occipital lobe in the rhesus monkey. *Brain Research*, 179(1):3–20.

Roelfsema, P. R. and Holtmaat, A. (2018). Control of synaptic plasticity in deep cortical networks. *Nature Reviews Neuroscience*, 19(3):166–180.

Roth, B. L. (2016). DREADDs for Neuroscientists. *Neuron*, 89(4):683–694.

Roth, M. M., Dahmen, J. C., Muir, D. R., Imhof, F., Martini, F. J., and Hofer, S. B. (2016). Thalamic nuclei convey diverse contextual information to layer 1 of visual cortex. *Nature Neuroscience*, 19(2):299–307.

Saleem, A. B., Ayaz, A. I., Jeffery, K. J., Harris, K. D., and Carandini, M. (2013). Integration of visual motion and locomotion in mouse visual cortex. *Nature Neuroscience*, 16(12):1864–1869.

Sandell, J. H. and Schiller, P. H. (1982). Effect of cooling area 18 on striate cortex cells in the squirrel monkey. *Journal of Neurophysiology*, 48(1):38–48.

Saravanan, V., Berman, G. J., and Sober, S. J. (2020). Application of the hierarchical bootstrap to multi-level data in neuroscience. *Neuron Behav Data Anal Theory*, 3(5):100–106.

Sato, T. K., Häusser, M., and Carandini, M. (2014). Distal connectivity causes summation and division across mouse visual cortex. *Nature Neuroscience*, 17(1):30–32.

Scholl, B., Tan, A. Y., Corey, J., and Priebe, N. J. (2013). Emergence of orientation selectivity in the mammalian visual pathway. *Journal of Neuroscience*, 33(26):10616–10624.

Schwartz, O., Hsu, A., and Dayan, P. (2007). Space and time in visual context. *Nature Reviews Neuroscience*, 8(7):522–535.

Self, M. W., Kooijmans, R. N., Supèr, H., Lamme, V. A., and Roelfsema, P. R. (2012). Different glutamate receptors convey feedforward and recurrent processing in macaque V1. *Proceedings of the National Academy of Sciences of the United States of America*, 109(27):11031–11036.

Self, M. W., van Kerkoerle, T., Supèr, H., and Roelfsema, P. R. (2013). Distinct Roles of the Cortical Layers of Area V1 in Figure-Ground Segregation. *Current Biology*, 23(21):2121–2129.

Sharpee, T. O., Sugihara, H., Kurgansky, A. V., Rebrik, S. P., Stryker, M. P., and Miller, K. D. (2006). Adaptive filtering enhances information transmission in visual cortex. *Nature*, 439(7079):936–942.

Shen, S., Jiang, X., Scala, F., Fu, J., Fahey, P., Kobak, D., Tan, Z., Reimer, J., Sinz, F., and Tolias, A. S. (2020). Distinct organization of two cortico-cortical feedback pathways. *bioRxiv*.

Sherman, S. M. (2016). Thalamus plays a central role in ongoing cortical functioning. *Nature Neuroscience*, 19(4):533–541.

Sherrington, C. (1904). Observations on the scratch-reflex in the spinal dog. *Response*.

Shimaoka, D., Harris, K. D., and Carandini, M. (2018). Effects of Arousal on Mouse Sensory Cortex Depend on Modality. *Cell Reports*, 22(12):3160–3167.

Shushruth, S., Mangapathy, P., Ichida, J. M., Bressloff, P. C., Schwabe, L., and Angelucci, A. (2012). Strong recurrent networks compute the orientation tuning of surround modulation in the primate primary visual cortex. *Journal of Neuroscience*, 32(1):308–321.

Siegle, J. H., Jia, X., Durand, S., Gale, S., Bennett, C., Graddis, N., Heller, G., Ramirez, T. K., Choi, H., Luviano, J. A., Groblewski, P. A., Ahmed, R., Arkhipov, A., Bernard, A., Billeh, Y. N., Brown, D., Buice, M. A., Cain, N., Caldejon, S., Casal, L., Cho, A., Chvilicek, M., Cox, T. C., Dai, K., Denman, D. J., de Vries, S. E., Dietzman, R., Esposito, L., Farrell, C., Feng, D., Galbraith, J., Garrett, M., Gelfand, E. C., Hancock, N., Harris, J. A., Howard, R., Hu, B., Hytnen, R., Iyer, R., Jessett, E., Johnson, K., Kato, I., Kiggins, J., Lambert, S., Lecoq, J., Ledochowitsch, P., Lee, J. H., Leon, A., Li, Y., Liang, E., Long, F., Mace, K., Melchior, J., Millman, D., Mollenkopf, T., Nayan, C., Ng, L., Ngo, K., Nguyen, T., Nicovich, P. R., North, K., Ocker, G. K., Ollerenshaw, D., Oliver, M., Pachitariu, M., Perkins, J., Reding, M., Reid, D., Robertson, M., Ronellenfitch, K., Seid, S., Slaughterbeck, C., Stoecklin, M., Sullivan, D., Sutton, B., Swapp, J., Thompson, C., Turner, K., Wakeman, W., Whitesell, J. D., Williams, D., Williford, A., Young, R., Zeng, H., Naylor, S., Phillips, J. W., Reid, R. C., Mihalas, S., Olsen, S. R., and Koch, C. (2021). Survey of spiking in the mouse visual system reveals functional hierarchy. *Nature*, 592(7852):86–92.

Smith, S. L., Smith, I. T., Branco, T., and Häusser, M. (2013). Dendritic spikes enhance stimulus selectivity in cortical neurons in vivo. *Nature*, 503(7474):115–120.

Sohal, V. S. and Rubenstein, J. L. (2019). Excitation-inhibition balance as a framework for investigating mechanisms in neuropsychiatric disorders. *Molecular Psychiatry*, 24(9):1248–1257.

Stachniak, T. J., Ghosh, A., and Sternson, S. M. (2014). Chemogenetic Synaptic Silencing of Neural Circuits Localizes a Hypothalamus→Midbrain Pathway for Feeding Behavior. *Neuron*, 82(4):797–808.

Stringer, C., Pachitariu, M., Steinmetz, N., Reddy, C. B., Carandini, M., and Harris, K. D. (2019). Spontaneous behaviors drive multidimensional, brainwide activity. *Science*, 364(6437).

Suter, B. A., O'Connor, T., Iyer, V., Petreanu, L. T., Hooks, B. M., Kiritani, T., Svoboda, K., and Shepherd, G. M. (2010). Ephus: Multipurpose data acquisition software for neuroscience experiments. *Frontiers in Neural Circuits*, 4(AUG):1–12.

Takahashi, N., Ebner, C., Sigl-Glöckner, J., Moberg, S., Nierwetberg, S., and Larkum, M. E. (2020). Active dendritic currents gate descending cortical outputs in perception. *Nature Neuroscience*, 23(10):1277–1285.

Takahashi, N., Moberg, S., Zolnik, T. A., Catanese, J., Sachdev, R. N., Larkum, M. E., and Jaeger, D. (2021). Thalamic input to motor cortex facilitates goal-directed action initiation. *Current Biology*, 31(18):4148–4155.

Tohmi, M., Meguro, R., Tsukano, H., Hishida, R., and Shibuki, K. (2014). The extrageniculate visual pathway generates distinct response properties in the higher visual areas of mice. *Current Biology*, 24(6):587–597.

Van Hateren, J. H. and Van der Schaaf, A. (1998). Independent component filters of natural images compared with simple cells in primary visual cortex. *Proceedings of the Royal Society B: Biological Sciences*, 265(1394):359–366.

Van Horn, S. C., Erişir, A., and Sherman, S. M. (2000). Relative distribution of synapses in the A-laminae of the lateral geniculate nucleus of the cat. *Journal of Comparative Neurology*, 416(4):509–520.

Vangeneugden, J., van Beest, E. H., Cohen, M. X., Lorteije, J. A., Mukherjee, S., Kirchberger, L., Montijn, J. S., Thamizharasu, P., Camillo, D., Levelt, C. N., Roelfsema, P. R., Self, M. W., and Heimel, J. A. (2019). Activity in Lateral Visual Areas Contributes to Surround Suppression in Awake Mouse V1. *Current Biology*, 29(24):4268–4275.

Vazey, E. M. and Aston-Jones, G. (2014). Designer receptor manipulations reveal a role of the locus coeruleus noradrenergic system in isoflurane general anesthesia. *Proceedings of the National Academy of Sciences of the United States of America*, 111(10):3859–3864.

Vezoli, J., Magrou, L., Goebel, R., Wang, X. J., Knoblauch, K., Vinck, M., and Kennedy, H. (2021). Cortical hierarchy, dual counterstream architecture and the importance of top-down generative networks. *NeuroImage*, 225(April 2020):117479.

Vinck, M., Batista-Brito, R., Knoblich, U., and Cardin, J. A. (2015). Arousal and Locomotion Make Distinct Contributions to Cortical Activity Patterns and Visual Encoding. *Neuron*, 86(3):740–754.

Vinje, W. E. and Gallant, J. L. (2000). Sparse coding and decorrelation in primary visual cortex during natural vision. *Science*, 287(5456):1273–1276.

Vinje, W. E. and Gallant, J. L. (2002). Natural Stimulation of the Nonclassical Receptive Field Increases Information Transmission Efficiency in V1. *Journal of Neuroscience*, 22(7):2904–2915.

Vries, S. E. J. D., Lecoq, J. A., Buice, M. A., Groblewski, P. A., Ocker, G. K., Oliver, M., Feng, D., Cain, N., Ledochowitsch, P., Millman, D., Roll, K., Garrett, M., Keenan, T., Kuan, L., Mihalas, S., Olsen, S., Thompson, C., Wakeman, W., Waters, J., Williams, D., Barber, C., Berbesque, N., Blanchard, B., Bowles, N., Caldejon, S. D., Casal, L., Cho, A., Cross, S., Dang, C., Dolbeare, T., Edwards, M., Galbraith, J., Gaudreault, N., Gilbert, T. L., Griffin, F., Hargrave, P., Howard, R., Huang, L., Jewell, S., Keller, N., Knoblich, U., Larkin, J. D., Larsen, R., Lau, C., Lee, E., Lee, F., Leon, A., Li, L., Long, F., Luviano, J., Mace, K., Nguyen, T., Perkins, J., Robertson, M., Seid, S., Shea-brown, E., Shi, J., Sjoquist, N., Slaughterbeck, C., Sullivan, D., Valenza, R., White, C., Williford, A., Witten, D. M., Zhuang, J., Zeng, H., Farrell, C., Ng, L., Bernard, A., Phillips, J. W., Reid, R. C., and Koch, C. (2019). A large-scale standardized physiological survey reveals functional organization of the mouse visual cortex. *Nature Neurosci.*, 23:138–151.

Wang, C., Huang, J. Y., Bardy, C., FitzGibbon, T., and Dreher, B. (2010). Influence of 'feedback' signals on spatial integration in receptive fields of cat area 17 neurons. *Brain Research*, 1328:34–48.

Wang, C., Waleszczyk, W. J., Burke, W., and Dreher, B. (2000). Modulatory influence of feedback projections from area 21a on neuronal activities in striate cortex of the cat. *Cerebral Cortex*, 10(12):1217–1232.

Wang, C., Waleszczyk, W. J., Burke, W., and Dreher, B. (2007). Feedback signals from cat's area 21a enhance orientation selectivity of area 17 neurons. *Experimental Brain Research*, 182(4):479–490.

Wang, Q., Sporns, O., and Burkhalter, A. (2012). Network Analysis of Corticocortical Connections Reveals Ventral and Dorsal Processing Streams in Mouse Visual Cortex. *Journal of Neuroscience*, 32(13):4386–4399.

Weber, A. I., Krishnamurthy, K., and Fairhall, A. L. (2019). Coding Principles in Adaptation. *Annual Review of Vision Science*, 5:427–449.

Wiegert, J. S., Mahn, M., Prigge, M., Printz, Y., and Yizhar, O. (2017). Silencing Neurons: Tools, Applications, and Experimental Constraints. *Neuron*, 95(3):504–529.

Willmore, B. D., Mazer, J. A., and Gallant, J. L. (2011). Sparse coding in striate and extrastriate visual cortex. *Journal of Neurophysiology*, 105(6):2907–2919.

Xia, J., Marks, T. D., Goard, M. J., and Wessel, R. (2021). Stable representation of a naturalistic movie emerges from episodic activity with gain variability. *Nature Communications*, 12(1).

Yaeger, C. E., Ringach, D. L., and Trachtenberg, J. T. (2019). Neuromodulatory control of localized dendritic spiking in critical period cortex. *Nature*, 567(7746):100–104.

Yates, S. C., Groeneboom, N. E., Coello, C., Lichtenthaler, S. F., Kuhn, P. H., Demuth, H. U., Hartlage-Rübsamen, M., Roßner, S., Leergaard, T., Kreshuk, A., Puchades, M. A., and Bjaalie, J. G. (2019). QUINT: Workflow for Quantification and Spatial Analysis of Features in Histological Images From Rodent Brain. *Frontiers in Neuroinformatics*, 13(December):1–14.

Yeh, C. I., Xing, D., Williams, P. E., and Shapley, R. M. (2009). Stimulus ensemble and cortical layer determine V1 spatial receptive fields. *Proceedings of the National Academy of Sciences of the United States of America*, 106(34):14652–14657.

Yoshida, T. and Ohki, K. (2020). Natural images are reliably represented by sparse and variable populations of neurons in visual cortex. *Nature Communications*, 11(1).

Young, H., Belbut, B., Baeta, M., and Petreanu, L. (2021). Laminar-specific cortico-cortical loops in mouse visual cortex. *eLife*, 10:1–25.

Zhang, S., Xu, M., Kamigaki, T., Do, J. P. H., Chang, W.-C., Jenvay, S., Miyamichi, K., Luo, L., and Dan, Y. (2014). Long-range and local circuits for top-down modulation of visual cortex processing. *Science*, 345(6197):660–665.

ITQB-UNL | Av. da República, 2780-157 Oeiras, Portugal
Tel (+351) 214 469 100 | Fax (+351) 214 411 277

www.itqb.unl.pt